



**HAL**  
open science

# Manufacturing of hemp/PP composites and study of its residual stress and aging behavior

Xiaohui Zhang

► **To cite this version:**

Xiaohui Zhang. Manufacturing of hemp/PP composites and study of its residual stress and aging behavior. Mechanics of materials [physics.class-ph]. Université de Technologie de Troyes, 2016. English. NNT : 2016TROY0015 . tel-03364312

**HAL Id: tel-03364312**

**<https://theses.hal.science/tel-03364312v1>**

Submitted on 4 Oct 2021

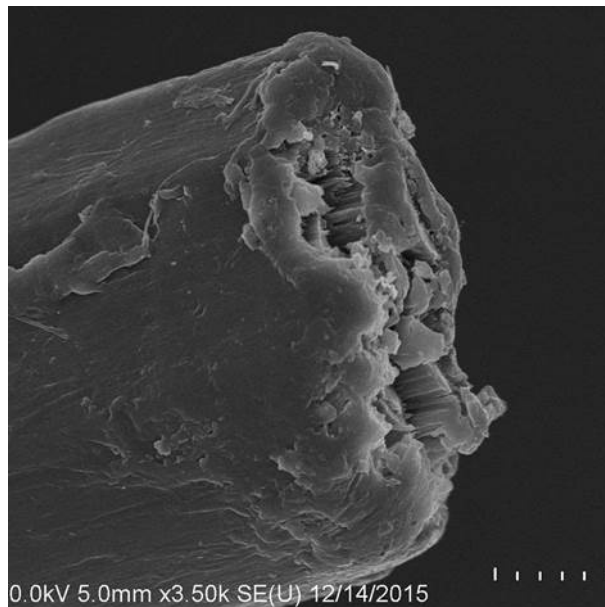
**HAL** is a multi-disciplinary open access archive for the deposit and dissemination of scientific research documents, whether they are published or not. The documents may come from teaching and research institutions in France or abroad, or from public or private research centers.

L'archive ouverte pluridisciplinaire **HAL**, est destinée au dépôt et à la diffusion de documents scientifiques de niveau recherche, publiés ou non, émanant des établissements d'enseignement et de recherche français ou étrangers, des laboratoires publics ou privés.

Thèse  
de doctorat  
de l'UTT

**XiaoHui ZHANG**

# Manufacturing of Hemp/PP Composites and Study of its Residual Stress and Aging Behavior



**Spécialité :**  
Matériaux, Mécanique, Optique et Nanotechnologie

2016TROY0015

Année 2016

---

---

# THESE

*pour l'obtention du grade de*

## DOCTEUR de l'UNIVERSITE DE TECHNOLOGIE DE TROYES

**Spécialité : MATERIAUX, MECANIQUE, OPTIQUE ET NANOTECHNOLOGIE**

*présentée et soutenue par*

**Xiaohui ZHANG**

*le 31 mai 2016*

---

---

### **Manufacturing of Hemp/PP Composites and Study of its Residual Stress and Aging Behavior**

---

---

#### JURY

M. R. AYAD	PROFESSEUR DES UNIVERSITES	Président
M. S. FONTAINE	PROFESSEUR DES UNIVERSITES	Rapporteur
M. X.-L. GONG	PROFESSEUR DES UNIVERSITES	Directeur de thèse
M. S. HE	PROFESSOR	Examineur
M. H. LIAO	PROFESSEUR DES UNIVERSITES	Rapporteur
M. G. MONTAY	MAITRE DE CONFERENCES - HDR	Directeur de thèse
M. D. SCIDA	MAITRE DE CONFERENCES	Examineur



# Acknowledgements

The experience to work at Université de Technologie de Troyes and to live in France is impressive, unforgettable and memorable. All of the work couldn't be accomplished without the assist of a number of people and the financial support of the China Scholarship Council (CSC). I would like to express my sincere appreciation of their generous help and support.

First and foremost I wish to thank my supervisors, Professor **Xiao-Lu GONG** and **Guillame MONTAY**. From the first day I came to Troyes, since when they have supported me not only by providing research aid over three years, but also academically and emotionally through this rough and colorful road to today. They have tirelessly guided me in the experiments and the analysis of the results.

Special thanks to my committee, **Prof. S. FONTAINE** and **Prof. H. LIAO** for their valuable comments on this research. And I would like to thank to the members of jury, R ézak AYAD, Si-Yuan He and Daniel SCIDA, for their attendance in my defense.

The same gratitude should be also given to the colleagues who helped me during my thesis. **B.LESAGE** and **F.WEIL** have helping me to conduct the experiments in Halle Industrielle and to repair the facilities. **X.GASSMANN** deserves the gratitude for his assistance in the chemistry laboratory. And thanks to **R.DETURCHE**, **B.GUELORGET** and all the researchers and technicians of the Institute Charles DELAUNAY.

I would also express my sincere gratitude to my PhD colleagues **HC.HAN**, **ZM.WEN**, **F.ZHU**, **C.ZHANG** and other colleagues at UTT. They have accompanied me all the way along my three-year life and work.

I would thank my parents, my sister and **Xin ZHENG** for their love, their confidence, encouragements and accompany.

XiaoHui ZHANG



# TABLE OF CONTENTS

<b>Acknowledgements .....</b>	<b>1</b>
<b>TABLE OF CONTENTS.....</b>	<b>I</b>
<b>Abstract.....</b>	<b>V</b>
<b>Résumé .....</b>	<b>VI</b>
<b>General Introduction .....</b>	<b>1</b>
<b>Chapter 1. Bibliography: Natural Fibres and Reinforced Composites.....</b>	<b>3</b>
1.1 Introduction.....	5
1.2 Natural Fibers.....	6
1.2.1 Chemical composition and structure.....	7
1.2.2 Physical and mechanical properties.....	10
1.3 Reinforced composites by natural fibers.....	12
1.3.2 Petrochemical composites.....	14
1.3.2.1 Thermoplastic .....	15
1.3.2.2 Thermosets.....	16
1.3.3 Bio-composites .....	16
1.3.4 Nanocomposites.....	16
1.3.5 All-cellulose composites.....	17
1.3.6 Mechanical properties of composites .....	17
1.4 Manufacturing/Processing .....	19
1.4.1 Compression molding.....	20
1.4.2 Factors influencing the process.....	21
1.4.2.1 Moisture .....	21
1.4.2.2 Fiber/polymer type and content .....	21
1.5 Long-term performance .....	22
1.5.1 Humidity .....	22
1.5.2 Thermal.....	27
1.5.3 Ultraviolet .....	28
1.6 Residual stresses in composites .....	30
1.6.1 Formation of residual stress.....	31
1.6.2 Determination of residual stress .....	33
1.6.3 Influence of residual stress .....	33
1.7 Conclusion .....	35
<b>Chapter 2. Elaboration and Performances of the Reinforced Composites.....</b>	<b>37</b>
2.1 Introduction.....	39
2.2 Materials and Methods.....	39
2.2.1 Materials .....	39
2.2.2 Characterization methods .....	41
2.2.2.1 Numerical microscopy .....	41

---

TABLE OF CONTENTS

---

2.2.2.2	Scanning electron microscopy (SEM) .....	41
2.2.2.3	Fourier transform infrared spectroscopy (FTIR) .....	41
2.2.2.4	Differential scanning calorimetry (DSC).....	41
2.3	Characterization of hemp fiber .....	41
2.3.1	Tensile tests .....	42
2.3.2	Measurement of the cross-section.....	43
2.3.3	Tensile properties .....	45
2.3.4	SEM observation.....	47
2.3.5	Spiral angle .....	49
2.4	Manufacture of reinforced composites .....	53
2.4.2	Choice of the fiber and polymer .....	54
2.4.3	Manufacturing process.....	54
2.4.3.1	Hemp preparation .....	54
2.4.3.2	Materials lay-up .....	55
2.4.3.3	Compression molding process .....	57
2.5	Properties of reinforced composites.....	57
2.5.1	Influence of temperature .....	57
2.5.1.1	Tensile properties .....	57
2.5.1.2	DSC analysis.....	59
2.5.1.3	Influence of temperature on hemp fibers .....	60
2.5.1.4	Micrographic observations .....	62
2.5.2	Influence of pressure.....	64
2.5.2.1	Tensile properties .....	64
2.5.2.2	SEM observation.....	65
2.6	Conclusion .....	67
<b>Chapter 3. Environmental Ageing and its Effects .....</b>		<b>69</b>
3.1	Introduction .....	71
3.2	Humidity ageing of composites .....	73
3.2.1	Experimental methods .....	73
3.2.1.1	Humidity ageing .....	73
3.2.1.2	Water uptake .....	74
3.2.1.3	Tensile tests .....	74
3.2.1.4	Scanning electron microscopy (SEM) .....	74
3.2.2	Results and discussion .....	75
3.2.2.1	Tensile test results .....	75
3.2.2.2	Water uptake .....	77
3.2.3	Diffusion of water .....	78
3.2.3.2	Kinetics of water diffusion.....	79
3.2.3.3	Fickian diffusion model .....	81
3.2.3.4	Dimension stability .....	83
3.3	UV ageing .....	85
3.3.1	Experimental methods .....	85
3.3.1.1	UV ageing .....	85
3.3.1.2	Tensile tests .....	86
3.3.1.3	Numerical microscopy .....	86
3.3.1.4	Scanning electron microscopy (SEM) .....	86
3.3.2	Results and discussion .....	86

---

TABLE OF CONTENTS

---

3.3.2.1	Tensile test results .....	86
3.3.2.2	UV ageing of PP/hemp composites .....	87
3.3.2.3	Fracture observation .....	89
3.3.2.4	UV ageing of pure PP .....	90
3.3.2.5	Degradation of lignin .....	93
3.4	Conclusion .....	94
<b>Chapter 4. Residual Stress and its Influence on the Mechanical Properties of the Composites .....</b>		<b>97</b>
4.1	Introduction .....	99
4.2	The hole drilling method.....	99
4.2.1	History of the hole drilling method.....	99
4.2.2	Incremental hole drilling method.....	103
4.3	Determination of the coefficients of calibration .....	109
4.4	The drilling process.....	113
4.4.1	Strain-gage rosette .....	113
4.4.2	Drilling dispositions.....	115
4.4.3	The hole drilling process.....	115
4.5	Residual stresses in the composites .....	116
4.5.1	Strains measured in the composites .....	117
4.5.2	Residual stresses in the composites .....	117
4.5.2.1	Influence of temperature .....	117
4.5.2.2	Influence of cooling rate .....	119
4.5.2.3	Influence of humidity ageing .....	120
4.6	Conclusion .....	122
<b>Chapter 5. Conclusions and Perspectives.....</b>		<b>125</b>
5.1	Conclusions.....	126
5.2	Perspectives .....	128
<b>Chapitre 6. Résumé en Français.....</b>		<b>129</b>
6.1	Introduction.....	131
6.2	Élaboration et performance des composites .....	133
6.2.1	Caractérisation de la fibre chanvre .....	133
6.2.1.1	Essai de traction .....	133
6.2.1.2	Angle spiral.....	135
6.2.2	Élaboration des composites .....	136
6.2.3	Propriétés des composites .....	137
6.2.3.1	Influence de la température.....	137
6.2.3.2	Influence de la température sur chanvre .....	138
6.2.3.3	Observation microscopique .....	139
6.3	Effets du vieillissement .....	140
6.3.1	Vieillessement en humidité relative.....	140
6.3.1.1	Résultats des essais de traction .....	141
6.3.1.2	Absorption de l'eau.....	142
6.3.2	Vieillessement au UV .....	144
6.3.2.1	Résultats des essais de traction .....	144
6.3.2.2	Observation d'apparence .....	145

## TABLE OF CONTENTS

---

6.4	Contraintes résiduelles dans les composites .....	146
6.4.1	La méthode du trou incrémentale .....	147
6.4.2	Détermination des coefficients de calibration.....	150
6.4.3	Contraintes résiduelles .....	152
6.4.3.1	Influence de température .....	152
6.5	Conclusions.....	153
	<b>List of Figures.....</b>	<b>155</b>
	<b>List of Tables.....</b>	<b>159</b>
	<b>References .....</b>	<b>161</b>

# Abstract

This thesis is composed of three parts: Manufacture and characterization of the hemp/polypropylene agro-composites; Ageing and its influence on the mechanical behaviors; Determination of the residual stresses in laminates of agro-composites. In the polypropylene matrix, the hems fibers were used as reinforcement in the composites. The composites were elaborated through compression molding method under different parameters as: temperature, pressure, time...etc. The influences of these parameters on the quality of the manufacturing process are analyzed. The results showed that the temperature has a significant effect on the mechanical properties of the agro-composites. The composite manufactured under 190 °C has the better mechanical properties than other composites. Moreover, the accelerated aging treatment is carried out with two factors: Relative Humidity and Ultra-Violet. Finally, we developed the incremental hole-drilling method to analyze the residual stress generated during the manufacturing process but also generated during aging process. Specific calibration coefficients for these materials were determined by the finite element method.

# Résumé

Cette thèse se compose de trois parties : Elaboration et Caractérisation des agro-composites chanvre/polypropylène, Vieillissement et son influence sur le comportement mécanique d'agro-composites et Détermination des contraintes résiduelles dans les agro-composites stratifiés. Dans la matrice de base en polypropylène, un tissu de chanvre a été utilisé comme renfort dans des composites. Ces derniers sont élaborés par compression thermique avec différents paramètres d'élaboration comme : la température, la pression et le temps...etc. Les influences de ces paramètres sur la qualité physique-mécanique de ces matériaux sont analysés. Les résultats ont montré que la température a un effet significatif sur les propriétés mécaniques des composites. Le composite fabriqué sous 190 °C présente de meilleures propriétés mécaniques que les autres composites. Nous avons ensuite étudié l'influence de deux types de vieillissement sur les propriétés du matériau : un vieillissement en Humidité Relative (RH) et puis un vieillissement aux Ultra-Violets (U.V). Enfin, nous avons développé la méthode du trou incrémental pour analyser les contraintes résiduelles générées lors du procédé de fabrication mais aussi générées pendant le vieillissement. Pour cela, des coefficients de calibration spécifiques à ces matériaux ont été déterminés par la méthode des éléments finis.

# General Introduction

There is a growing interest to use natural fibers as reinforcements in composites for their environmental advantages and to replace artificial fibers as glass or carbon fibers. The natural fibers present low cost, low density, biodegradability, flexibility during processing and storing carbon dioxide during growth make them attractive to researchers and manufacturers.

The principal objectives of this thesis are to manufacture the hemp fiber reinforced polypropylene composites, to characterize the performances of the composites, to study the ageing effects on the behaviors of the composites and to analyze the residual stresses induced in the composites.

In the polypropylene matrix, the hems fibers were used as reinforcement in the composites. The composites were elaborated through compression molding method under different parameters as: temperature, pressure, time...etc. The influences of these parameters on the quality of the manufacturing process are analyzed. The results showed that the temperature has a significant effect on the mechanical properties of the agro-composites. The composite manufactured under 190 °C has the better mechanical properties than other composites. Moreover, the accelerated aging treatment is carried out with two factors: Relative Humidity and Ultra-Violet. Finally, we developed the incremental hole-drilling method to analyze the residual stress generated during the manufacturing process but also generated during aging process. Specific calibration coefficients for these materials were determined by the finite element method.

In the chapter 1, in order to understand the state of the art of the agro-composites, we are concentrated on the bibliographic introduction of the natural fibers and their composites. Natural fibers reinforced polymer composites are of great attraction to applications in many fields. Different types of composites and their chemical and physical properties were presented. The manufacturing methods of the composites are summarized. For thermoplastic polymers, the compression molding method is emphasized. Furthermore, the durability of the natural fibers

reinforced composites, especially the humidity and ultraviolet ageing are introduced. At last, the residual stresses in the composites are introduced. The residual stresses can generate in three levels in the composites. The determination methods and the influences of the residual stresses on the composites are also discussed.

In the chapter 2, the hemp fibers are characterized, and different kinds of hemp reinforced polypropylene composites are elaborated. The hemp fabrics show a difference of properties in the longitudinal and transversal directions. The spiral angle of the hems is measured and analyzed. The hemp fiber reinforced polypropylene composites are manufactured by compression molding method.

In the chapter 3, the humidity ageing and the ultraviolet ageing of the composites are carried out. The effects of humidity ageing on the mechanical properties and the diffusion of water in the composites are discussed. The water uptake in different composite and the dimension stability are measured and analyzed. The effects of UV ageing on the morphology and the mechanical properties are discussed. The microscopic observation is also performed to identify the degradation difference during the UV ageing.

In the chapter 4, the residual stresses and their influences on the composites are discussed. The incremental hole drilling method is introduced. A finite element model is established. The coefficients of calibration are determined by employing this model. The hole drilling process is introduced. The residual stresses are determined by the hole drilling method in the composites. The influence of temperature, cooling rate and humidity ageing on the residual stresses are discussed.

In the end, a conclusion chapter is summarized to finish this thesis. And a resume in French of this thesis is also attached.

# **Chapter 1.**

## **Bibliography: Natural Fibers and Reinforced Composites**

# Chapter 1. Bibliography: Natural Fibers and Reinforced Composites

1.1	Introduction.....	5
1.2	Natural Fibers.....	6
1.2.1	Chemical composition and structure.....	7
1.2.2	Physical and mechanical properties.....	10
1.3	Reinforced composites by natural fibers.....	12
1.3.1	Petrochemical composites.....	14
1.3.1.1	Thermoplastic .....	15
1.3.1.2	Thermosets.....	16
1.3.2	Bio-composites .....	16
1.3.3	Nanocomposites.....	16
1.3.4	All-cellulose composites.....	17
1.3.5	Mechanical properties of composites .....	17
1.4	Manufacturing/Processing .....	19
1.4.1	Compression molding.....	20
1.4.2	Factors influencing the process.....	21
1.4.2.1	Moisture .....	21
1.4.2.2	Fiber/polymer type and content .....	21
1.5	Long-term performance .....	22
1.5.1	Humidity .....	22
1.5.2	Thermal.....	27
1.5.3	Ultraviolet.....	28
1.6	Residual stresses in composites .....	30
1.6.1	Formation of residual stress.....	31
1.6.2	Determination of residual stress .....	33
1.6.3	Influence of residual stress .....	33
1.7	Conclusion .....	35

## 1.1 Introduction

The first step, in this chapter, gives an overview of the wide variety of natural fibers and the corresponding composites. It also includes the frequently-used fabrication methods of composites. In a second step, work is presented across the environment influence on the long-term performances of the composites. Finally, attention is devoted to describing and analyzing the residual stresses in the laminated composites.

Composites materials are defined as materials that are composed of two or more different kinds of materials, which possess significantly different properties. These component materials are mixt to form a new material, on the macro-scale, with novel performances partially or entirely, through physical or/and chemical methods.

A composite generally consists of the matrix elements and the reinforcement elements. The matrix supports, maintains and stabilizes the reinforcements, protects the fibers, prevents the fibers from abrasion, erosion and ageing, delivers the loading from fibers to fibers, thus ameliorates certain properties of the composite. Macromolecular compounds (taking resin for an example), metals or ceramic materials are usually employed as the matrix. The reinforcement in the composites plays a primary part in the reinforcing and ameliorative effects, enhances and controls the main performances of the composites. The strength and stiffness of the composites are supplied by the reinforcements. As reinforcements, various kinds of fibers and particles materials are often utilized.

A composite owns certain attributes of the constituents physically and chemically, and some particularly enhanced properties with respect to those of the components. A great number of composites have been in service in our daily life, such as alloys, ceramic materials, concretes, metal-based composites, resin-based composites.

Among different kinds of composites, eco-composites (or bio-composites)

have been attracting more and more interests since a few decades, mainly because of their environmentally friendly characteristics. Matter the environment and sustainability issues, lots of current materials are irrespctive and unfavorable. Hence green technology and renewable resources have come into the awareness of human beings. Bio-composites, or agro-composites, are made up of natural fibers and green matrices. Natural fibers, hemp, flax, jute, kenaf, sisal (just to name a few), are sustainable and reproducible but, as a matter of fact, they are neither. The plants from which the natural fibers come are renewable, not the fibers themselves. So it is of importance that we manage and take advantages of the ecosystems in ways that we do not pose threat to them [1].

Besides the scarce non-sustainable resources, another crucial field that can broaden the applications of natural-fiber composites is the improvement of long-term properties. The resistance to ultra-violet, moisture and temperature are included. During employments, the environment effect will be a dominating issue. The UV radiation accelerates the degradation of both the matrices and the fibers. The ambient moisture promotes the absorption of water and fiber swelling, leading to accelerated degradation, bad interface adhesion respectively.

## **1.2 Natural Fibers**

The use of natural fibers dates back to about 8000 BC in human's history. Eliso Kvavadze et al. [2] have reported a finding of wild flax fibers at Dzudzuana Cave (Caucasus, Georgia), which indicates that prehistoric human made cords for hafting stone tools, weaving baskets, or sewing garments 32,000 to 26,000 years before the present. Different kinds of fibers are accessible all through the earth. Fibers are mainly divided into two categories, natural fibers and synthetic fibers. Natural fiber is one kind of fibers that comes from natural resources, of which cellulose comes from plants and protein from animals. Natural fibers comprise plant fibers (hemp, flax, jute, kenaf, nettle, ramie, sisal, cotton, etc.), animal fibers (silk, wool, hair, alpaca, etc.), and mineral fibers (asbestos). Nevertheless, synthetic fibers and animal fibers are not discussed in our work.

## 1.2.1 Chemical composition and structure

Plant fibers or vegetal fibers can be classified by their botanical type into: bast, leaf, seed, grass and reed, core, and other types of fibers. There are fibers which contains two or more kinds of fibers. For instance, hemp, flax and kenaf contains both bast and core fibers. Both fruit and stem fibers are included in coconut and oil palm. The complex structure of plant fiber is shown in Fig. 1-1 [3]. The cell wall of plant fibers is made up of several layers as followed: the secondary wall, the primary wall and the middle lamella. And the secondary wall is composed of three sub-layers from interior to exterior: S3, S2, S1 [4, 5]. The layer S2 is the thickest and governs the performance of the whole fiber. The hollow, named lumen, transports water and nutrients during the plant's growth and photosynthesis.

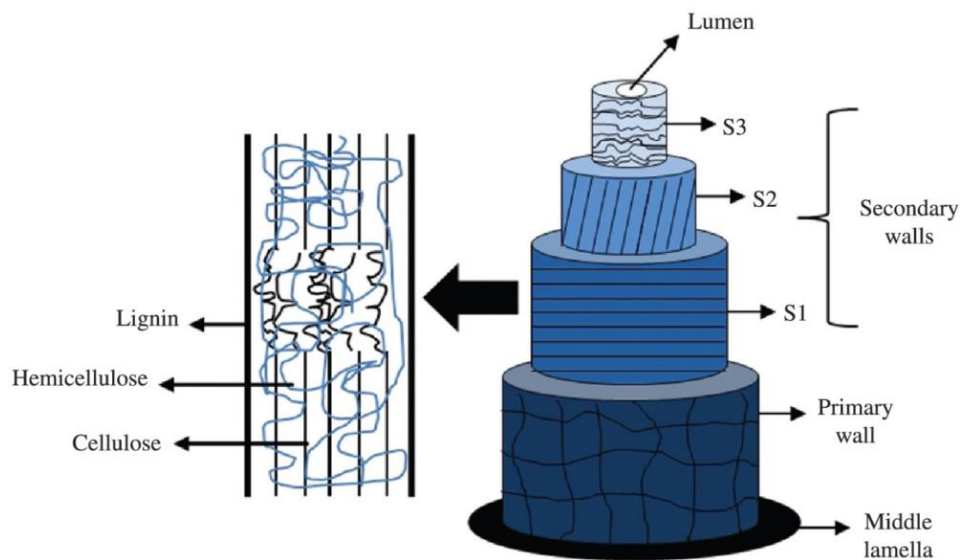


**Fig. 1-1 Schematic representation of plant fiber structure [3]**

The composition of plant fibers varies depending on the type of fiber. The primary constituents are sugar based polymers: cellulose, hemi-cellulose and lignin [6]. The remainder compositions are pectin, wax, protein and several water-soluble compounds. The chemical composition alters from plant to plant. Table 1-1 shows a wide range of the average chemical constituents for different plants [4, 7, 8].

## Cellulose

Cellulose is the most important chemical composition of plant cell walls. Cellulose is defined as a linear condensation polymer containing chain of variable length of 1-4 linked  $\beta$ -d-anhydroglucopyranose units [9], as shown in Fig. 1-2 [10]. This carbohydrate  $(C_6H_{10}O_5)_n$  can be degraded to only glucose  $(C_6H_{12}O_6)$ . Cellulose has good resistance to hydrolysis, oxidizing agents, alkali and temperature under 150 °C. Lots of reviews have detailedly discussed the structure and chemical continuants of the cellulose [11-14]. The degree of polymerization of natural cellulose molecules is between 7000 and 15000. The DP (Degree of Polymerization) of primary cell walls is between 2000 and 6000, and the secondary cell walls 1400, taking cotton fiber for an example.

**Table 1-1 Chemical composition of some natural fibers**

Type of fiber	Chemical composition (%)		
	Cellulose	Hemi-cellulose	Lignin
Abaca	56-63	20-25	7-9
Bagasse	55.2	16.8	25.3
Bamboo	26-43	30	21-31
Coir	32-43	10-20	43-49
Corn cobs	45	35	15
Corn stalks	35	25	35
Cotton	95	2	1
Curaua	73.6	9.9	7.5
EFB	50	30	17
Flax	71	18.6-20.6	2.2
Hemp	68	15	10
Henequen	78	4-8	13
Jute	61-71	14-20	12-13
Kenaf	72	20.3	9
Oil palm	65	-	29
Pineapple	81	-	12.7
Ramie	68.6-76.2	13-16	0.6-0.7
Rice straw	41-57	33	8-19
Sisal	65	12	9.9
Wheat straw	38-45	15-31	12-20

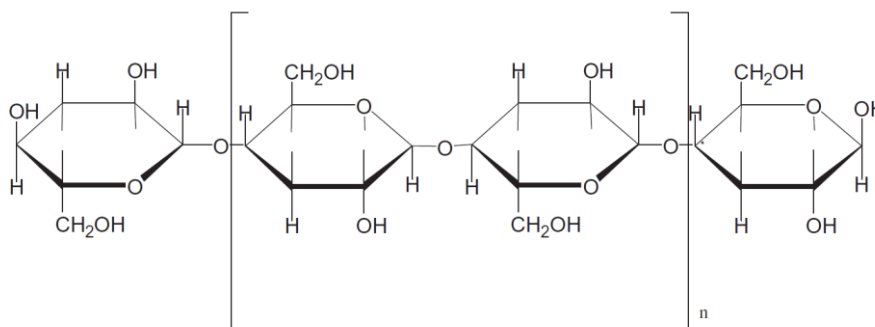


**Fig. 1-2 Chemical structure of cellulose**

### Hemicellulose

Hemicellulose is the second abundant constituent of natural-fiber cell walls. Hemicelluloses (Fig. 1-3 [15]) are lower molecule weight polysaccharides (including hexoses, pentoses, uronic acid residues, excluding pectin), often copolymers forming branch-containing random, amorphous branched and non-linear structures. Hemicellulose is easily hydrolyzed by dilute acids or alkalis; it remains linked with cellulose after removing the lignin. Hemicellulose controls the moisture absorption, biodegradation, and thermal degradation properties of all the natural cellulosic fibers [16-21].

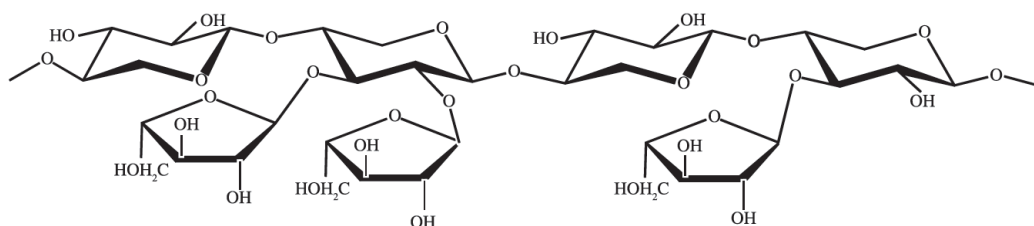


**Fig. 1-3 Example of hemicellulose structure: L-arabino-D-xylane [15]**

### Lignin

Lignin (Fig. 1-4) is formed by non-reversible removal of water from sugars (primarily xylose) to create aromatic structures [21], and it's the highly branched polymers. Lignin has been reported to be the most thermally stable among the three major components of plant cell walls, to confer mechanical stability to the plant, to protect the cellulose/hemicellulose from harsh environmental conditions like water.

But it's responsible for the degradation of fibers and sensitive to UV radiation [9, 21-24].

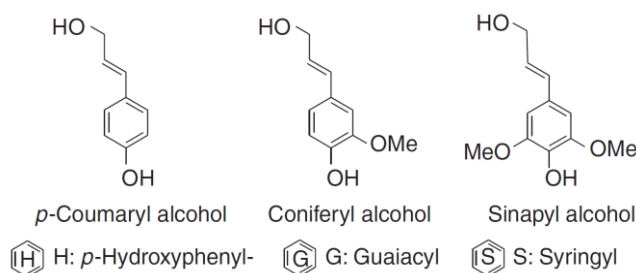


**Fig. 1-4 The three alcoholic monomers of lignin**

### Other components

Pectin is a structural hetero-polysaccharide contained in the primary cell walls of plants, and it gives plants flexibility. Waxes are a class of chemical compounds, consisting different types of alcohols. Waxes and oil consist on fiber surfaces protecting the fiber surfaces.

## 1.2.2 Physical and mechanical properties

There are lots of different species plant fibers, their appearance, physical and mechanical properties differ as well. Because they are in diverse growing conditions and can be affected by measuring methods. Table 1-2 summarizes the factors affecting the fiber quality of different stages [25]. Nishino [26] identified several factors which can influence the physical and mechanical properties of natural fibers, as shown in Table 1-3.

Because of many factors of fiber quality and properties, the fibers present different performances influenced by the cellulose content, degree of polymerization and microfibrillar angle. It has been reported that higher tensile resistance was found in natural cellulosic fibers of a higher content of cellulose and a higher degree of polymerization and a smaller microfibrillar angle. Table 1-4 shows the mechanical properties of different fibers. Due to their high variability in the same species, most of the natural fibers display large ranges of the values of the properties.

**Table 1-2 Factors effecting fiber quality at various stages of natural fiber production**

Stage	Factors effecting fiber quality
Plant growth	Species of plant, local climate, cop cultivation, cop location, fiber location in plant
Harvesting stage	Fiber ripeness, which affects: cell wall thickness, coarseness of fiber, adherence between fibers and surrounding structures
Fiber extraction stage	Decortication process, type of retting method
Supply stage	Transportation conditions, storage conditions, age of fiber

**Table 1-3 Factors affecting the physical and mechanical properties**

Materials	Microscopic: crystallinity, microfibril angle, crystal modifications Macroscopic: fineness, porosity, size and shape of lumen Factors as in table 2.
Measurement conditions	Tensile speed, initial gauge length, moisture, temperature, different cross-section of fibers at different points

Mwaikambo L. Y. [27] studied the tensile properties of alkalinized jute fibers. The tensile strength and Young's modulus of jute fiber was found to depend on the physical characteristics of its internal structure (cellulose content, crystallinity index, and micro-fibril angle). Marie Genet et al. [28] revealed that fiber tensile strength was significantly and positively related to percentage cellulose in roots of Sweet chestnut. But high variability of cellulose content was observed, which could be explained by other chemical and anatomical parameters. They could affect the tensile strength of roots. Sefain M.Z. [29] found that wood pulp was more reactive because of a lower degree of polymerization. Sawpan M.A. [30] observed that tensile strength and Young's modulus of untreated and treated (alkali, silane, maleic anhydride, acetylation) hemp fibers increased with increased crystallinity index. Mwaikambo L.Y. et al. [31, 32] estimated the effect of fiber diameter, cellulose content, crystallinity index and micro-fibril angle on the tensile properties of treated hemp and sisal fibers. Fibers with small diameter, relatively high cellulose content, lower crystallinity (different from Sawpan M.A.) had high strength and modulus. Asim Shahzad [33] identified that fiber strength was inversely related to fiber width, showing that as the fiber width increased, fiber strength decreased.

**Table 1-4 Physio-mechanical properties of some natural fibers with comparative values for E-glass**

Fiber	Density (g/cm <sup>3</sup> )	Tensile strength (MPa)	Young's modulus (GPa)	Elongation at break (%)	References
Abaca	1.5	400	12	3-10	[7]
Coir	1.2	175	4-6	30	[34]
Cotton	1.5-1.6	287-597	5.5-12.6	7.0-8.0	[35, 36]
Flax	1.5	345-1035	27.6	2.7-3.2	[37, 38]
Flax	1.53	1339±486	58±15	3.27±0.4	[39]
Hemp	1.48	690	70	1.6	[40]
Hemp	1.52	920	70	1.7	[41]
Jute	1.3	393-773	26.5	1.5-1.8	[35, 42, 43]
Kenaf	-	930	53	1.6	[40]
Kenaf	1.19	240-600	14-38	-	[21]
Sisal	1.5	511-635	9.4-22	2.0-2.5	[44]
E-glass	2.55	3400	71	3.4	[41]

As the surface impurities present in plant materials, the interface between fiber and matrix is impaired. So some chemical and physical methods are developed with the purpose of taking good advantages of the physical and structural performances of the fibers. In Beckermann G.W.'s study [45], after alkali treated (a solution of 5wt.% NaOH/2 wt.% Na<sub>2</sub>SO<sub>3</sub>), the crystallinity index of hemp fiber was elevated, the fiber lignin contents was reduced, the thermal stability increased, and the tensile strength and Young's modulus were enhanced. And also, the tensile strength of composites consisting of treated hemp fibers proved to be higher than that of untreated.

### 1.3 Reinforced composites by natural fibers

Composites were defined in different ways by different researchers. On a broader scale a composite is defined as: a combination of two different materials is enhanced than the individual component. As for composites reinforced by

natural fibers, the matrix is a polymer, the reinforcement is natural fibers. The matrices play an important role in holding the fibers, transferring loads along the reinforcements, determining the composites' surface appearance and environmental durability. The fibers dominate the overall properties of composites [46], carrying most of the loads, provide strength and stiffness for instance.

Like agriculture, natural fibers have been a part of human life since the dawn of civilization. Fragments of cotton articles dating back to 5000 BC have been unearthed in Mexico and Pakistan [47]. It was as early as 3,000 years ago in ancient Egypt that the natural fibers were employed as component in composites materials [48]. During last century, natural fibers are getting more and more attention. In 1941, hemp and flax fibers were used in resin matrix composites for the bodywork of a Henry Ford car [49]. Beginning in 1990s, renewed interest in natural fiber composites emerged.

As the universal awareness of environment pollutions, sustainable development and recyclable resources, a number of researchers, entrepreneurs, manufacturers and even government are trying to find alternative materials in most fields. Natural fibers reinforced polymer composites present a lot of advantages such as comparable specific strength, toughness, considerable flexibility, eco-friendliness, recyclability and easy processing. And natural fiber is considered as a substitute of glass fiber, ceramics or perhaps carbon fiber. Table 1-5 summarized the principal advantages and disadvantages of natural fibers as reinforcements in composites materials [50]. Germany has been at the front rank using natural fiber reinforced composites for automobile applications. The annual average consumption of natural fibers doubled from 12 million tons in the 1960s to 24 million tons in the 2000s, resulting in the decrease of the average share of natural fibers in total textile fiber consumption from 71% to 42% in the same period.

According to the matrix involved, the corresponding composites can be

fully biodegradable, or non-biodegradable. The development of synthetic resins during and just after the Second World War led to a highly growing production of synthetic composites and the consequent declination of natural fibers in composites.

**Table 1-5 Principal advantages and disadvantages of natural fibers as reinforcements in composites materials**

Advantages	Disadvantages
<ul style="list-style-type: none"> <li>• Low cost;</li> <li>• High specific mechanical properties (resistance and rigidity);</li> <li>• Biodegradability;</li> <li>• Non-abrasive for tooling;</li> <li>• Neutral for the emission of CO<sub>2</sub>;</li> <li>• Require little energy to be produced;</li> <li>• No residue after incineration;</li> <li>• No irritation during the manipulation of the fibers;</li> <li>• Good thermal and acoustic insulation;</li> <li>• Renewable resource.</li> </ul>	<ul style="list-style-type: none"> <li>• Absorption of water;</li> <li>• Low thermal resistance (200 to 230 °C max);</li> <li>• Biodegradability;</li> <li>• Weak dimensional stability;</li> <li>• Anisotropic fiber;</li> <li>• Discontinuous reinforcement;</li> <li>• Request managing of stock for industrial application;</li> <li>• Variation in quality depending on the place of growth, weather.</li> </ul>

### 1.3.2 Petrochemical composites

The polymer market is dominated by commodity plastics with 80% consuming materials based on non-recyclable conventional petroleum resources. The petrochemical based matrix comprises two large kinds of plastics, thermoplastics and thermosets. Because of the low thermal resistance of natural fibers (shown in table 5), so the reported polymer matrices are dedicated to polymers with a relatively low processing temperature. Polypropylene (PP), polyester (PE), polystyrene (PS) and polyvinyl chloride (PVC) are employed in thermoplastic matrices, whereas polyester, epoxy resin, phenol formaldehyde and vinyl esters are utilized as thermosets. The thermoset matrix is the most widely used for natural fiber reinforced composites.

### 1.3.2.1 Thermoplastic

PE matrix based composites reinforced by natural fibers are investigated by many researchers, in lots of aspects, such as the hygrothermal weathering properties, isothermal crystallization behavior, single fiber pullout, interfacial properties, surface modifications and mechanical properties. To vary the content of fibers and to control the bonding between fibers and matrices could improve the strength and stiffness.

The coupling agents added to RHDPE/fiber (pine, bagasse) composites could increase or decrease the crystallinity level [51]. The modulus, tensile strength and impact strength occurred maxima for the RHDPE/bagasse at 4.5% content MAPE, while the RHDPE/pine at 2.4%. Angelo G. Facca [52] predicted the stiffness of some commercially important natural fiber composite formulations employing available micromechanical models. The Halpin-Tsai equation was found to be most accurate to predict the experimental data for natural fiber reinforced thermoplastics. Similar investigations (polyethylene based composites) were carried out using sisal [53, 54], curaua [55] fibers, and LDPE as matrices with coconut [56], technocel, alfa, pine, avicel [57], sisal [58] and coir fibers [59].

Zampaloni M. [60] focused on the manufacture of sheet form composites with chopped kenaf fiber and polypropylene powder through compression molding. Kenaf/PP composites showed a higher modulus/cost (140-150 \$/kg) and a higher specific modulus (55-60 kN·m/kg) than other natural fibers and E-glass fiber. Mohanty A. K. [61] studied the natural fibers reinforced PP composites employing powder impregnation processing. And through suitable blend of surface treated bast and leaf fibers, the desired properties of the composite materials were obtained. And mechanical and thermal properties [62, 63], water absorption [64], flame retardant properties [65] interface investigations, fiber and matrix modifications [66, 67], compatibilizer [68] were studied by other scientists.

### **1.3.2.2 Thermosets**

Thermosets are characterized by their high modulus, strength, thermal and chemical resistances, however, they also present low impact resistance and cannot be reformed.

K. Al-Kaabi and A. Al-Khanbashi [69] found that fiber content and fiber surface treatments had effects over the flexural properties and impact strength of date palm fiber/polyester. Fibers were strengthened through soda treatment. It's at 9 wt.% and 2 cm that the fiber fraction and fiber length were optimized. Piedad Ganan et al. [70] evaluated the mechanical and thermal properties of sisal fiber reinforced epoxy matrix composites as a function of modification of sisal fiber by mercerization and silane treatment. M.S. Sreekala et al. [71] studied the stress relaxation in phenol-formaldehyde composites reinforced with short oil-palm empty fruit bunch fibers as a function of fiber loading, fiber treatment, physical aging and strain level.

### **1.3.3 Bio-composites**

Alternatives to petroleum resources are under pursuing, because of the global concern about the environment and climate changing. In the last two decades, biopolymers have driven great public attention. Bio-composites, containing bio-polymer, are biodegradable. Biopolymers are developed from naturally renewable resources, such as starch, Polylactide acid (PLA) and Polyhydroxybutyrate (PHB). Biopolymers are mainly used in short-life application like packaging. Biopolymers are entirely biodegradable and much more attracting with respect to the partially degradable natural fiber reinforced composites.

### **1.3.4 Nanocomposites**

Nanocomposites are generally two-phase materials in which one of the phases has at least one dimension in the nanometer range (1-100nm). The

advantages of nanocomposites materials are their superior thermal, mechanical, barrier properties at low reinforcement levels (e.g.,  $\leq 5$  wt.%) compared with conventional composites, and the same good recyclability, biodegradability and low weight as the conventional composites [72]. It's possible to produce films with high transparency and with improved oxygen barrier properties, the electronic devices in industry and the potential reinforcing materials in roll-to-roll technologies and so on. But The hydrophilicity and high energy consumption are the major obstacles for the application and commercialization [72].

### **1.3.5 All-cellulose composites**

A new all-cellulose composite (ACC) appeared in recent years, cellulose reinforced cellulose-based composite. A number of publications have reported exceptional mechanical properties of ACCs over those of traditional bio-composites [73-77]. The hydrophilicity of cellulose will require additional processing to recede or avoid the swelling and degradation in long-term service.

### **1.3.6 Mechanical properties of composites**

In order to exploit the applications of natural fibers, it is important recognize their certain mechanical properties, among which are tensile, flexural, impacts, dynamic mechanical and creep properties.

The tensile properties belong to the most widely tested properties of natural fiber reinforced composites. The strength is a major criterion for the selection of a certain application. A tensile test is the reflection of the average property through the thickness, and is uniform throughout the cross-section. A flexural stress varies from 0 in the middle to maximum in the top and bottom surfaces. The flexural stiffness reflects the deformability. Impact strength is the ability of a material to resist fracture under stress applied at a high speed [7]. Creep behavior is the tendency of a solid material to move slowly or deform permanently under the influence of mechanical stresses. Cyclic dynamic mechanical properties and the

creep behavior of natural fiber reinforced composites is still poorly studied.

The generally famous rule-of-mixtures (ROM) equation can predicting the various properties of a composite material, and it is applicable when the reinforcements are continuous and well aligned and the basic assumption of equal strain in the two components is correct. It gives the form as following:

$$E_c = V_f E_f + V_m E_m \quad (1-1)$$

where E and V are moduli and volume fractions, respectively, and the subscripts c, f and m are composites, fibers and matrices, respectively. And the semi-empirical Halpin-Tsai equations are widely used to predict the elastic properties of short fiber reinforced thermoplastics (SFRT) [78], as found in the following form in the one-direction:

$$E_1 = E_m \left( \frac{1+\xi\eta V_f}{1-\eta V_f} \right) \quad (1-2)$$

In Eq. (1-2)  $\eta$  is referred to as:

$$\eta = \frac{(E_f/E_m)-1}{(E_f/E_m)+\xi} \quad (1-3)$$

where  $\xi$  in Eqs. (1-2) and (1-3) is a shape fitting parameter to fit the Halpin-Tsai equation to the experimental data. If the tensile modulus in the principle fiber direction is desired, and the fibers are rectangular or circular in shape,  $\xi$  is thus given by the equation as follows:

$$\xi = 2 \left( \frac{L}{T} \right) \quad \text{or} \quad \xi = 2 \left( \frac{L}{D} \right) \quad (1-4)$$

where L is the length of a fiber in the one-direction, and T or D is the thickness or diameter of the fiber in the three-direction respectively. As  $L \rightarrow \infty, \xi \rightarrow \infty$ , the Halpin-Tsai equation reduces back to the ROM equation (1-1).

In practical terms, there always is porosity, which can influence the actual predictions and cannot be neglected. Porosity is referred to as air-filled cavities,

which is an unavoidable part in all composites materials. Porosity can be developed and generated during the mixture and solidification of two different materials. According to MacKenzie's study [79], on adding spherical holes into materials, the effect of porosity on material stiffness can be approximated by,

$$E_p = E_d \cdot (1 - V_p)^2 \quad (1-5)$$

where the E and V are the stiffness and volume of porosity respectively, and the subscripts p and d are referred to as the fully dense material and the porous material, respectively. And there are interactions between these three parts being called volumetric interaction by Bo Madsen [80]. A model was developed to predict the porosity as a function of the fiber weight fractions and to calculate the density of the composite. Four porosity sub-components were identified, three of which were assumed to be fiber correlated, fiber porosity, interface porosity and impregnation porosity, and one matrix-correlated matrix porosity. The model was in good agreement with the experimental data.

## 1.4 Manufacturing/Processing

In the present researches, natural fiber reinforced polymer composites have generally suffered a number of manufacturing processes. In one hand, all of the methods should be operated at a certain temperature, because the flowability of the polymers is one guarantee to enclose the natural fibers. In another hand, the cellulosic fibers cannot suffer a too high temperature, which could induce fiber degradation and cellulose decomposition to a certain extent. Otherwise, a significant decrease of mechanical properties will be avoided. Natural fibers were processed under a range of temperatures from 160 °C to 220 °C [57, 64, 80-87], depending on the varieties of the fibers used. As a consequence of this constraint, appropriate matrix and fiber systems and suitable processing methods need to be selected. Most synthetic composites processing methods which don't require intense heat are also compatible with cellulosic fibers.

In general, natural fiber reinforced composites are elaborated by traditional manufacturing techniques, such as compounding, pultrusion, extrusion, injection molding, compression molding, resin transfer molding (RTM), vacuum bagging (including autoclave cure) and liquid moulding technologies (LMT) or liquid composite moulding (LCM).

### **1.4.1 Compression molding**

Compression molding is applicable to many cases, thermosets or thermoplastics, particle fibers, short fibers or continuous fibers, composite sheets or laminates. Depending on its ease of use and stability, compression molding has been widely employed, especially for laminates composites.

Abdelmouleh M. [57] and his colleague manufactured a 0.5 mm thick sheets by compression molding at 180 °C with cellulose reinforced LDPE (the low density polyethylene). The molding cycle consisted of 5 min preheating, compression under a force of 10 ton for 3 min, and air cooling under load until the mold reached 40 °C. Mechanical properties, thermal properties and water absorbance behavior were characterized. The mechanical properties increased with increasing the average fiber length. Composites containing fibers treated with MPS and MRPS displayed better mechanical performances than fibers treated with HDS. Seung-Hwan Lee et al. [82] compression molded the composites with a thickness of 0.4 mm, at 200 °C for 10 min. The hardness and elastic modulus of the composites were investigated. It was found that the width of the property transition zone is less than 1 µm. Bo Madsen et al. [87] studied the physical and mechanical properties of unidirectional polypropylene based composites reinforced by textile monofilament flax yarn fibers. The composites were prepared through film-stacking technique and processed by vacuum heating at 190 °C during 15 min and press consolidation under 2.2 MPa and 1 min. A modified version of the “rule-of-mixture”, incorporated parameters of porosity content and anisotropy of fiber properties, were developed to improve the prediction of composites tensile properties.

## **1.4.2 Factors influencing the process**

During processing, the composites quality and its final properties can be influenced by several factors, such as the environment moisture, the water residue in fibers and matrices, the fiber qualities and components etc.

### **1.4.2.1 Moisture**

Water presence in the fiber before and during the processing, and ambient moisture could lead to a harmful effect on the mechanical and chemical properties of the composites. The natural fibers are hydrophilic; this nature can play a role as a separating agent between the fiber surface and the matrix surface. Additionally, the water evaporation during elaboration under a relatively high temperature induces voids in the matrix. Consequently drying fiber before manufacture is an important step.

Ana Espert et al. [64] have investigated to relate kinetics and characteristics of the water absorption in natural fibers/polypropylene composites. Water absorption on natural fibers/PP composites followed the kinetics of a Fickian diffusion process, where the kinetics parameters are influenced by the fiber content, the matrix type and the temperature by means of the Arrhenius law. Water-saturated samples showed poor mechanical properties. At low fiber content, the composite presented a slightly higher value, which disappeared with the increase in temperature. Suhara Panthapulakkal and Mohini Sain [88] found that the flaws and gaps at the interface of the filler and high density polyethylene (HDPE) are the main factors for moisture diffusion in the wheat straw and cornstalk filled composites without compatibilizer.

### **1.4.2.2 Fiber/polymer type and content**

The hydrophilic natural fiber has an important effect on the processing, for example, their types, contents, lengths, aspect ratio (length/diameter), and chemical compositions. There are different chemical structures, surface

morphology and so on. Increasing the fiber content in the composites increases the composites' stiffness. However, increased fiber content increases the composites' odor and the water absorption. And a high aspect ratio induces the high mechanical properties of the fibers/composites.

## **1.5 Long-term performance**

Despite of their advantages such as low density and relatively comparable mechanical properties, the natural fiber reinforced composites are still mainly limited to interior applications in automotive industries, furniture and packaging. The disadvantages are a main concern narrowing down their expansions, including incompatibility between fibers and matrices, low durability performances, variability in quality and composition, low processing and/or service temperatures.

Natural fibers/polymer composites exposed in an outdoor environment may suffer accelerated degradation, because of influencing factors of relative humidity, temperature, ultraviolet radiation. Furthermore, biodegradation could be induced by microbes, for instance, bacteria and fungi, which are not taken into our consideration in this section.

### **1.5.1 Humidity**

Because of the hydrophilicity of natural plant fibers, natural fiber/polymer composites present a moisture absorption in humid environment. It is the results of the presence of the hydroxyl groups and other polar groups in natural fibers. This hydrophilicity leads to incompatibility between the hydrophilic fibers and the hydrophobic polymer matrices. The higher content of fibers presents in the composites, the more water absorption is obtained. Accordingly, undesirable poor fiber-matrix adhesion occurred, resulting in poor stress transfer, low mechanical properties and short-term service.

Normally, the transfer of water can take place in three mechanisms, diffusion

inside the matrix, imperfections within the matrix (micro space, pores or cracks) or capillarity along the fiber/matrix interface [89, 90]. It was observed that the moisture absorption at room temperature respects the Fick's law. The water diffusion takes places from higher concentration areas to lower concentration areas due to the concentration gradient. In the beginning, moisture absorption is linear, then slows and approaches a saturation state after a certain time.

Water, which is absorbed in polymers, is composed of free water and bound water [12], as shown in Fig. 1-5. Free water is able to move independently through voids and microspaces. But bound water is bounded to the polar groups of the polymers. As a natural fiber reinforced polymer composite take in moisture, water molecules penetrate into the composite, and grab the hydrophilic, forming intermolecular hydrogen bonding with fibers, thus weaken the interfacial adhesion fiber/matrix. The fiber swell when absorbing more and more water, and the swelling develops stress at the fiber/matrix interfaces, thus microcracks occur in the matrix surrounding the swollen fibers. Due to the microcracks developed previously, more water is absorbed, and fiber swelling and microcracks furtherly prograde. Meanwhile, water soluble substances begin to dissolve and drop from the fibers and matrices, leading to dramatically fiber/matrix debonding. This progress is diagrammed in Fig. 1-6 [12].

Athijayamani et al. investigated the effect of moisture absorption of randomly oriented natural fibers/polyester composites. The moisture absorption increased with increasing fiber content and fiber length, in the case of 50mm/100mm/150mm fiber length reinforced composites. The surface morphology of the moisture absorbed composite was different with that of dry composite in terms of voids, porosity, swelling, sorption in micro-cracking, disbanding around filler [91].

The **hemicelluloses** consist of low molecular weight polysaccharides; they are the dominant factors in moisture composition, moisture absorption and

biodegradation. Higher hemicellulose content leads to relatively higher moisture absorption. The hemicellulose content of water hyacinth, 16.78 w.t.%, was higher than that of sisal, 5.63 w.t.%. And the moisture content of water hyacinth and sisal were 9.46 w.t.% and 7.02 w.t.% respectively. It suggested that natural fibers with

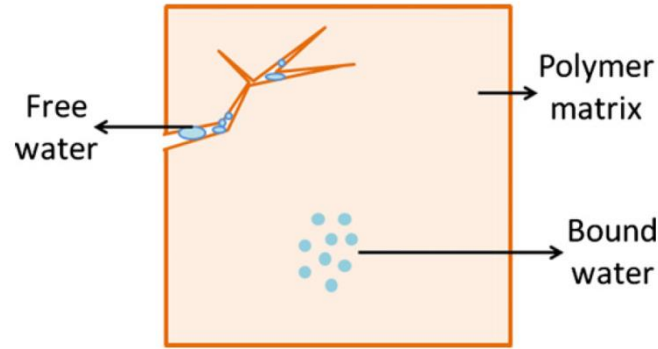


Fig. 1-5 Free water and bound water in polymer matrix [12]

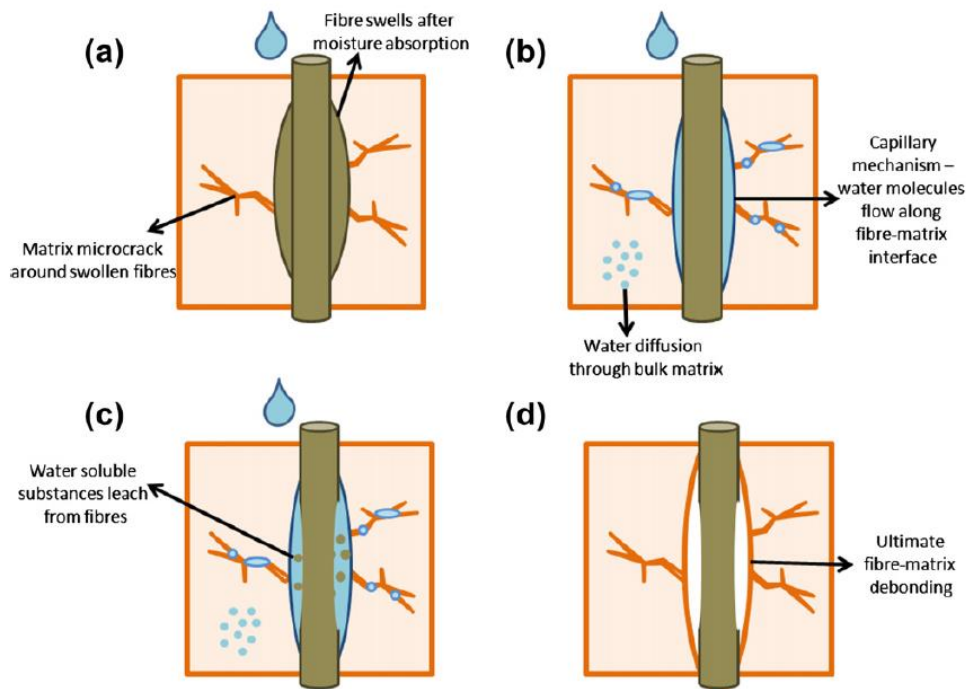
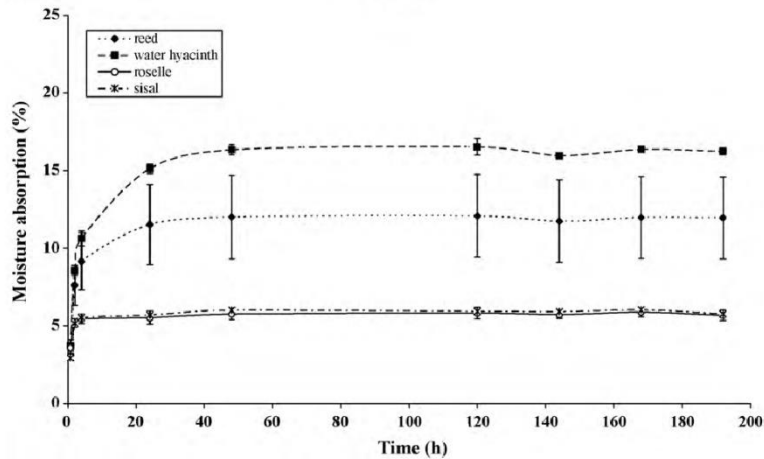


Fig. 1-6 Effect of water on fibre–matrix interface [12]



**Fig. 1-7** Moisture absorption of the studied natural fibers at 23 °C/ 75% RH [92]

a high hemicellulose content could have a high moisture composition. As time progressed, the moisture absorption was more rapid at the initial stage and lower amount of water was taken in as time increased until it reached a balanced level comparing with the surrounding RH (as shown in Fig. 1-7). The moisture absorption of sisal and roselle was very close together and less than that of reed and water hyacinth [92].

It was found that the surrounding **Relative Humidity** (RH) was a factor which influenced the moisture absorption capacity of the natural fibers [92]. At 33% RH, almost no moisture absorption (less than 1%) was detected in the studied fibers. At 75% RH, the moisture absorption of studied fibers is shown in Fig. 1-8. At 97% RH, moisture absorption of reed, roselle and sisal fibers remarkably increased approximately as 5 times higher than that at 75% RH. And the moisture absorption of the remaining water hyacinth remarkably increased 8 times higher.

**Temperature** can be an important factor which may affect the moisture absorption behavior. According to H.N. Dhakal and his co-workers, the water uptake process for all specimens except CSM, which hardly absorbs any water, was in accordance with Fickian diffusion process at room temperature. The water uptake process was linear in the beginning, then slowed and approached saturation after prolonged time. But, at boiling temperature, the water uptake

seemed to obey non-Fickian behavior compared to room temperature. This is attributed to the moist, high temperature environment, and micro-cracks developed on the surface and inside the materials [12, 93]. Fig. 1-8 a) and b) show typical graphs of Fickian diffusion and non-Fickian diffusion, respectively.

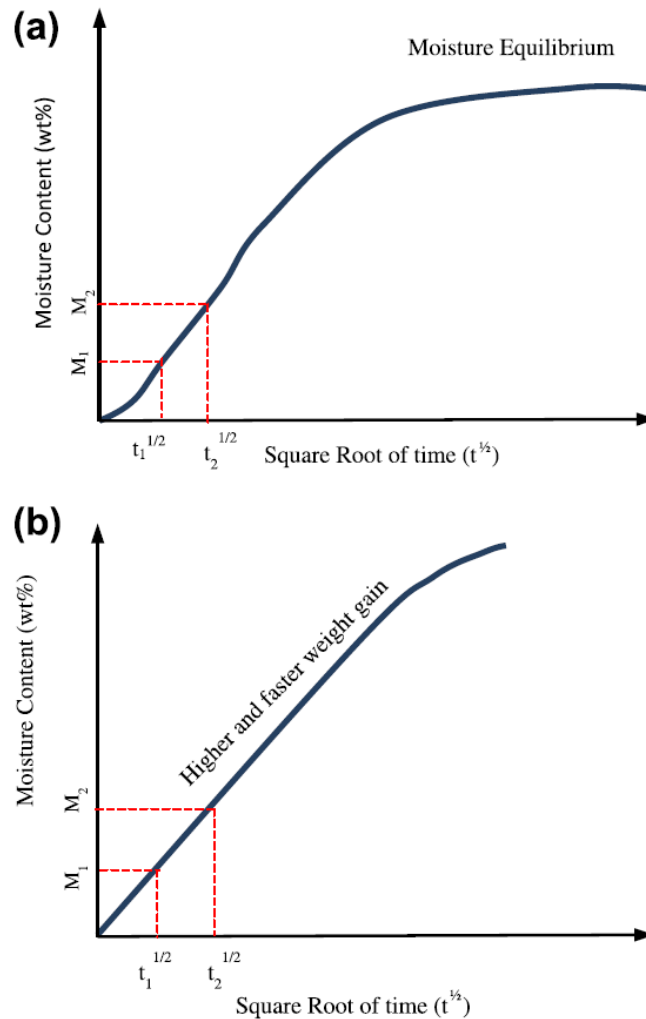


**Fig. 1-8 a) fickian diffusion at room temperature, b) non-fickian diffusion at elevated temperature [12]**

**Influence: Moisture content** in fibers influences the degree of crystallinity, crystalline orientation, tensile strength, swelling behavior, and porosity of fibers. Higher moisture absorption increases the ease of microbial attack (biodegradation). Cellulose fibers are difficult to dissolve due to their high crystallinity, enabling them to retain liquids in the interfibrillar space. The degree of sorption and swelling obtained are determined by the ability of the liquid to

interact with the cellulosic fiber [92, 94]. Moisture content in the fibers also influences the degree of crystallinity, crystalline orientation, tensile strength, swelling behavior and porosity of the fibers [92].

## 1.5.2 Thermal

Temperature can be an important factor which may affect the moisture absorption behavior. According to H.N. Dhakal and his co-workers, the water uptake process was in accordance with Fickian diffusion process at room temperature. The water uptake process was linear in the beginning, then slowed and approached saturation after prolonged time. But, at boiling temperature, the water uptake seemed to obey non-Fickian behavior compared to room temperature.

A typical thermogravimetric graph for the decomposition process of natural fibers is shown in Fig. 1-9. Thermal decomposition processes of different lignocellulosic fibers have similar TG and DTG curves because of their similar chemical composition and physical and mechanical properties. The weight loss of natural fibers during fire is classified into three main stages in Table 1-6.

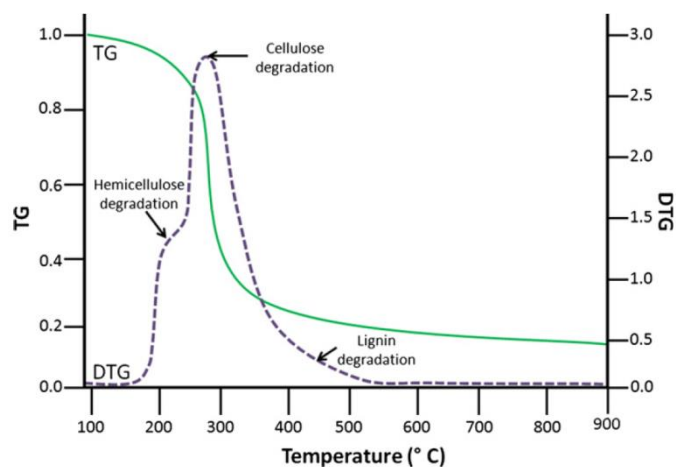


Fig. 1-9 Typical thermogravimetric decomposition process of natural fibres [95, 96]

**Table 1-6 Three main stages of weight loss of natural fibers**

Stage 1	Stage 2	Stage 3
50–100 °C: Evaporation of moisture in the fibers	200–300 °C: Decomposition of hemicelluloses	400–500 °C: Weight loss due to lignin and cellulose degradation
300 °C: Corresponds to the thermal decomposition of hemicellulose and the glycosidic links of cellulose	360 °C: Corresponds to the thermal decomposition of $\alpha$ -cellulose	200–500 °C, max at 350 °C: Lignin peak is wider and appears superposed on the other two peaks
250–300 °C: Characteristic of low molecular weight components, such as hemicelluloses	300–400 °C: Corresponds to the thermal degradation of cellulose	Near 420 °C: Due to lignin decomposition
220–315 °C: Pyrolysis of hemicelluloses	315–400 °C: Pyrolysis of cellulose	160–900 °C: Pyrolysis of lignin
97 °C: Attributed to water loss	325 °C: Attributed to protein degradation	Major thermal decomposition of the composites began at about 260 °C and beyond 390 °C the rate of decomposition was slow

### 1.5.3 Ultraviolet

Ultraviolet (UV) is another important factor which greatly influences the ageing of natural fibers reinforced composites. It can result in breaking the covalent bonds in organic polymers and fibers, thus leading to color fading, yellowing, weight loss, surface roughening and mechanical property deterioration [97].

Lignin has been reported to be the most thermally stable among the major components of plant cell walls, to protect the cellulose/hemicellulose from harsh environmental condition. It's responsible for the degradation of fibers and sensitive to UV radiation. Lignin has a phenolic structure, and acts as the binder between the microfibrils in the cell walls of the tracheid. Fig. 1-10 shows a model of lignin's partial structure, in which the two chromophoric groups A and B absorb UV light. The mechanism of lignin photodegradation is complicated, with different pathways leading to chain cleavage and yellowing. One of the main phenoxy radicals is a long life guaiacoxyl radical; it undergoes transformation into

quinoid structures which are the origin of the yellowing of the surface of the wood [98]. The surfaces of samples were observed to change in form of color fading and partial shrinkage resulting in bending of samples. This was due to, during weathering, leaching of lignin and water soluble products from the samples [89].

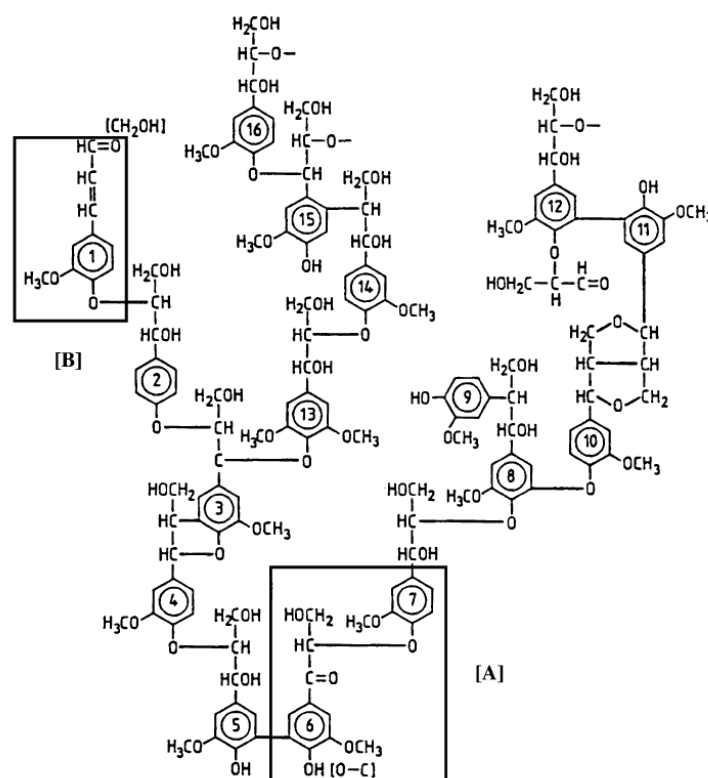


**Fig. 1-10 Model of the structure of softwood lignin showing two chromophoric groups (A and B) [98]**

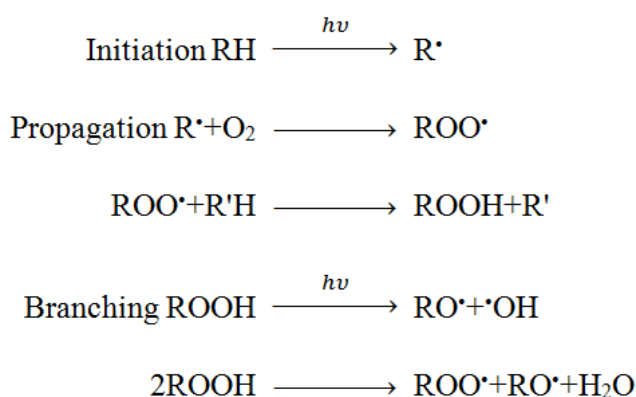


**Fig. 1-11 Oxidation reactions initiated by ultraviolet radiation [94]**

Polymers' photodegradation during irradiation for a long-time duration can

be a detriment to composites' structures and properties. Oxidative reactions induced by ultraviolet radiation are shown in Fig. 1-11 [94]. The degradation of PP is attributed to photooxidation promoted by UV irradiation. PP molecules after extensive photodegradation is shown in Fig. 1-12 [94]. Photodegradation induces changes in all scales of polymer dimension, including the monomer unit (oxidation), the chain (chain scission or crosslinking), the morphology (breakdown of tie molecules and crystal), and on the macroscopic scale.

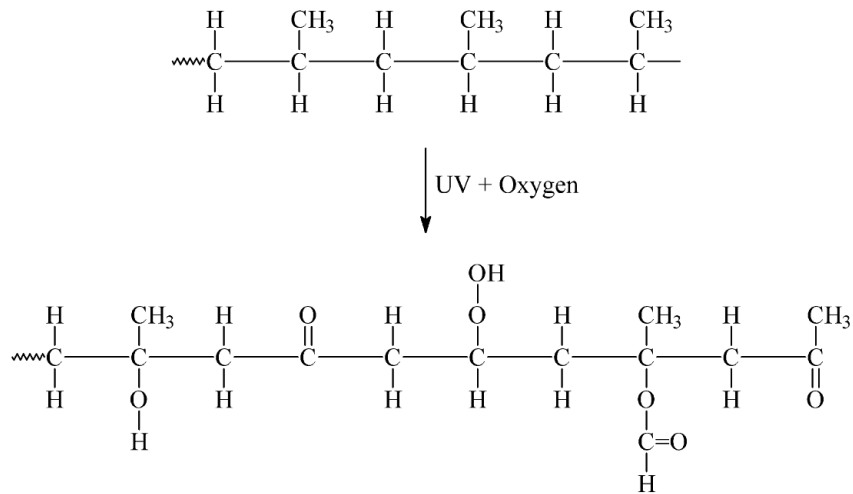


**Fig. 1-12 Schematic representation of PP molecules after extensive photodegradation [94]**

As was discussed, lignin is considered to be most responsible for UV degradation, whereas, hemicelluloses are suggested as more important for moisture and biological degradation. Cellulose is greatly contributed to strength.

## 1.6 Residual stresses in composites

In this part, the phenomenon of the emergence and the development of residual stress in composite laminates will be discussed. And the influence of residual stress on the properties of composites is of great interest as well.

In the manufacturing process of composites, thermal residual stresses emerge on account to the shrinkage and mismatch of thermal expansion coefficients between the fibers and matrices, between the plies with different orientations for

composite laminates. Since residual stresses exist in almost all composite materials, influence and even deteriorate the properties of composites, leading to the failure of a component below the design load or prior to its design service life under fatigue load [99-101]. It is of great importance to identify, determine the residual stresses and take them into consideration during composite component design and modelling.

### 1.6.1 Formation of residual stress

According to the origins of the residual stresses which occur after the processing and succeeding consolidation of the composite laminates, they can be categorized into three different levels: the micro (fiber/matrix) level, the macro (lamination) level and the global level [99, 102-105].

**On the micro-mechanical level** On the micro-scale, the disequilibrium in the thermal expansion coefficients between the fibers and matrices play an important role. The thermoplastic matrix is heated to a processing temperature above its glass transition or melting temperature, and subsequently solidified to the service or room temperature. There won't be chemical reactions occur, but the volumetric shrinkage of the thermoplastic matrix and the fiber. Due to the significantly higher shrinkage of the matrix than that of the fiber, an important driving force facilitates the formation of residual strains in the fibers and the ambient matrices [99, 106]. Under the hypothesis which fiber-matrix bonding exists during cooling, Fig. 1-13 shows the resulted residual stress distribution. A residual compressive stress in the fiber longitudinal axis as well as in the radial direction and a residual tensile stress in the matrix in the longitudinal and radial direction form and develop.

**On the macro-mechanical level** On the macro or lamination level, the lamina residual stress is present. The residual stress develops, attributed to the difference in the transverse and longitudinal ply thermal-expansion coefficients. As shown in Fig. 1-14, for example, in the cross-ply composites, the 90° fibers impose a mechanical constraint on the 0° fibers during cooling and vice versa.

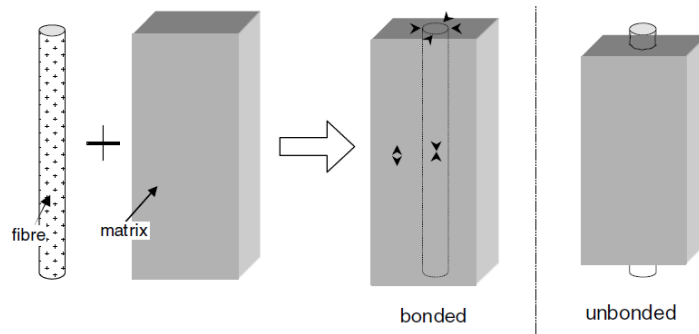


**Fig. 1-13 Schematic view of the effect of cooling on the matrix around a fibre. The bonded (constrained) case represents the situation after processing [99]**

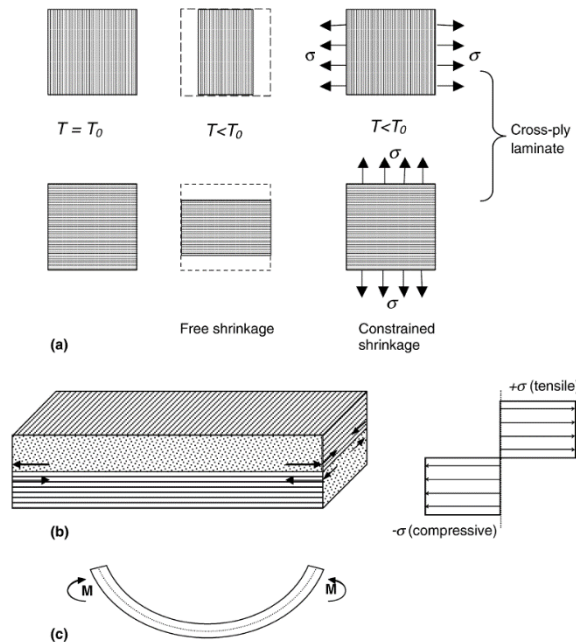


**Fig. 1-14 Schematic view of residual stress formation in unbalanced cross-ply laminate [99]**

**On the global level** On the composite scale, a gradient in cooling rate, temperature and moisture conditions throughout the thickness of the composite laminate may lead to a residual stress distribution through the whole thickness of the composite laminate. Generally, a thick-enough composite structure will suffer a slower cooling rate in the center of the structure than at the surface. In a certain time, the central part may still need to cool down, while the surfaces have already solidified. Fig. 1-15 show the result of this process.

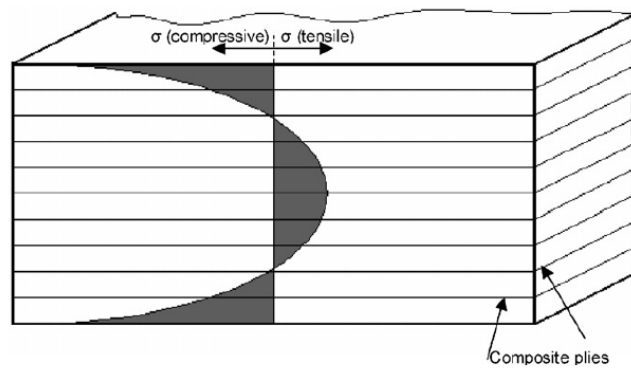


Fig. 1-15 Laminate skin-core residual stress distribution (grey area) [99]

## 1.6.2 Determination of residual stress

Since the residual stress exists in almost all composite materials and it affects the performances of the composites, it is of great significance to take it into consideration in during design and producing. Table 1-7 reviews the experimental techniques used to determine the residual stresses [107-111].

These techniques are divided into two categories: destructive techniques and non-destructive techniques. Destructive methods depend on releasing internal stresses by removing material. Releasing these stresses causes deformations in the samples, which can be measured, and compared to the deformation state before this removal step. Or otherwise, the non-destructive techniques avoid any material removal and some must use some identification of a reference of “stress free” state. Even, the components may be returned to service after the measurement and the evaluation of the residual stress.

## 1.6.3 Influence of residual stress

Because of their self-equilibrating character, the presence of residual stresses may not be apparent, but they indeed affect the properties of components. A short summary is given below on the effects of residual stresses [101, 104, 107, 112-114]:

- Environmental resistance is a matrix-dominated composite property which

may be affected by residual stresses, resulting in damage due to changes in physical and/or chemical properties of the matrix, such as  $T_g$  and toughness.

- Debonding of fiber-matrix interphase may appear.
- The mechanical properties of thermoplastic composite laminates may be decreased by thermal residual stresses.
- Defects may be generated, such as fiber waviness, warpage and transverse cracking.
- Dimensional instability or “spring-in”.

**Table 1-7 Overview of experimental techniques for residual stresses determination, percent accuracy estimates are for measurements of large stresses (~50% of yield stress), percentage numbers will be greater when measuring small stresses [107]**

Methods	Precision	Depth penetration	Advantages	Limitations
Splitting	20-50%	Specimen thickness	Routine comparative quality control	Non-uniform and untypical stresses
Layer removal	10-30%	Specimen thickness	Flat plates and cylinders of uniform thickness	Time consuming procedure subject to measurement drift
Hole drilling	5-30%	Up to 2mm typically	Near surface measurements of in-plane uniform stresses	Stresses often are not uniform, max=70% of yield
Deep hole	5-15%	Specimen thickness	Large components	Now done only by specialists and compromised by plasticity
Slitting	5-20%	Specimen thickness	1-D perpendicular stress in prismatic shaped specimens	Stresses that are non-uniform across width
XRD	~20MPa	<0.03mm	Near surface measurements on crystalline materials	Variations in grain structure and surface texture
Synchrotron diffraction	~50 MPa	>5mm	Deeper non-destructive measurements than X-ray	Requires synchrotron radiation source and 0 stress reference
Ultrasonic	>25 MPa	1-20mm	Low cost comparative	Requires material-specific calibration
Photoelastic	10-30%	Specimen thickness	Full-field measurements in transparent materials	Transparent materials, not quantitative
Indentation	Qualitative	<1mm	Comparative measurements	Results are not quantitative

## 1.7 Conclusion

As the concern about the environment, the urgency of sustainable development and consideration on the commercial profits increase, the interests in biodegradable materials are becoming more and more indispensable, especially in Europe. Among the fiber reinforced composites, the natural fibers are promising alternatives to substitute glass fibers, due to their comparable physical and mechanical performances and, the most important, environmental friendliness.

Nevertheless, it is necessary to acknowledge and overcome the drawbacks of natural fibers, such as the variations in fiber structures, compositions and properties due to the rather big variations in growing conditions. The natural hydrophilicity of natural fibers and the hydrophobicity of the polymer matrices result in bad fiber-matrix interfacial adhesions and dimensional instabilities. Although the short natural fiber (from several micrometers to dozens of millimeters) reinforced composites have attracted much attention, there are still few discussions on the continuous or woven yarns fibers. Additionally, the majority of natural fibers suffer low degradation temperatures ( $\sim 220$  °C), which is incompatible with higher processing temperatures.

Because of the hydrophilic natural fibers, moisture presence and water absorption during processing and under service environment will lead to the degradation of the composites and the durability of the composites. It is also of importance to study the durability under different humid, thermal and irradiant conditions. And the residual stresses originated from the three levels can affect the properties of the composites. Several destructive and non-destructive methods are developed to help us measure and evaluate the residual stresses in composites.



## **Chapter 2.**

# **Elaboration and Performance of the Reinforced Composites**

## Chapter 2. Elaboration and Performance of the Reinforced Composites

2.1	Introduction.....	39
2.2	Materials and Methods.....	39
2.2.1	Materials .....	39
2.2.2	Characterization methods .....	41
2.2.2.1	Numerical microscopy .....	41
2.2.2.2	Scanning electron microscopy (SEM) .....	41
2.2.2.3	Fourier transform infrared spectroscopy (FTIR) .....	41
2.2.2.4	Differential scanning calorimetry (DSC).....	41
2.3	Characterization of hemp fiber .....	41
2.3.1	Tensile tests .....	42
2.3.2	Measurement of the cross-section.....	43
2.3.3	Tensile properties .....	45
2.3.4	SEM observation.....	47
2.3.5	Spiral angle .....	49
2.4	Manufacture of reinforced composites .....	53
2.4.1	Choice of the fiber and polymer .....	54
2.4.2	Manufacturing process.....	54
2.4.2.1	Hemp preparation .....	54
2.4.2.2	Materials lay-up .....	55
2.4.2.3	Compression molding process .....	57
2.5	Properties of reinforced composites.....	57
2.5.1	Influence of temperature .....	57
2.5.1.1	Tensile properties .....	57
2.5.1.2	DSC analysis.....	59
2.5.1.3	Influence of temperature on hemp fibers .....	60
2.5.1.4	Micrographic observations .....	62
2.5.2	Influence of pressure.....	64
2.5.2.1	Tensile properties .....	64
2.5.2.2	SEM observation.....	65
2.6	Conclusion .....	67

## **2.1 Introduction**

In this chapter, the first objective is to characterize the performance of the hemp fibers and polypropylene. Secondly, the hemp fiber reinforced composites are supposed to be manufactured. At last, we want to know the mechanical behaviors of the reinforced composites.

Due to their environmental friendliness, the natural fibers have been getting more and more interests, especially as reinforcements in thermoplastic composites. Different fibers have been studied in the range: 10  $\mu\text{m}$  – 4cm in length, 1  $\mu\text{m}$  – 300  $\mu\text{m}$  in diameter [35, 61, 64, 81-85, 87, 115-121]. And thermoplastic composites have been suffering manufacturing techniques such as compounding, pultrusion, extrusion, injection and compression molding etc. During the processing of thermoplastic composites, different parameters could influence the structures and properties of final samples.

A woven hemp fabric was firstly characterized through tensile tests and SEM observations, and then the hemp fiber reinforced polypropylene composites were manufactured by compression molding method. The performances of the composites were studied. The processing parameters (processing temperatures, pressures and time and so on) which may influence the properties of the composites are of importance to be studied and discussed.

## **2.2 Materials and Methods**

### **2.2.1 Materials**

The hemp fiber fabric, “BRISON naturel”, was supplied by Enterprise Naturellement Chanvre. The weight of the hemp-fiber fabrics is 290  $\text{g}/\text{m}^2$ , and it was supplied in the dimension, 1500 mm in length. The detailed information about this kind of hemp as follows:

**Table 2-1 Information on hemp fiber fabric**

Composition	100% Hemp
Weight	290 g/m <sup>2</sup>
Width	148 cm ±3%
Origin	Culture and Fabrication Europe
Chain/Tram	10/1

The polypropylene was provided by DOW, FRANCE. The basic properties of polypropylene are shown in Table 2-2.

Fig. 2-1 shows the received state of hemp fiber fabric and polypropylene.

**Table 2-2 Basic properties of polypropylene**

Density (g/cm <sup>3</sup> )	0.91
Melt Flow Rate (230 °C/2.16kg)	3.2
Thickness (mm)	0.8
Width (mm)	1000

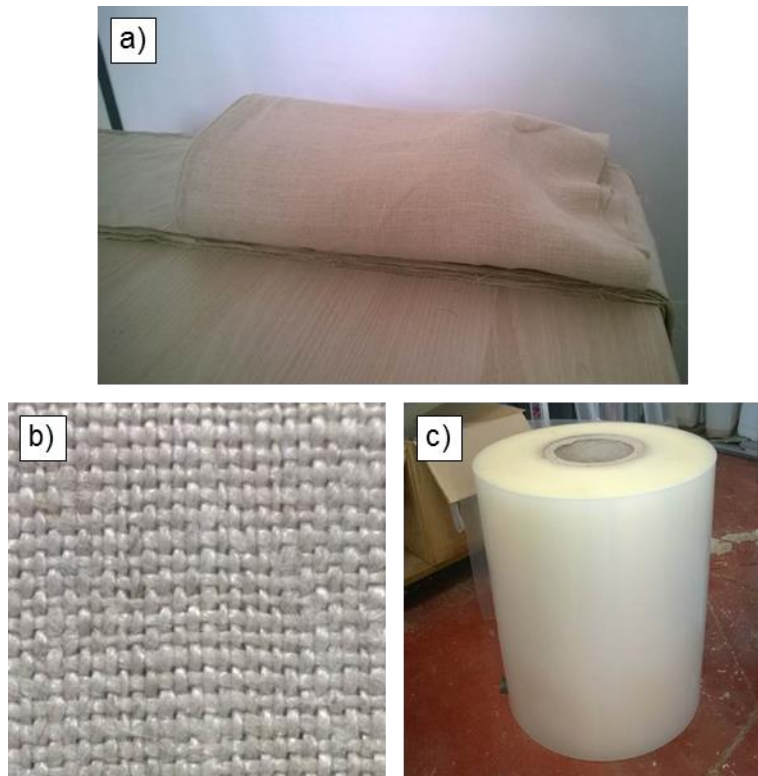


**Fig. 2-1 The received state of received (a) (b) hemp fabric and (c) polypropylene**

## **2.2.2 Characterization methods**

### **2.2.2.1 Numerical microscopy**

The hemp fiber fabric was observed under a numerical microscope, KEYENCE VHX-S15, assembled with an objective (magnification 100×~1000×). To observe the morphology and the dimension of one yarn of the hemp fiber fabric, the fibers were pulled tightly.

### **2.2.2.2 Scanning electron microscopy (SEM)**

The fiber surface morphology and the fracture topography were scanned by SEM. The hemp fibers were stuck to a paper, and coated with carbon with a SEM coater CC7650 to facilitate the electron beam incident. The composite samples were observed using a HITACHI S 3500 N or a HITACHI SU 8030 microscope.

### **2.2.2.3 Fourier transform infrared spectroscopy (FTIR)**

A Perkin-Elmer system 2000 FTIR Spectrometer Two was used with an Universal Attenuated Total Reflectance Accessory (UATR) to gather the IR spectra of the samples. The measurements were performed at the range 400 – 4000 cm<sup>-1</sup>.

### **2.2.2.4 Differential scanning calorimetry (DSC)**

Differential scanning calorimetry (DSC 131 EVO analyzer) was used for the thermal analysis of the hemp fibers and polypropylene. The samples were placed in hermetic 10 mg aluminum crucibles. During analysis, approximate 20 mg of samples were heated from Room Temperature to about 600 °C at a heating rate of 10 °C/min and then cooled down.

## **2.3 Characterization of hemp fiber**

It was necessary to recognize the properties and the performances of the as-received hemp fibers, so the tensile test was firstly realized. The objective of this

step is to determine the longitudinal and transversal resistance of the hemp fiber fabric.

### 2.3.1 Tensile tests

The tensile tests were performed in a static tension machine Instron 4484 at room temperature. The tensile test was based on the standard test method ASTM D 3039/D 3039M – 08 (ASTM\_International 2008). The samples were cut into rectangular strips, as shown in Fig. 2-2. Tensile tests were employed in the two directions, longitudinal and transversal. The samples were dried before the tests. The configurations of tensile tests are listed below:

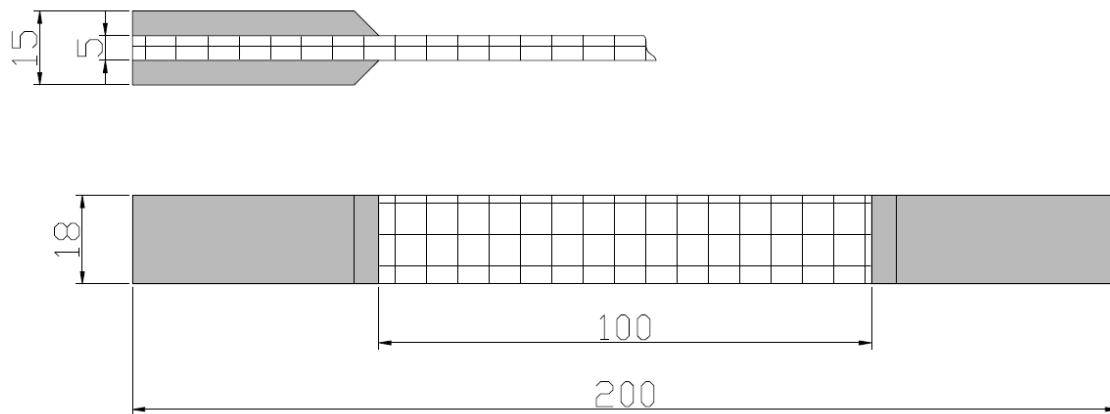


**Fig. 2-2 Dimensions and shape of the test samples**

Materials: hemp fiber fabrics;

Dimensions: 200 mm × 18 mm × 0.4 mm;

Speed of testing: 2 mm/min;

Temperature: Room Temperature;

Extensometer: an initial opening length of 12.5 mm;

Tab: tabs were attached to both ends, two-sides of the samples with specific glue.

Fig. 2-3 shows the typical force-displacement curve of the hemp fabric samples. From this figure, three main parts were marked, OA, AB, BC. At OA stage, the slope of the curve increased slowly at the beginning and faster later. Between AB, the force and displacement presented a linear relationship, and the force reached to an extremum. After B, the force fell at a high speed, until C, which meant to be fracture of the samples.

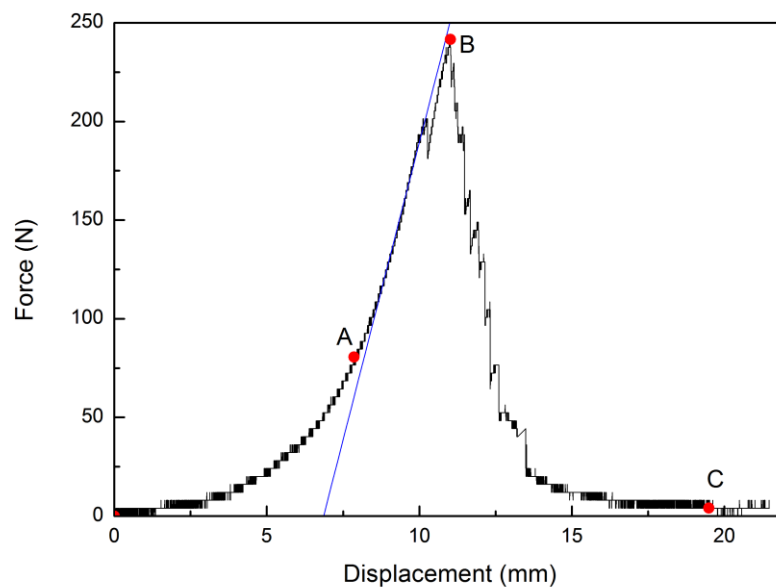
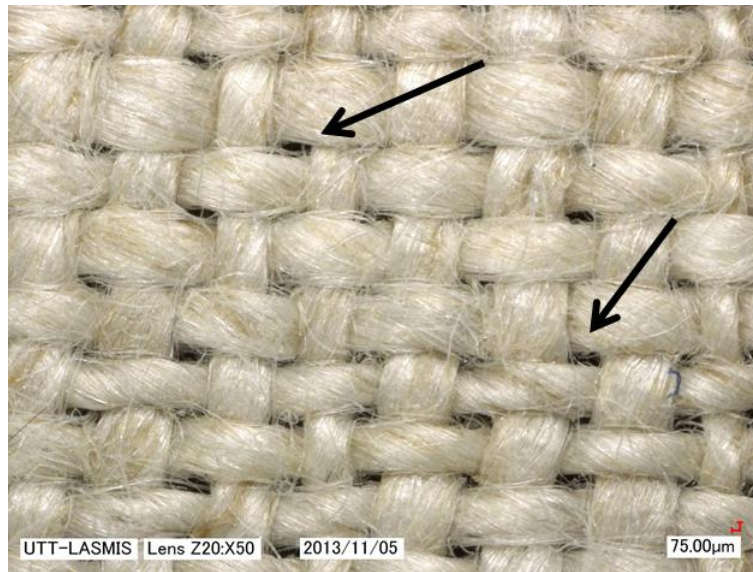


Fig. 2-3 The typical curve of the hemp fabric samples

### 2.3.2 Measurement of the cross-section

The hemp fiber fabrics were woven with hemp fiber yarns, as shown in Fig. 2-4, and there were gaps between the yarns. So the real force-bearing section should be measured by eliminating the gaps between the yarns in the two directions, longitudinal and transversal.



**Fig. 2-4 Gaps between hemp yarns**



**Fig. 2-5 Measurement of the width of the force-bearing hemp**

Three batches of samples with 10, 20 and 30 yarns were prepared. The width of every hemp yarn was measured through numerical microscope and Vernier Caliper respectively. For every sample, more than one hundred of values were obtained, and the average values were calculated. The width of every yarn was measured via numerical microscope (as shown in Fig. 2-5), and remeasured by Vernier Caliper. The comparison between the width measured by numerical microscope and that measured by Vernier Caliper was shown in Fig. 2-6. A

proportional relationship between the two kinds of dimensions was found,

$$W_r = W_{NM} = \alpha \cdot W_{VC} \quad (2-1)$$

where,  $W_r$  is the real width which support the force;  $W_{NM}$  and  $W_{VC}$  were the widths measured by numerical microscope and Vernier Caliper, respectively;  $\alpha$  is the proportional coefficient. It means that we could get the width from this formula:  $\alpha = \frac{W_{NM}}{W_{VC}} = 0.626$ .

To verify this relationship, another 3 batches (8, 18 and 32 yarns) of samples were re-prepared. The experimental results and the measured results showed a good and reliable fitness, as shown in Fig. 2-7. This appropriate coefficient will make the measurements timesaving and easy-to-use.

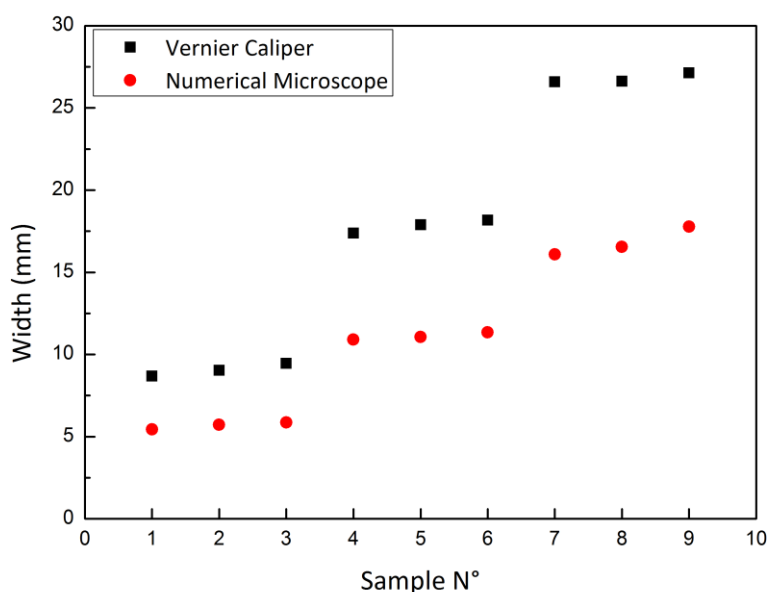


Fig. 2-6 Widths measured by numerical microscope and Vernier Caliper

### 2.3.3 Tensile properties

Five samples were tested for each batch, and an average value was calculated. Each hemp sample was considered as a rectangular section, and the ultimate strength was calculated from the maximal tensile force divided by the initial cross-

section.

$$\sigma_m(MPa) = \frac{F_m(N)}{S_0(mm^2)} = \frac{F_m(N)}{bc(mm^2)} \quad (2-2)$$

where  $F_m$  is the maximal tensile force and  $S_0$  is the initial cross-section,  $b$  is the width and  $c$  is the thickness of the sample.

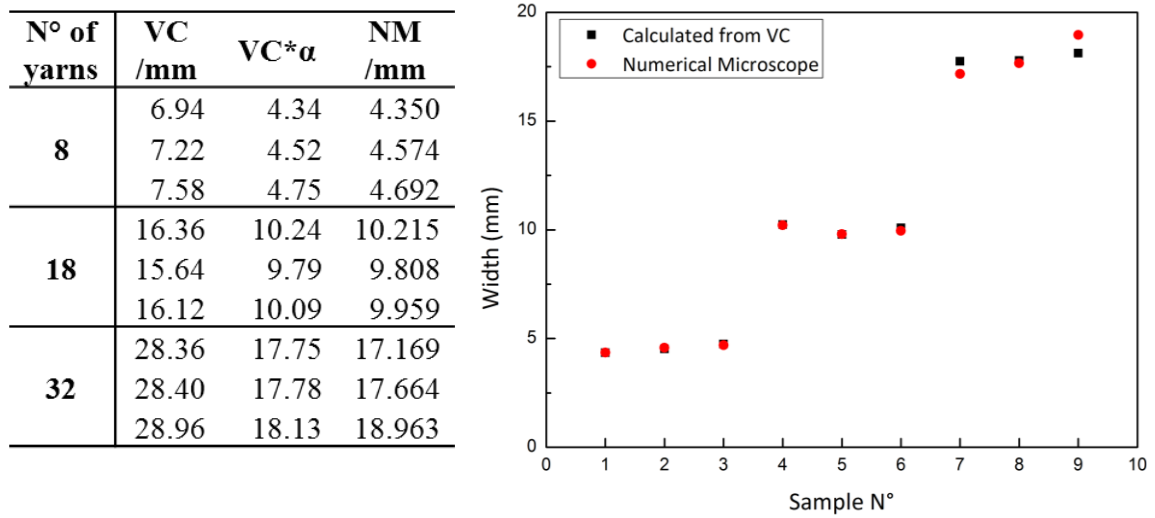


**Fig. 2-7 Verification of the relationship coefficient between numerical microscope and Vernier Caliper**

The strain was computed by the ration of elongation  $\Delta L$  to initial length  $L_0$ , as follows,

$$\varepsilon(\%) = \frac{\Delta L(mm)}{L_0(mm)} \times 100\% \quad (2-3)$$

The Young's modulus  $E$  could be calculated from the linear part of the stress-strain curve (like the linear part between A and B in Fig. 2-3),

$$E(GPa) = \frac{\sigma_m(MPa)}{\varepsilon \times 1000} \quad (2-4)$$

From the stress-strain curve, the tensile properties of the hemp fabric were figured out in the longitudinal and transversal directions. Fig. 2-8 shows the

mechanical properties of the hemp fabric in the two perpendicular directions. Although they were derived from the same fabric, but their mechanical properties show some difference. The tensile strength in the longitudinal direction is  $165.89 \pm 8.22$  MPa, which is 63.8% higher than that in the transversal direction. The Young's modulus in the two perpendicular directions approximate with each other,  $4.86 \pm 0.32$  GPa longitudinal, and  $4.78 \pm 0.59$  GPa transversal respectively. In contrast, however, the fracture strain of hemp fiber in longitudinal direction is  $11.35 \pm 0.68\%$ . But it shows a higher strain in the transversal direction.

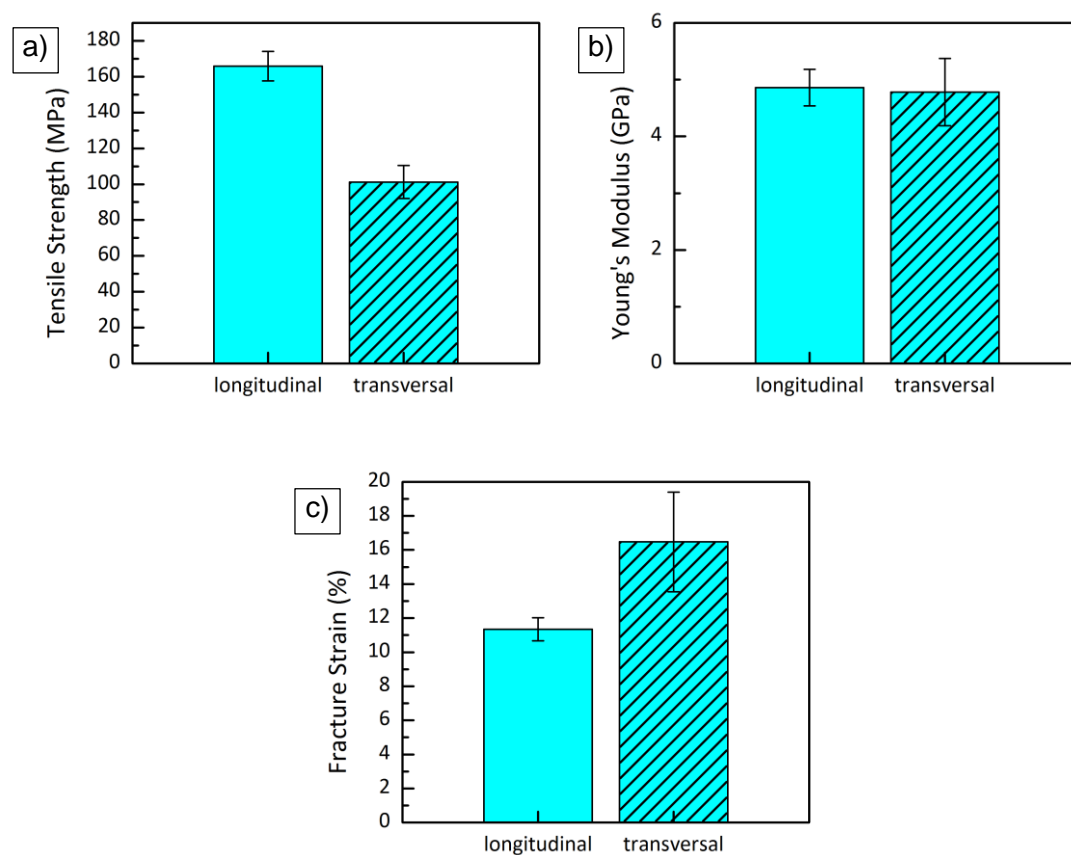


**Fig. 2-8 Mechanical properties of hemp fabric, a) Tensile Strength; b) Young's Modulus; c) Fracture Strain.**

### 2.3.4 SEM observation

From the micro scale, the hemp fibers were observed through SEM. The morphology of the untested and tested hemp fibers were analyzed, as shown in

Fig. 2-9.

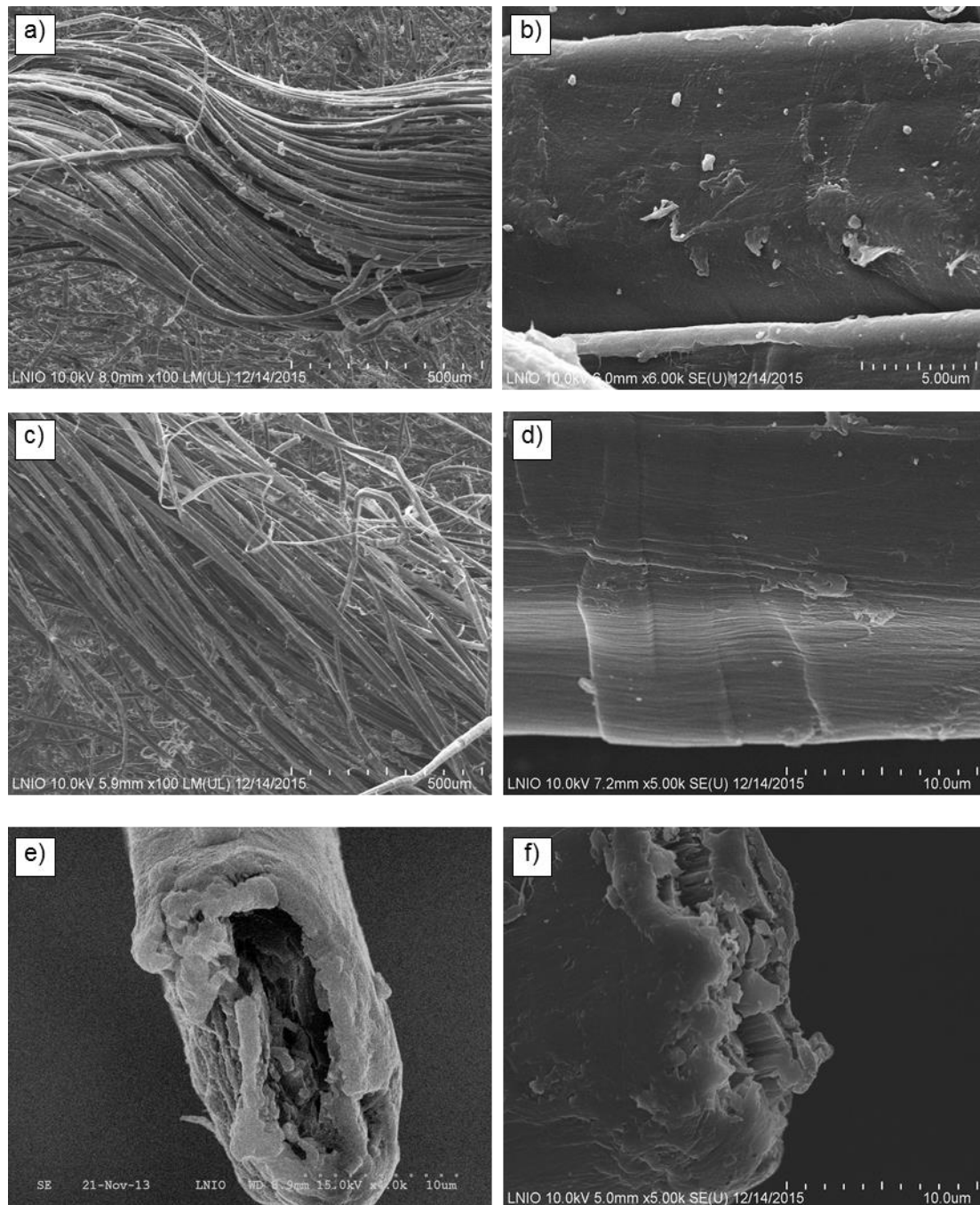


**Fig. 2-9 SEM micrographs of the hemp fibers. a) and b) hemp fiber untested; c), d), e) and f) hemp fibers tested.**

The hemp fibers untested present a curved outline, and they were found to be twisted together. From Fig. 2-9 a) and b), the surface of the untested fiber is covered a layer of rough substances. Small branches were found on the surface of the fibers. According to the cellulosic fiber's structure, some lignin and hemicellulose

(amorphous regions of cellulosic microfibrils) are connected with the cellulose (crystalline regions of cellulosic microfibrils). After tensile tests, the fibers were much aligned along the fibers direction than the untested ones. The surface of the tested fibers was less rough than the untested fibers. From Fig. 2-9 e) and f), a hollow lumen was observed at the center, as presented in Fig. 1-1. And the aligned crystalline celluloses are surrounded by the amorphous hemicellulose and the lignin.

### 2.3.5 Spiral angle

To explain the difference of mechanical properties between the two perpendicular directions, complementary experiments, tests and observations need to be realized. While being observed, a bundle of hemp fibers was found to be twisted together. Before tensile tests, a certain angle in each bundle was observed (Fig. 2-10). We thought that it may have an influence on the mechanical properties of the hemp fibers. So the alteration of the spiral angle was measured and analyzed.



**Fig. 2-10 The spiral angle presents in the hemp yarns**

As the width or diameter of the hemp yarns was different from each other in one sample, more than one hundred points were collected to ensure a stable value. The spiral angle of the hemp yarns before and after tensile tests was measured in

both longitudinal and transversal directions. In Fig. 2-11, the measuring method via numerical microscope was presented.

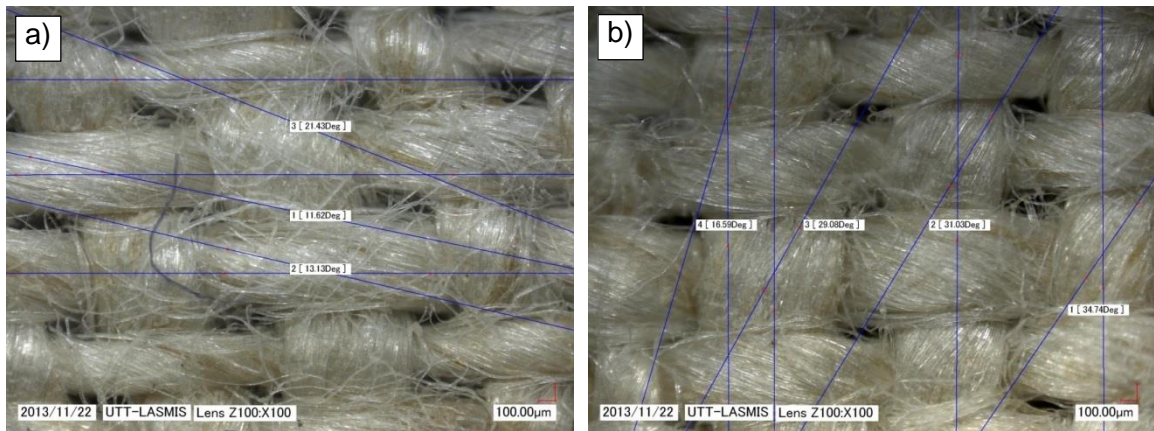


**Fig. 2-11 Measurement of the spiral angle, a) Longitudinal direction; b) Transversal direction.**

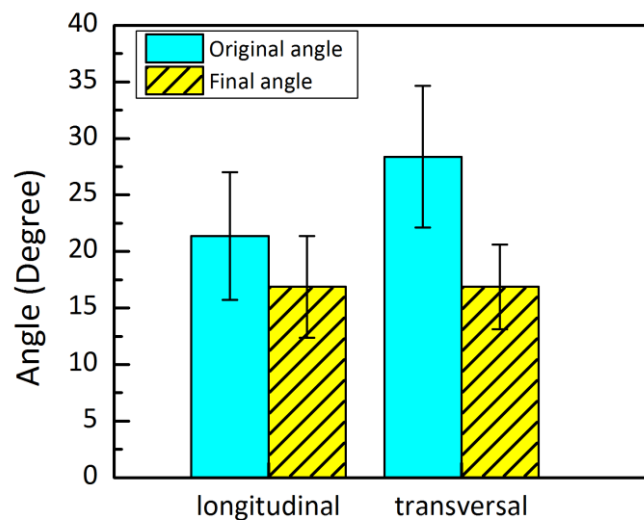


**Fig. 2-12 Spiral angle alteration**

From Fig. 2-12, the alteration of the spiral angle in both longitudinal and transversal directions was presented. The spiral angles decreased after tensile tests for both directions. The spiral angle of the transversal hemp yarns was  $28.37^{\circ} \pm 6.27^{\circ}$ , while that of the longitudinal direction was 24.7% lower,  $21.36^{\circ} \pm 5.65^{\circ}$ .

But, the final spiral angle after the tensile test show quasi-equal values. During the tensile test process, the spiral angle suffered a decrease of 20% and

40%, in longitudinal and transversal directions, respectively.

As for plant fibers, made up with cellulose and hemicellulose, characterize the structure of cellulose oriented in helix, following a microfibril angle. It was also stated in Literature [50], Fig. 2-13. Generally, the reinforcement percentage and the orientation of the fibers determine the elastic and fracture characteristics. As reported, the microfibril angle of hemp and flax is about  $6.2^\circ$  and  $10^\circ$  respectively.

According to literature [122], the variation mechanism of flax fiber was discussed. The global deformation (Fig. 2-14) is:

$$\varepsilon = \ln \left( 1 + \frac{\Delta L}{L_0} \right) = -\ln(\cos \alpha) \quad (2-5)$$

For a deformation of  $1.4\% \pm 0.7\%$ , the derived angle  $\alpha$  is  $9.4^\circ \pm 2.4^\circ$ . This microfibril angle corresponds with that of the flax. So for the hemp fiber with a microfibril angle of  $6.2^\circ$ , the estimated strain is about 0.59.

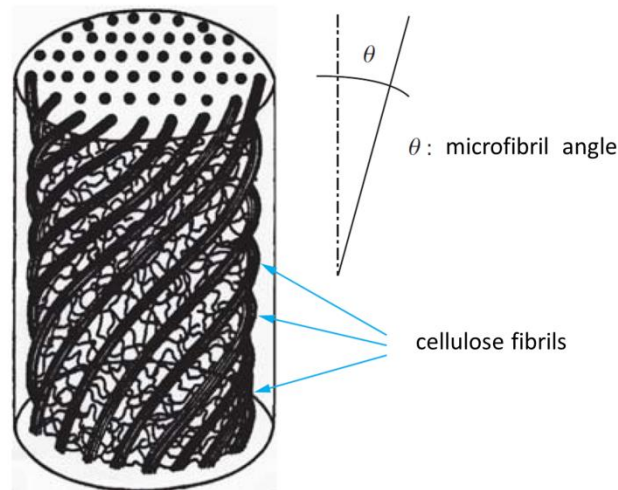


**Fig. 2-13 Basic diagram of the structure of a plant fiber [50]**

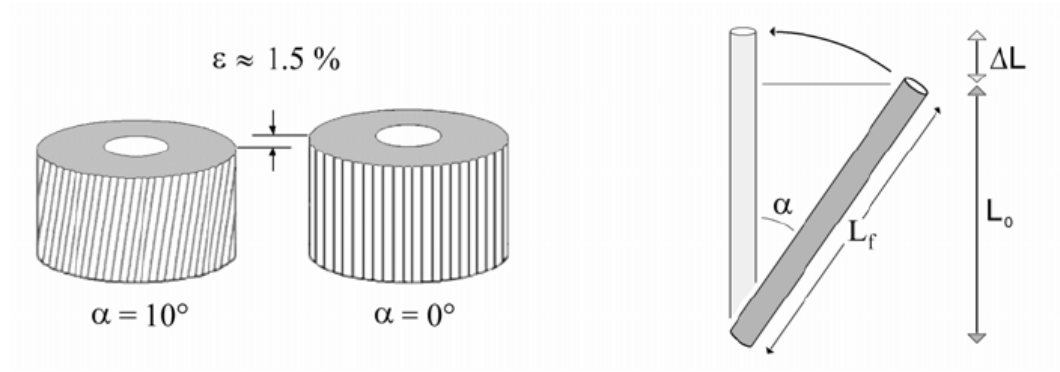


**Fig. 2-14 Simple representation of the reorientation of the microfibrils [122]**

The strain difference between the two directions of hemp may be concerned with the spiral angle of the hemp yarns, as shown in Fig. 2-15. Assign  $L_0$  to be the initial length of the samples with a fiber orientation of an initial angle  $\alpha_1$ , and make  $L_f$  be the final length of the samples with a reduced angle  $\alpha_2$ . We hypothesize that the rearrangement process of fiber yarns is limited to the elastic deformation stage, and that the strain due to the hemp microfibril angle can be neglected. The real length of one hemp yarn without angle  $L$ :

$$L = \frac{L_0}{\cos \alpha_1} = \frac{L_f}{\cos \alpha_2} \quad (2-6)$$

The strain of the reorientation of the samples  $\varepsilon$ :

$$\varepsilon = \frac{\Delta L}{L_0} = \left( \frac{\cos \alpha_2}{\cos \alpha_1} - 1 \right) \times 100\% \quad (2-7)$$

The longitudinal reorientation  $\varepsilon_{LR} = 2.76\%$ ;

The transversal reorientation  $\varepsilon_{TR} = 8.75\%$ .

The strain difference due to the hemp yarn reorientation is 5.99%, and this correspond with the fracture strain difference 5.12%. So the main reason of the fracture strain difference is attributed to the different spiral angle of the hemp yarns.

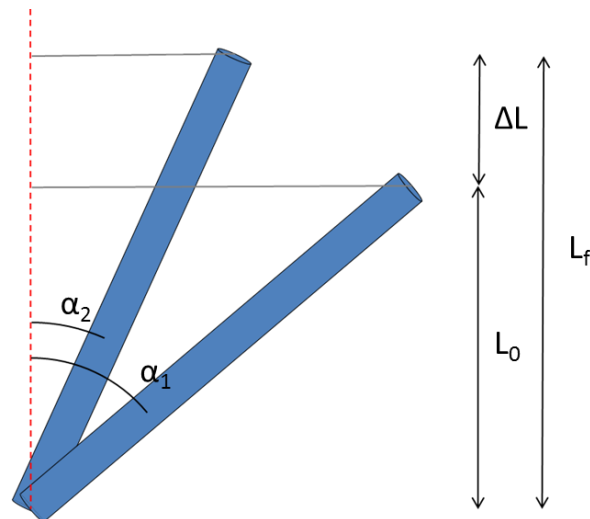


Fig. 2-15 Basic diagram of the reorientation of the hemp yarns

## 2.4 Manufacture of reinforced composites

In this part, the objective is to manufacture the composites laminates based on hemp fibers through compression moulding. Before the manufacturing process was finally determined, several attempts had been tried. Granules, strips and sheets have been used to manufacture the composite; the resulted composites are presented in Fig. 2-16. As can be seen, all of the three composites can form a complete sheet, but composites made from hemp fiber, PP granules (or strips) show poor penetration and poor mixture. There are some locations where the hemp fibers are exposed. Whereas the composites made from PP sheets and hemp fibers present a better formability.

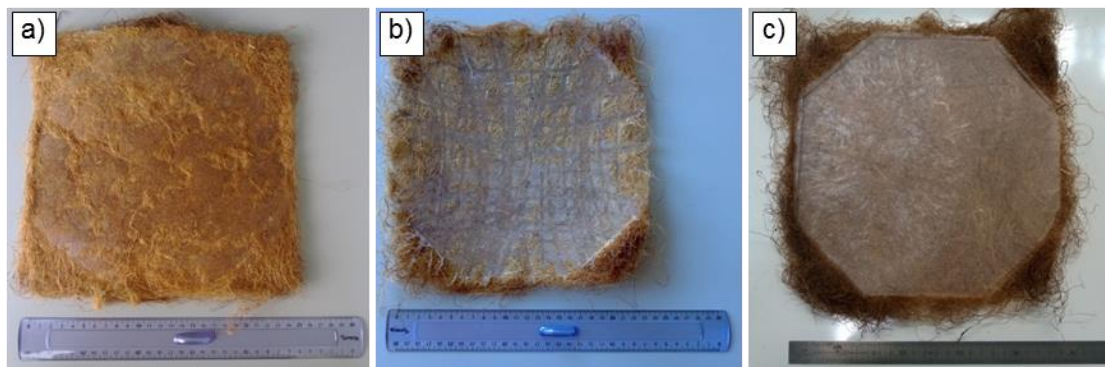


Fig. 2-16 Composites manufactured with different PP forms. a) PP granules, b) PP strips, c) PP sheets.

## **2.4.2 Choice of the fiber and polymer**

Throughout the process above, the PP form affects the formability and the completeness of the final composites. Prefabricated PP films could facilitate the composite manufacturing process. So we firstly chose PP films as a raw material of this thesis.

Secondly, woven fabrics of hemp yarns were utilized as the reinforcements of the composites. A hemp fiber is in the range of 5-55 mm in length and 10-51  $\mu\text{m}$  in diameter [123, 124], and hemp fibers are twisted together to make up a hemp yarn, which are woven at last to form a fabric.

## **2.4.3 Manufacturing process**

The main procedures of the manufacture of the composites as follows:

- (1) Preheat the hemp fibers to eliminate the moisture containing in the fibers, reducing the influence of the moisture as less as possible;
- (2) Assembly of the molds and the raw materials, where the hemp fibers and the PP films were laid up with a prescribed proportion;
- (3) Continuously heat the molds in an oven via a pre-programmed way;
- (4) Realize the compression molding process;
- (5) Cool down the molds and demold.

### **2.4.3.1 Hemp preparation**

As the plant fibers contain hydrophilic hydroxyl groups and polar groups, the plant fibers would absorb moisture in the normal environment. So it is of importance to eliminate the stubborn moisture in the fibers.

Different hemp samples were prepared and heated at a certain temperature. And a Sartorius MA150 Moisture Analyzer was used to analyze the moisture loss.

A weight index was calculated to characterize the moisture content in the hemp fibers:

$$\text{Weight Index} = M_1/M_0 \quad (2-8)$$

where  $M_0$  is the weight before heating, and  $M_1$  is the fiber weight after a certain heating time. Fig. 2-17 shows the weight index of different temperatures.

As presented in Fig. 2-17, hemp fibers have the same moisture content ratios at different temperatures and the weight of the samples tend to be stable after a certain time. So the first step was to prepare the hemp fibers by heating them for 20 minutes in an oven at 160 °.

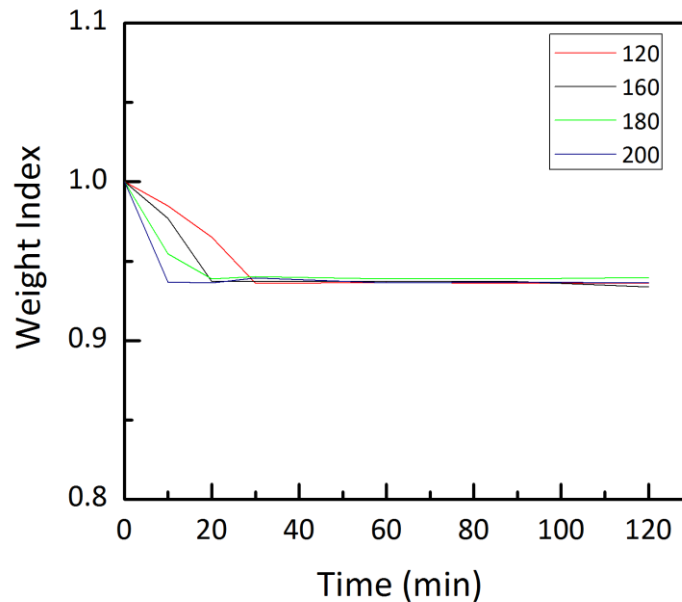


Fig. 2-17 Weight change of hemp when heated at a temperature

#### 2.4.3.2 Materials lay-up

In this study, we utilized the volume fraction  $V_f$  expressed in % other than the mass fraction  $W_f$ . The relation between  $V_f$  and  $W_f$  is expressed as following:

$$V_f = \frac{M_f/\rho_f}{M_f/\rho_f + M_m/\rho_m} \quad (2-9)$$

and

$$M_f = \frac{V_f \cdot \rho_f}{V_f \cdot \rho_f + V_m \cdot \rho_m} \quad (2-10)$$

$M_m + M_f = 1$ , where  $M_m$  and  $M_f$  are the mass fraction of matrix and fiber, respectively,

$V_m + V_f = 1$ , where  $V_m$  and  $M_f$  are the volume fraction of matrix and fiber, respectively,

$\rho_m$  and  $\rho_f$  are the density of matrix and fiber, respectively.

The hemp fibers and polypropylene films were cut into  $200 \times 200$  mm squares. The dimensions were determined by the molds, as shown in Fig. 2-18. The materials were laid up one layer after another to form a laminate.

A mold release agent was sprayed onto the surface of the mold cavity. Then the laminate was placed into the molds.

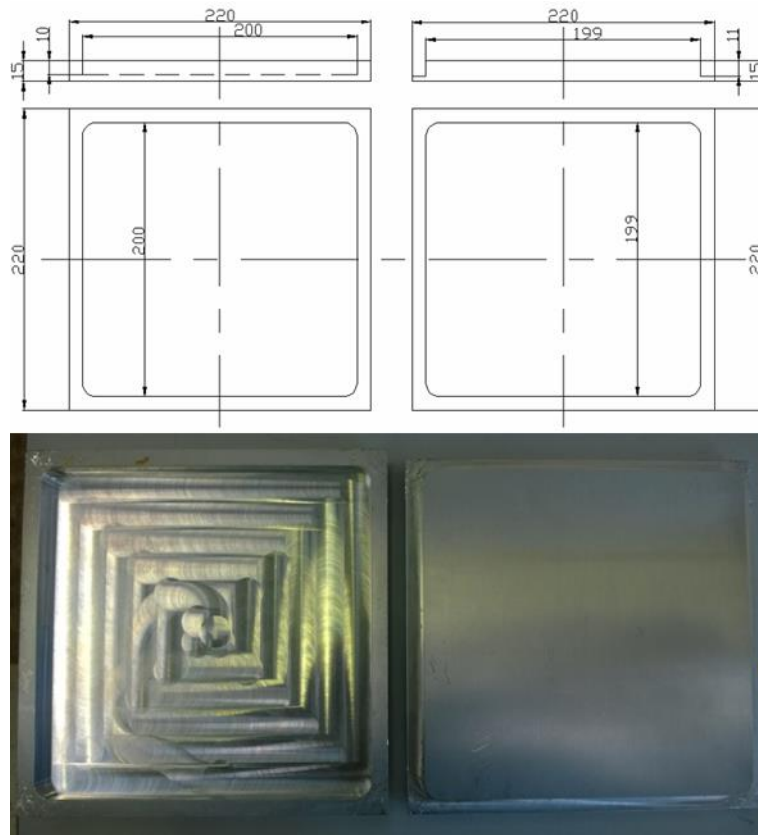


**Fig. 2-18** The diagram of the moulds

### **2.4.3.3 Compression molding process**

The laminates were heated in an oven via different parameters. The compression molding machine was also launched to get the scheduled temperature. After a scheduled time, the molds were transported immediately in the compression molding machine to apply the compression molding. All the parameters used during this procedure are as follows:

1. The laminates were heated up to  $X$  °C in 30 minutes; preserve the temperature  $X$  °C in 120 minutes.
2. Compression mold under  $Y$  MPa during  $Z$  minutes;
3. Cool down and demould after a certain time.

## **2.5 Properties of reinforced composites**

The mechanical properties of hemp reinforced polypropylene composites were characterized through different methods. The mechanical properties show an attraction to us. The influence of different parameters on the mechanical properties was discussed in this section.

### **2.5.1 Influence of temperature**

Firstly, the influence of temperature on the performances of the composites was discussed. The formula discussed in section 2.4.3.3 was specified as  $X=160, 170, 180, 190, 200$  °C;  $Y=0.4$  MPa;  $Z=10$ . The samples were cooled down at ambient temperature. The mass fraction of hemp in composites  $V_m=28.76\%$ , and the calculated volume fraction  $V_f=19.70\%$ .

#### **2.5.1.1 Tensile properties**

After the compression molding, a tensile test was accomplished. An extensometer of 12.5 mm initial opening length was mounted at the center of

composites samples. For each kind of composites, five samples were tested. Fig. 2-19 shows the mechanical properties of hemp reinforced polypropylene composites.

We can see that in Fig. 2-19 a), the tensile properties of the composites were higher than the pure polypropylene samples, and much lower than that of hemp fibers. As the temperature increased, the tensile strength of the composites tended to decrease. The tensile strength decreased from 43.34 MPa to 35.00 MPa, except at 190 °C where there was a rise. The Young's modulus of the composites was slightly enhanced from 1.70 GPa to 1.88 GPa as the temperature increased from 160 °C to 190 °C, except the samples where there was a reduction of 11.6 % at 200 °C (Fig. 2-19 b)). It showed that the compression temperature influenced the properties of the composites. The fracture strain of the composites presented the same trend as the case of the tensile strength (Fig. 2-19 c)).

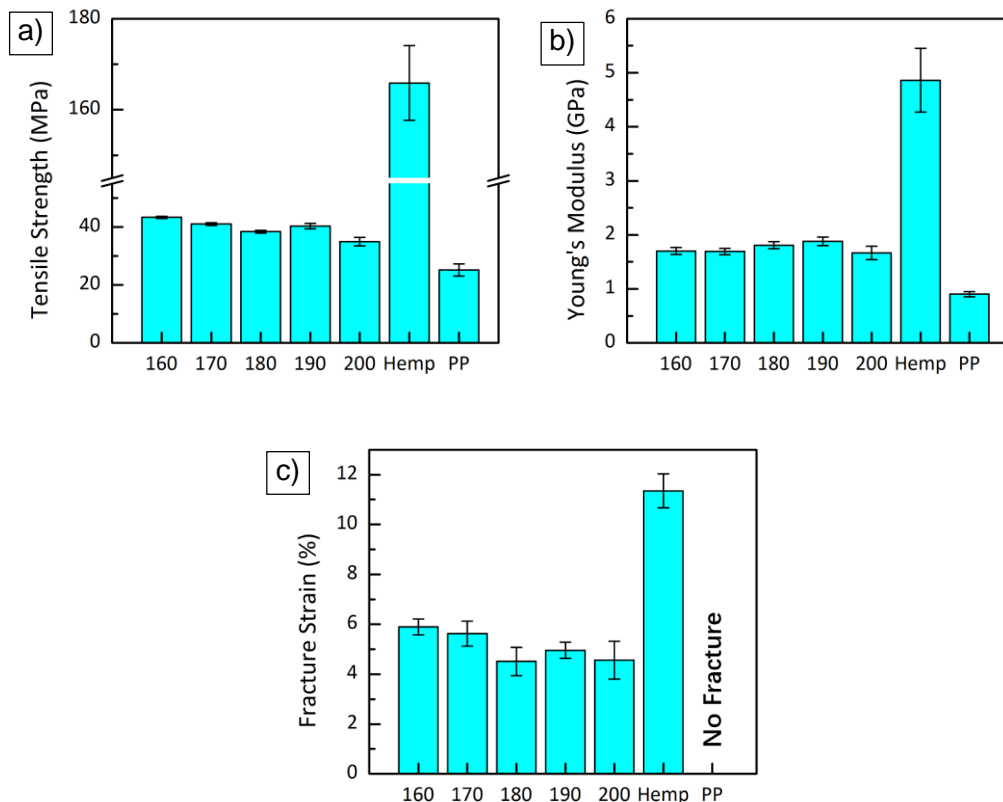


**Fig. 2-19 Mechanical properties of PP/hemp composites: a) Tensile Strength; b) Young's Modulus; c) Fracture Strain.**

The tensile properties of the composites at 190 °C are higher than the other counterparts, although the tensile strength and the fracture strain of the composites at 190 °C are slightly lower than that of 160 °C. So it is possible to elevate the tensile properties of the PP/hemp composites by improving the manufacturing temperature.

To analyze the difference among the samples, extra experiments and analyses need to be carried out.

### 2.5.1.2 DSC analysis

Thermal analysis can be performed to evaluate the thermal stability and determine the moisture content and volatile substances in composites [125-127]. And it also enables the identification of chemical activity occurring in the fibers as the temperature increases. The degradation temperatures of hemicellulose, cellulose and lignin are 200-320 °C, 300-400 °C and 150->500 °C, respectively [128].

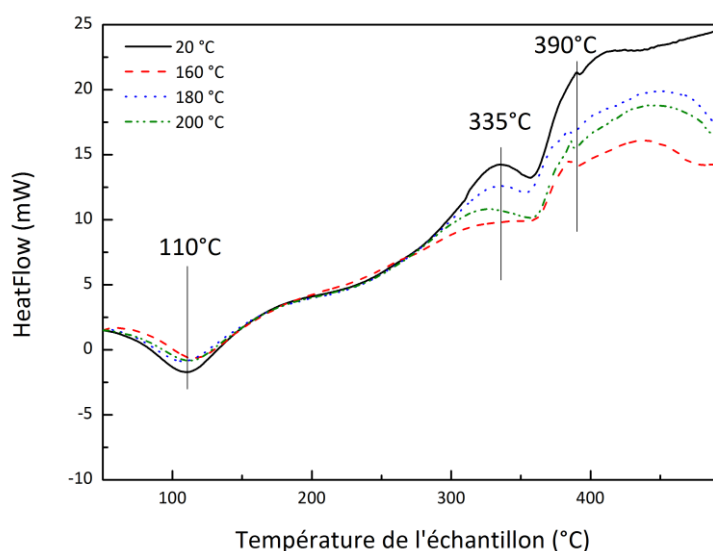


**Fig. 2-20 DSC thermograms of hemp fibers**

Differential thermal analysis curves of the hemp fibers are shown in Fig. 2-20. A broad endothermic peak observed in the range of 50 - 175 °C in all of the

samples indicates the presence of water molecules and volatile components in the fibers. There are two or three exothermic peaks observed in the DSC thermograms. Akita and Kase [127] have reported that for natural fibers, lignin degrades at the temperature around 200 °C while the other constituents such as cellulose and hemicellulose degrade at higher temperatures. The region between 150 and 260 °C shows no endothermic and exothermic peaks, which indicates that the fibers are stable between these temperatures. Therefore the exothermic peaks in Fig. 2-20 correspond to the decomposition of lignin, hemicellulose and cellulose of the fibers. Between these temperatures 150 - 260 °C, a gradual degradation occurs which includes depolymerisation, hydrolysis, oxidation, dehydration and decarboxylation [125].

The heat-treated hemp fibers present lower exothermic peaks than the first untreated fibers at 335 °C, and the second at 390 °C. From the exothermic peaks, it can be concluded that the hemp fibers were changed after heated. S.H. Aziz et al. [125] reported a decrease in the decomposition temperature of the untreated plant fibers, which indicates thermally less stable.

### **2.5.1.3 Influence of temperature on hemp fibers**

To verify the influence of temperature on the hemp fibers, tensile tested were firstly performed. The hemp fibers were heated in an oven under different temperatures and a certain time, then a comparison of their appearance and the mechanical properties.

Hemp fibers were treated in an oven in 120 minutes and at different temperatures, 160 °C, 180 °C, 200 °C, 220 °C, 240 °C, 260 °C and 280 °C. they were compared with the untreated fibers, in Fig. 2-21. As can be seen, the fibers treated at 160 °C, 180 °C and 200 °C present almost the same color as the untreated fibers. Nevertheless, the color of samples treated over 200 °C show a dark-brown appearance. As the temperature increases from 220 °C to 260 °C, the color gets darker and darker. Finally, the hemp fibers becomes carbonized when treated at 280 °C, it shows a totally dark color from the outer surface.

This corresponds to the DSC analysis, from 200 °C, a gradual degradation occurs which includes depolymerisation, hydrolysis, oxidation, dehydration and decarboxylation.

Fig. 2-22 shows the tensile properties of the untreated and heat-treated hemp fibers. The tensile strengths of the treated hemp fibers show a reducing trend, and are lower than the untreated of the untreated fibers. Before 200 °C, the tensile strength of the hemp fibers decline gradually. However, the hemp fibers treated at 220 °C shows a sudden fall than that at 200 °C. After 200 °C, the tensile strength of the fibers decreases markedly until at 280 °C, it vanishes. The Young's moduli of the hemp fibers present a similar characterization with regard to the tensile strength. But, from 160 °C to 200 °C, the Young's modulus shows a slightly increase. This can be an explanation for the same phenomenon of the composites in section 2.5.1.1. As for the fracture strain, it firstly increases as the temperature improves. Then, it decreases, as the temperature elevates continuously. An obvious reduction appears and a zero property at 280 °C.

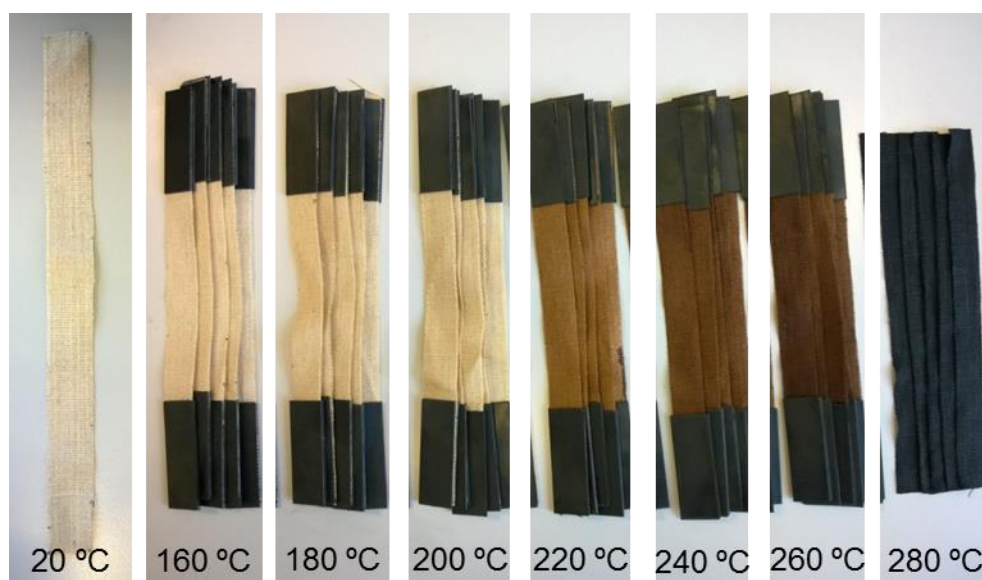


**Fig. 2-21**Color comparison of hemp fibers after treated under different temperatures

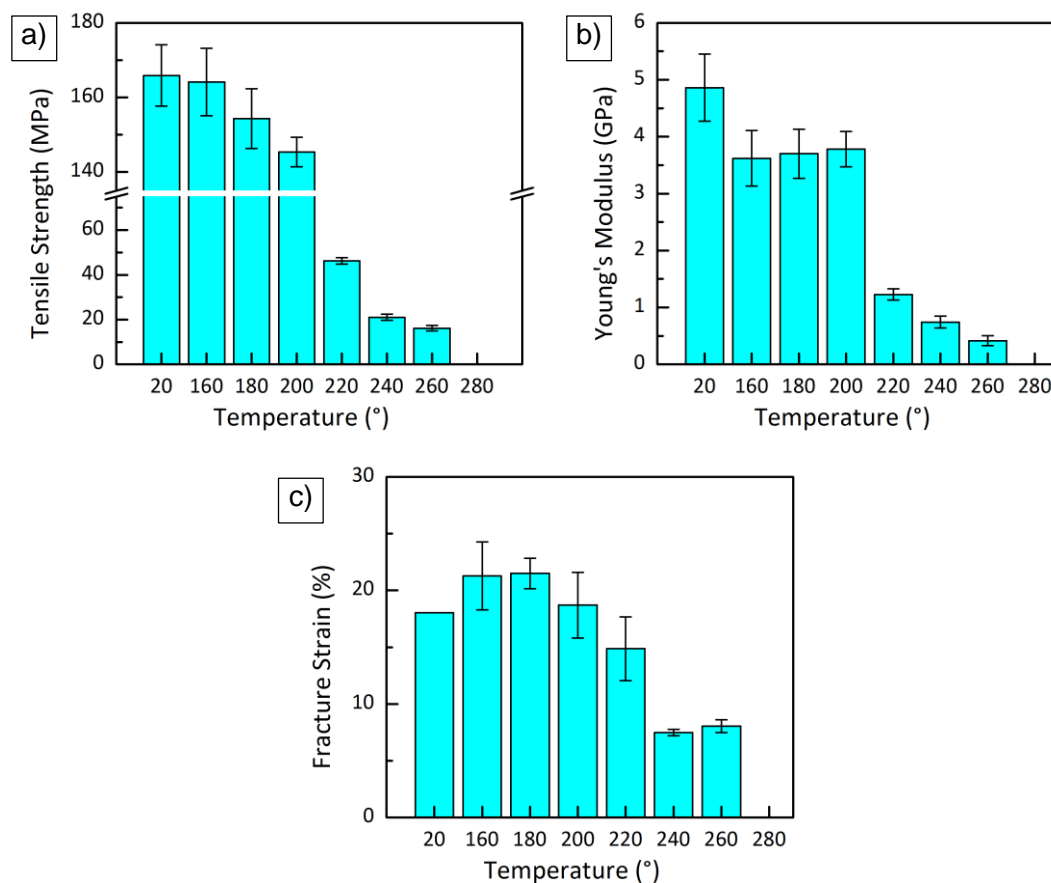


**Fig. 2-22 mechanical properties of hemp fibers treated under different temperatures. a) Tensile Strength, b) Young's Modulus, c) Fracture Strain.**

#### 2.5.1.4 Micrographic observations

From the micro scale, the hemp fibers were observed through SEM. The morphology of the untreated and treated hemp fibers were analyzed, as shown in Fig. 2-23.

Fig. 2-23 presents the morphology by SEM of the hemp fabrics non-treated, and heated at 160 °C, 180 °C, 200 °C, 220 °C, 240 °C. Hemp fiber is mainly composed of cellulose (67.0-78.3 w.t. %), hemicelluloses (5.5-16.1 w.t. %), lignin (2.9-3.3 w.t. %) and pectin (0.8-2.5 w.t. %) [21]. Compared with the non-treated hemp (Fig. 2-23 a)), there was not much difference of the hemp at 160 °C from that of the non-treated hemp. From 180 °C, differences began to be presented. At 180 °C (Fig. 2-23 c)), there occurred some thin branches on the surface of the

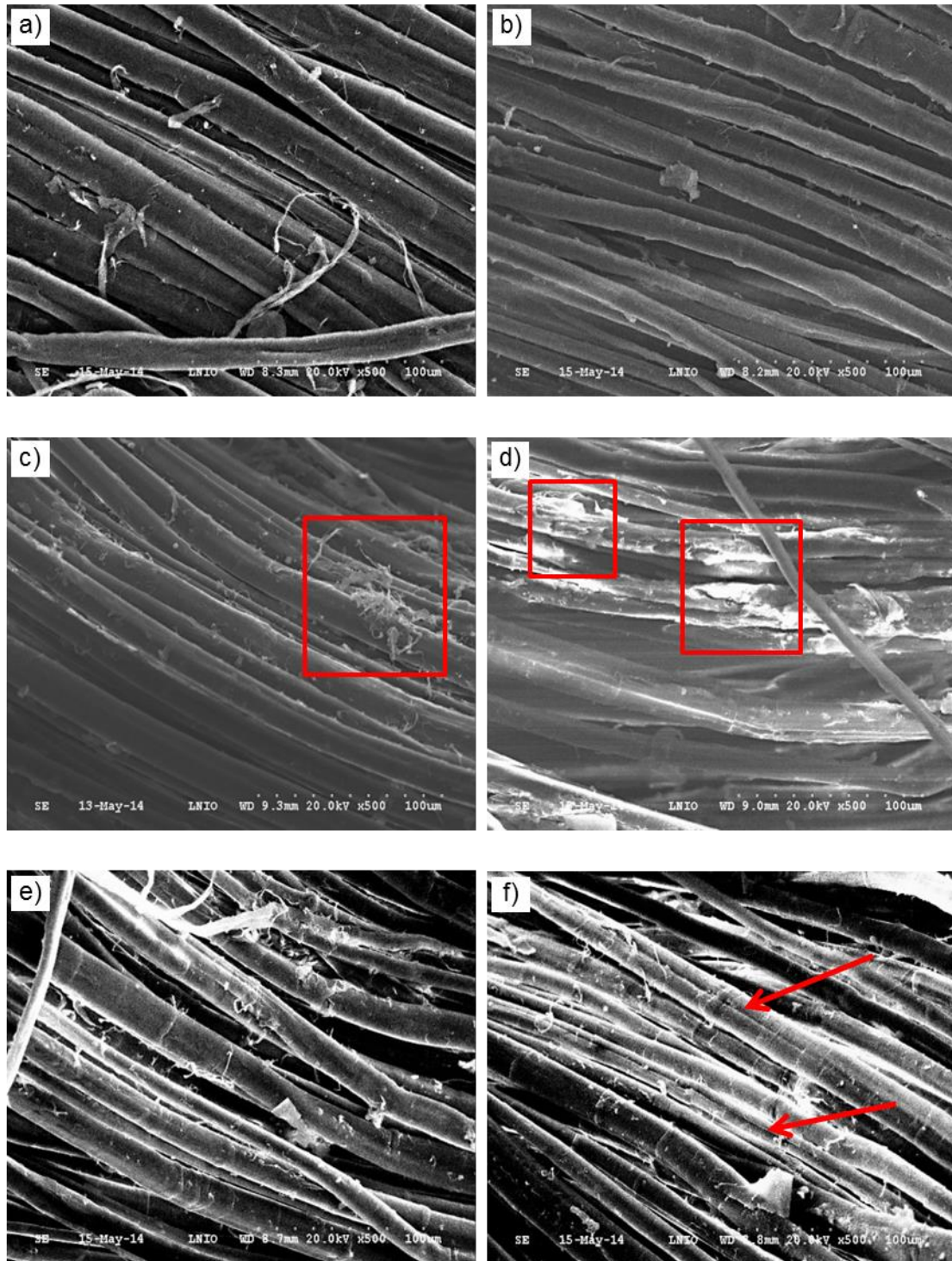


**Fig. 2-23 SEM micrographs fo hemp fibers non-treated and treated under different temperatures: a) untreated fibers; b) treated at 160 °C; c) at 180 °C; d) at 200 °C; e) at 220 °C; f) at 240 °C.**

hemp fibers. It could result in more contact surface between polypropylene and the hemp fibers. But at 200 °C (Fig. 2-23 d)), the hemp surfaces were badly burnt, in this case they couldn't grasp the PP matrix. As the temperature increased, the lignin and pectin were burnt out, even the celluloses cracked (Fig. 2-23 f)). The reinforcement of the hemp on PP would be greatly weakened.

The samples manufactured at 190 °C presents higher tensile properties than the others. It is possible that when the temperature goes higher, the PP will also be more easily penetrates into the space between the hemp threads, and the hemp fibers' thin branches result in more surface contact with the polypropylene matrix. When the temperature is higher than 200 °C, the strength decreases markedly.

## **2.5.2 Influence of pressure**

The influence of temperature on the performances of the composites as studied in this part, following the discussion of temperature. The formula discussed in section 2.4.3.3 was specified as X=190 °C; Y=0.3 MPa, 0.4 MPa, 0.5 MPa, 0.6 MPa, 0.7 MPa; Z=10. The samples were cooled down at ambient temperature.

The mass fraction of hemp in the composites  $V_m$  is 28.76%, and the calculated volume fraction  $V_f$  is 19.70%.

### **2.5.2.1 Tensile properties**

Fig. 2-24 shows the tensile properties of the hemp/PP composites under different manufacturing pressures.

The tensile strength of the composites doesn't show a monotonous trend. According to Fig. 2-24, the tensile strength at 0.6 MPa is the highest among the five kinds of samples. It is 3.34% higher than the tensile strength of the composites at 0.4 MPa. The other three composites show less difference. Fig. 2-24 b) shows an increasing Young's modulus of the composites, while a decrease occurs at 0.5 MPa. The Young's modulus of 0.7MPa is 8% higher than that of 0.4MPa. The fracture strain decreases slowly as the manufacturing pressure improves.

To explain this difference of the properties of the hemp/PP composites, the volume fraction of the fibers in the composites was firstly verified. The volume fractions of the five composites are 19.4 w.t.%, 20.1 w.t.%, 20.0 w.t.%, 20.9 w.t.% and 20.0 w.t.%, respectively. The volume fractions correspond to the tensile strength of the composites, 39.3 MPa, 40.3 MPa, 39.4 MPa, 41.7 MPa and 39.5 MPa. The volume fractions of hemp fibers are found to be responsible for the difference of the mechanical properties of the composites.

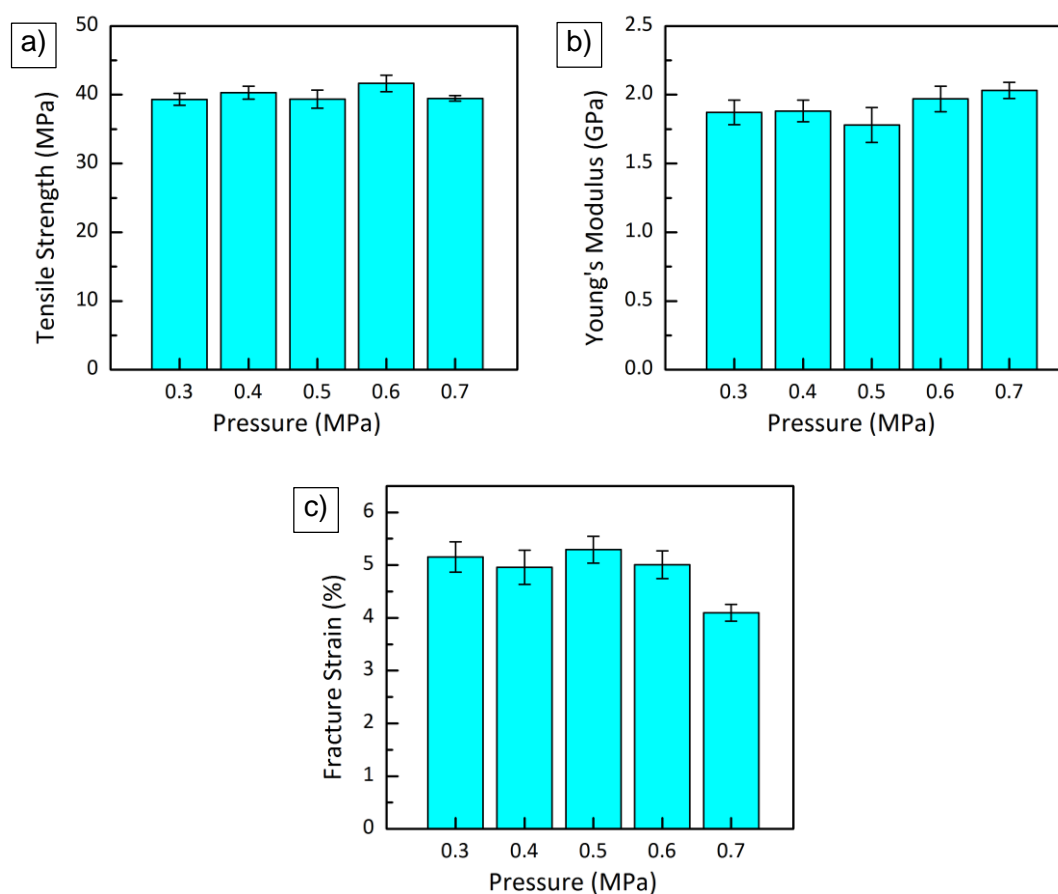


**Fig. 2-24 Tensile properties of PP/hemp composites under different pressures. a) Tensile Strength; b) Young's Modulus; c) Fracture Strain.**

### 2.5.2.2 SEM observation

Fig. 2-25 shows the SEM images of PP reinforced polypropylene composites suffered different manufacturing pressures. For the composites of 0.3 MPa, we

can find the positions where poor adhesion (gaps or voids) occurred between the fiber and matrix. As the manufacturing pressure increases, the interface became better adhered. This can be reflected in the mechanical properties of the composites. As a consequence, to increase the manufacturing pressure could improve the fiber matrix adhesion and the mechanical properties of the composites.

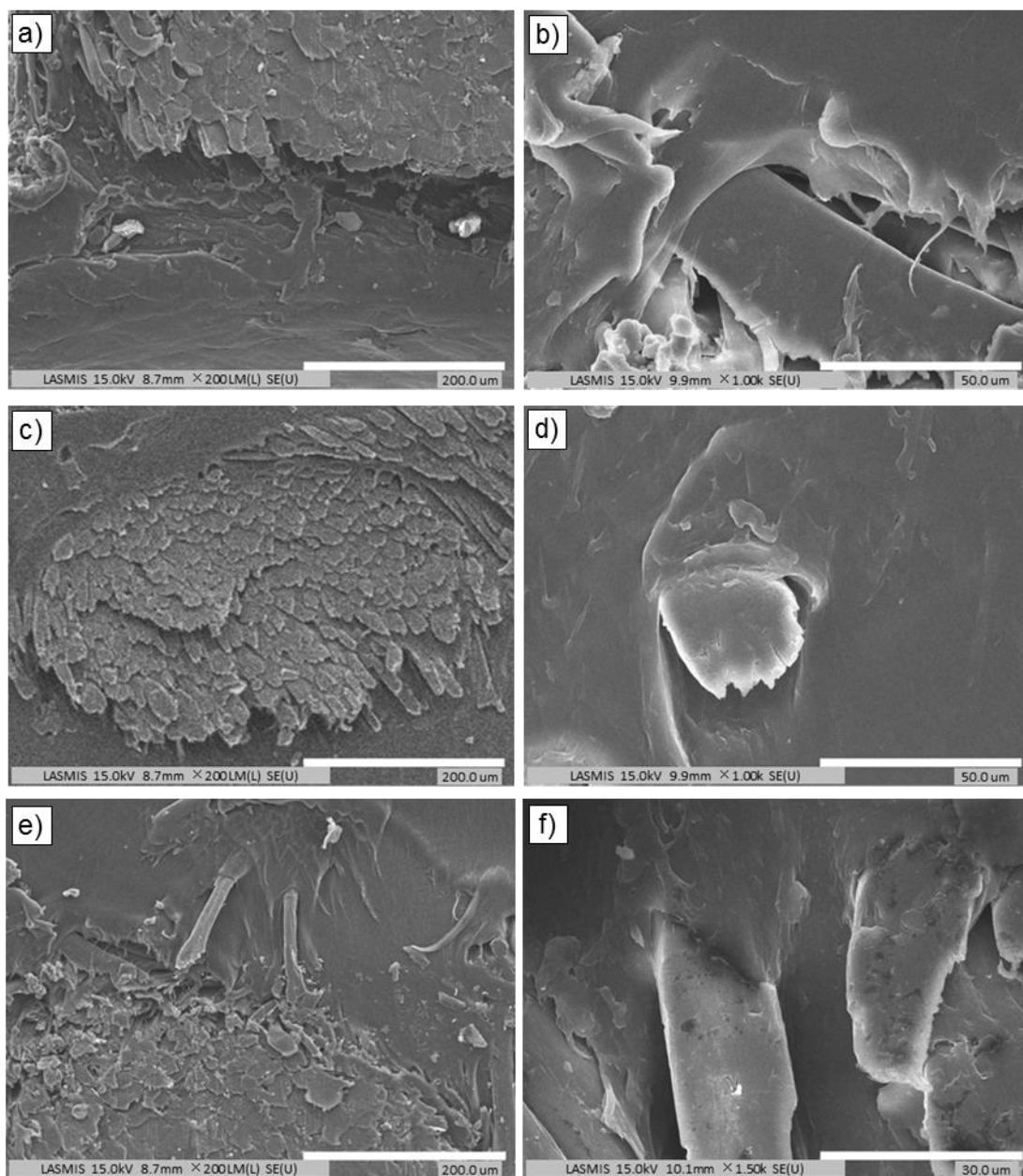


**Fig. 2-25 SEM images of hemp/PP composites under different manufacturing pressure: a) b) 0.3 MPa; c) d) 0.5 MPa; e) f) 0.7 MPa.**

## 2.6 Conclusion

The mechanical properties of the hemp fibers are attractive according to our study. The hemp fibers show different performances in the longitudinal and the transversal direction. The mechanical properties of the manufactured composites were affected by the different parameters.

The hemp fibers show elevated tensile properties in the longitudinal direction than those in the transversal direction. A remeasurement of the cross-section of the fibers was performed; a relationship of the dimensions between by the numerical method and by the Vernier Caliper was established. The spiral angle of the hemp yarns was responsible for the difference of the tensile properties of the hemp fibers.

The hemp/PP composites were manufactured through compression molding method under different parameters. The parameters have an influence on the mechanical properties of the composites. Composites manufactured at 190 °C show higher performances than the others. The hemp fibers were affected by the temperature according to the DSC analysis, color appearance and the tensile properties results. When the temperature goes higher, the PP will be more easily penetrates into the space between the hemp yarns, and the hemp fibers' thin branches result in more surface contact with the polypropylene matrix. When the temperature is higher than 200 °C, the strength decreases markedly.



**Chapter 3.**  
**Environmental Ageing and Its  
Effects**

## Chapter 3. Environmental Ageing and Its Effects

3.1	Introduction .....	71
3.2	Humidity ageing of composites .....	73
3.2.1	Experimental methods .....	73
3.2.1.1	Humidity ageing .....	73
3.2.1.2	Water uptake .....	74
3.2.1.3	Tensile tests .....	74
3.2.1.4	Scanning electron microscopy (SEM) .....	74
3.2.2	Results and discussion .....	75
3.2.2.1	Tensile test results .....	75
3.2.2.2	Water uptake .....	77
3.2.3	Diffusion of water .....	78
3.2.3.1	Kinetics of water diffusion .....	79
3.2.3.2	Fickian diffusion model .....	81
3.2.3.3	Dimension stability .....	83
3.3	UV ageing .....	85
3.3.1	Experimental methods .....	85
3.3.1.1	UV ageing .....	85
3.3.1.2	Tensile tests .....	86
3.3.1.3	Numerical microscopy .....	86
3.3.1.4	Scanning electron microscopy (SEM) .....	86
3.3.2	Results and discussion .....	86
3.3.2.1	Tensile test results .....	86
3.3.2.2	UV ageing of PP/hemp composites .....	87
3.3.2.3	Fracture observation .....	89
3.3.2.4	UV ageing of pure PP .....	90
3.3.2.5	Degradation of lignin .....	93
3.4	Conclusion .....	94

## 3.1 Introduction

In the previous chapter, the manufacturing process of the composites, the mechanical properties of the manufactured composites, and the influence of different parameters on the composites were discussed. It is of great interest that natural fibers show many attracting merits, such as low cost, environmental friendliness and bio-degradability, comparable specific mechanical properties as glass fibers, ease of availability, low energy consumption, acoustical properties etc.. However, the high hydrophilicity of the cellulosic fibers and the poor wettability, incompatibility with the polymer matrices become the main disadvantage which influence their elaboration, utility and application. The cellulosic fibers exposed to solar radiation, humid and thermal environment are subject to fiber degradation, including colour changes, defibration, graying and dimensional change [129]. In this chapter, the influence of different ageing conditions on the composites will be investigated. Firstly, the relative humidity ageing will be carried out. The moisture absorption, mechanical experiments and the diffusion of water will be discussed. Secondly, the UV ageing will be performed. The degradation of composites will be discussed.

Because of the hydrophilicity of cellulosic fibers, they are subjected to moisture changes when exposed in humid environment. The water uptake and release result in tension within the composites, causing surface defects such as cracking and flaking, fiber-matrix interface debonding and dimensional modifications, thus limit their wide applications [129-131]. The water-induced fiber swelling may be also responsible for the debonding of the interfacial adhesion. The water absorption of the composites can induce the decrease of the mechanical properties of composites. Pothan L.A. et al [132] have found that a 32 % decrease in tensile strength of banana fiber reinforced polyester composites when subjected to accelerated water ageing.

Degradation exists not only in humid environment, but also under radiation.

The main reason is the UV light transparency of the PP and the reactivity of the fibers to UV light, particularly lignin absorbs the radiation relatively strongly. The degradation happens not only under UV light, but also under the shorter wavelengths of visible light [98]. More recent researches have highlighted the importance of the shorter visible wavelengths of light in causing lignin degradation. Wavelengths up to 450 nm have shown changes in surface properties and the mechanical properties. It is thought that the reaction results are the same as for UV light but they simply occur slowly. The mechanism of lignin photodegradation is complex, with different pathways giving free phenoxy radicals leading to chain cleavage and yellowing. Fig. 3-1 shows the mechanism of the free radical formation from lignin degradation [98, 133].

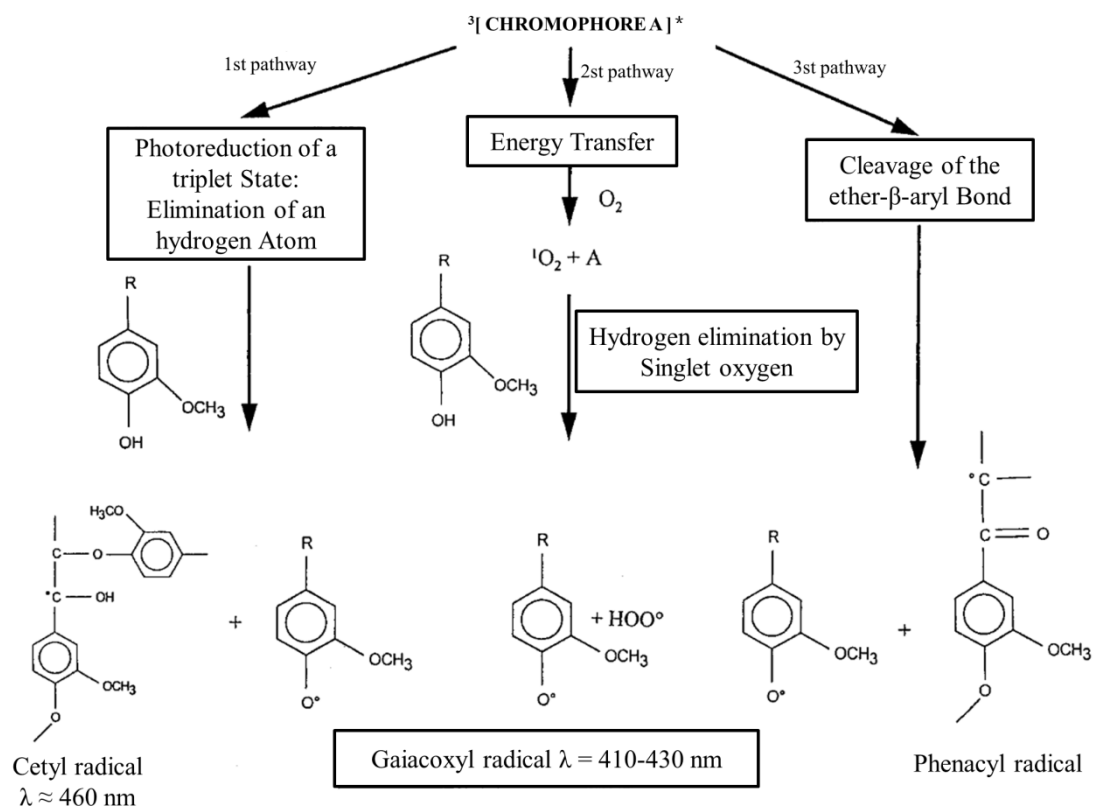


Fig. 3-1 Mechanism of free radical formation from lignin degradation [98, 133]

In order to understand the influence of the degradation of every climate element on the PP/hemp composites, different ageing procedures and the relative analyses were realized

## 3.2 Humidity ageing of composites

### 3.2.1 Experimental methods

#### 3.2.1.1 Humidity ageing

Humidity ageing was performed in ATLAS SUNTEST XXL/XXL+, as is shown in Fig. 3-2. It is equipped with a source of xenon lamp. The three lamps are located at the top the chamber, so all the samples can receive the same level of illuminance. It is also furnished with a ventilation system, to ensure a homogeneous environment in the oven.

The ageing condition as follows: relative humidity  $80 \pm 5$  %, chamber temperature  $20 \pm 2$  °C, without illumination.



**Fig. 3-2 Ageing oven ATLAS SUNTEST XXL/XXL+**

### 3.2.1.2 Water uptake

Because of the hydrophilicity of the natural fibers, water absorption tests were carried out. The composite samples were dried at 80 °C for 24 hours to a constant weight of a precision of 0.001 g, designated as  $M_0$ . The samples were next immersed in water at room temperature. The weights of the samples were measured at regular intervals after being dried, designated as  $M_t$ . The percentage gain at any time ( $w_t$ ) as a result of water absorption was determined by :

$$w_t (\%) = \frac{M_t - M_0}{M_0} \times 100\% \quad (3-1)$$

In the water absorption tests, the samples were immersed until they were saturated. The diffusion coefficient and the maximum water absorbed can be obtained by considering the Fick's law diffusion model.

### 3.2.1.3 Tensile tests

The tensile tests were performed in a static tension machine Instron 4484 at room temperature with a displacement rate of 2 mm/min. An extensometer with a 12.5 mm initial opening length was placed at the center of the specimens to measure the deformation. The tensile test was based on the standard test method ASTM D 3039/D 3039M – 08 (ASTM International 2008).

### 3.2.1.4 Scanning electron microscopy (SEM)

The fiber surface morphology and the fracture topography were scanned by SEM. The hemp fibers were stuck to a paper, and coated with carbon with a SEM coater CC7650 to facilitate the electron beam incident. The composite samples were observed using a HITACHI S 3500 N or a HITACHI SU 8030 microscope.

## 3.2.2 Results and discussion

### 3.2.2.1 Tensile test results

Tensile test results of PP/hemp composites under different configurations (as shown in Table 3-1) up to 8 weeks humidity ageing are shown in Fig. 3-2.

**Table 3-1 Different configurations of the aged composites**

Composites	Temperature of fabrication/ °C	Fiber volume fraction/ %	Pressure/ MPa
HR1	190	11	0.4
HR2	190	19.5	0.4
HR3	190	19.5	0.6

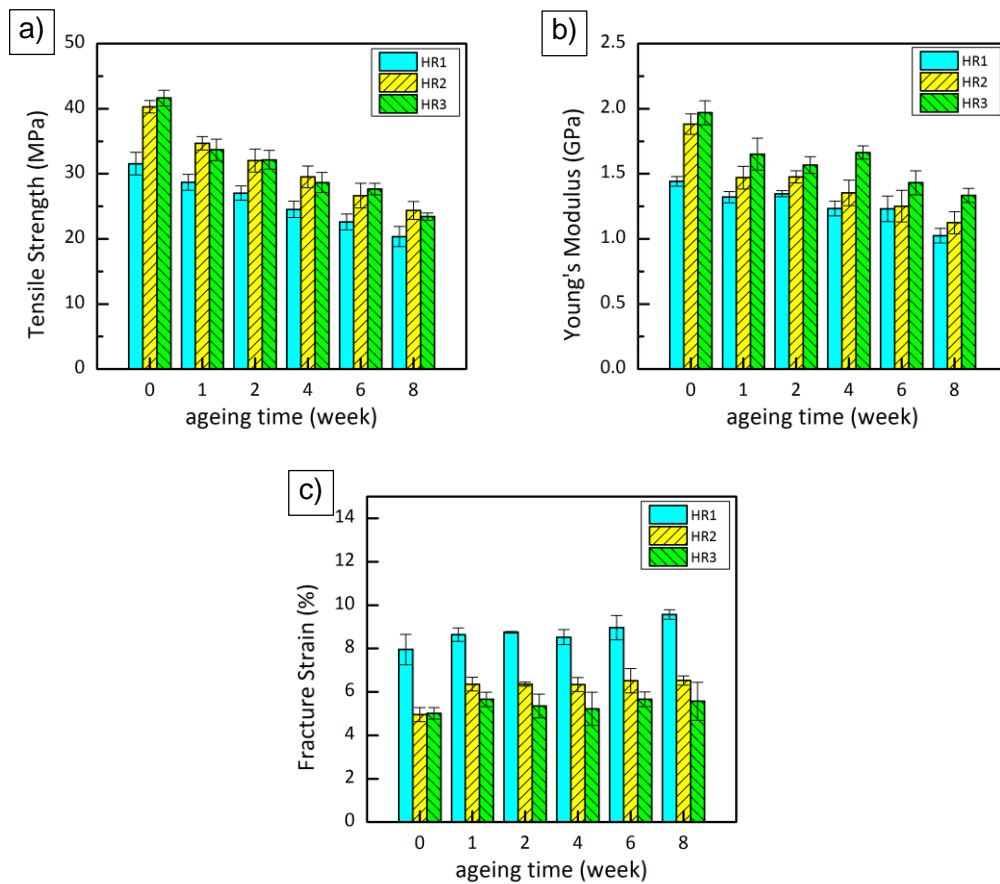


**Fig. 3-3 Mechanical properties of relative humidity-aged PP/hemp composites under different conditions: 190 °C/0.4MPa/11%hemp; 190 °C/0.4MPa/19%hemp; 190 °C/0.6MPa/19%hemp, a) Tensile Strength; b) Young's Modulus; c) Fracture Strain**

The tensile properties of these composites are remarkably affected by the humidity ageing. According to the results, the tensile strengths of the composites decrease after humidity ageing. The Young's moduli of the composites present the same tendency as the tensile strengths. The tensile strengths dramatically decreased after 2 weeks, 14.3%, 20.5% and 22.8% for composites HR1, HR2 and HR3, respectively. Because of the higher fiber volume fraction of HR2 and HR3 (19% hemp in volume fraction) than HR1, water is much easier to penetrate into the composites. After 8-week humidity ageing, the composites suffered 35% and 40% drain of the tensile strength for 11% and 19% fiber fraction, respectively.

After 8 weeks humidity ageing, the Young's modulus of the composites decreased by 29% (HR1), 40% (HR2) and 32% (HR3) respectively. In the first two weeks, the Young's modulus of the composites decreased by 7% (HR1), 21.5% (HR2), 20% (HR3) respectively. In the one hand, a high fiber fraction can improve the tensile properties of the composites; in the other hand, a relatively high fiber fraction in composites may absorb more water during its service. Thus water absorption may influence its application, especially in humid environment. Composite HR3 showed lower reduction in tensile strength than HR2, which may be due to the higher manufacturing pressure. And an increase was noted after 4 weeks ageing. The polypropylene penetrated well into the hemp, and formed a better protection to the hemp fibers. The decrease of the tensile properties was retarded.

Composite HR1 has a higher fracture strain than HR2 and HR3, and the fracture strain of HR1 increased gradually during humidity ageing. But the fracture strain of HR2 increased slowly, and the fracture strain of HR3 changed slightly. A decrease was found after 4 weeks humidity ageing, which corresponded to the increase of the Young's modulus after 4 weeks ageing. The fiber fraction had a distinct effect on the strain of the composites.

### 3.2.2.2 Water uptake

Fig. 3-4 shows the percentage moisture absorption  $w_t$  (%) of pure PP and PP/hemp composites HR1, HR2 and HR3, as a function of time at room temperature. An initial increase in  $w_t$  (%) is observed in each cases, followed by an equilibrium state or saturation indicated by a plateau region.

Pure PP was found to be the lowest water absorption, because of its hydrophobic nature. PP does not absorb water significantly, because of being a non-polar polymer. At 19% fiber loading, the composite exhibited higher water absorption values than 11% fiber loading for all immersion times. It indicates that the higher fiber loading facilitates water absorption. As is shown in Fig. 3-4, composite HR2 reached equilibrium state earlier (about after 39 days of immersion), compared with HR3 (approximately after 42 days of immersion).

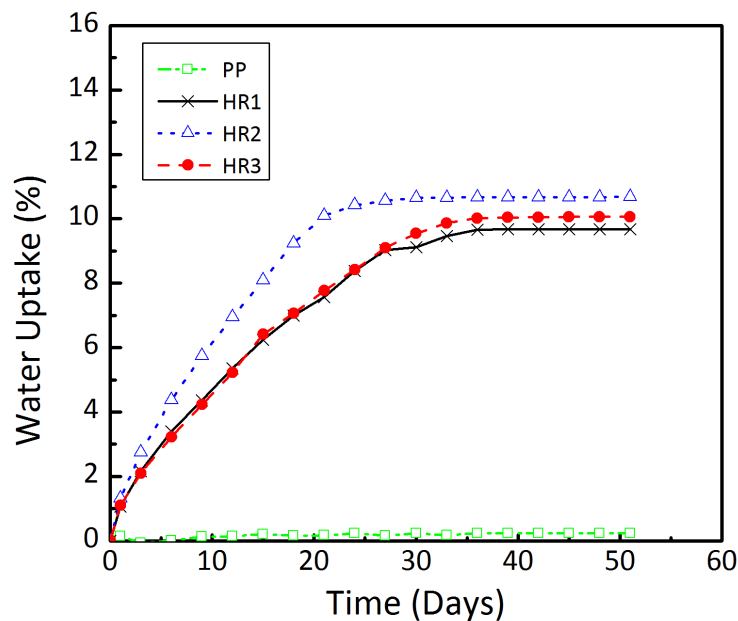


**Fig. 3-4 Evolution of water uptake of composites: pure PP, HR1, HR2, HR3.**

Natural fibers are apt to absorb moisture and water because the constituents, such as cellulose and hemicellulose, are hydrophilic [131, 134]. As shown in Fig. 1-2, cellulose is a linear condensation polymer containing chain of variable length

of 1-4 linked  $\beta$ -d-anhydroglucopyranose units, which contain hydroxyl groups. Hemicelluloses (Fig. 1-3) are lower molecule weight polysaccharides forming branch- containing random, amorphous branched and non-linear structures, which also contain hydroxyl groups. These hydroxyl groups may form hydrogen bonds with the molecule itself or with the other polar molecules. Water, a polar molecule, can react with the cellulose and hemicellulose to form hydrogen bonds. Consequently, higher fiber loading leads to higher water and moisture absorption. Composites HR2 and HR3 absorbed more water than HR1 in Fig. 3-4. Besides, porosity and microgaps (for insufficient fiber/polymer interfacial adhesion) can hold water molecules. This would facilitate the water absorption and water transfer.

### **3.2.3 Diffusion of water**

When the polymer composites are exposed to a humid environment or immersed in aqueous solution, they tend to absorb water molecules through the surfaces directly contacting with the foreign environment. With the penetration of water into the materials, a mass gain occurs versus time.

Diffusion is the most important mechanism which conducts the water penetration or water absorption into the composite materials. And the other two minor mechanisms are capillarity and transport by micro-spaces. Diffusion mechanism implies direct water molecules diffusion or absorption into the matrices and fibers. Water transport by micro-spaces involves flow and storage of water in microcracks, microgaps, porosity and other forms of microdamages formed during the manufacturing process or resulting from environmental effects. Capillarity involves flow of water molecules along the fiber-matrix interface, which is produced by weak interfacial adhesion and/or fiber-matrix debonding. When the composite materials are exposed to humid environment, all these three mechanisms occur simultaneously, but the overall absorption behavior can be modeled only considering the diffusion mechanism.

Two kinds of diffusion behaviors are classified in most cases: Fickian diffusion law and non-Fickian diffusion. They can be distinguished from the curve of water absorption versus the square root of time (Fig. 3-5).

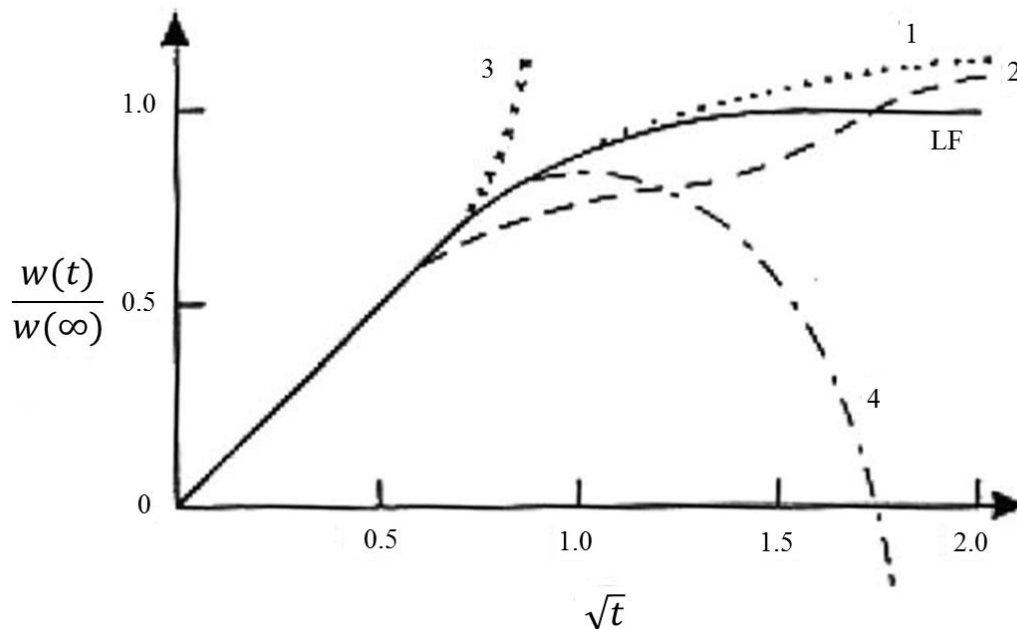


**Fig. 3-5 Schematic curves representing four categories of recorded non-Fickian weight-gain sorption data in polymers and polymeric composites [135].**

The curve of Fickian diffusion (LF) is based on the Fickian diffusion model. In the first part, water absorption corresponds to a linear mass gain as a function of the square root of time. Then a plateau region is achieved, indicating an equilibrium state or saturation at a certain time. And curves 1, 2, 3 and 4 correspond to variations thereof. A two-stage saturation diffusion (2), a successive mass gain (1, 3) or a contrary mass loss (4) may occur for different materials in different liquids [134, 135].

### 3.2.3.2 Kinetics of water diffusion

Different kinds of diffusion behavior, Fickian or non-Fickian diffusion, can be distinguished theoretically by the formulation following [136]:

$$\frac{w_t}{w_m} = k \cdot t^n \quad (3-2)$$

where  $w_t$  is the water mass gain at time  $t$ ,  $w_m$  is the maximum water mass gain at saturation, and  $k$  and  $n$  are the diffusion kinetic parameters,  $k$  is the slope of the linear part of the curve  $w_t = f(\sqrt{t})$ . The mode of diffusion is represented by the exponent  $n$ . When  $n$  is equal to 0.5, diffusion obeys Fick's law. When  $n = 1$  (or  $n > 1$ ), it is non-Fickian diffusion. The diffusion is anomalous when  $n$  is between 0.5 and 1.

To determine the diffusion mechanism and the kinetics of water absorption of the PP/hemp composites,  $n$  can be determined by the following equation:

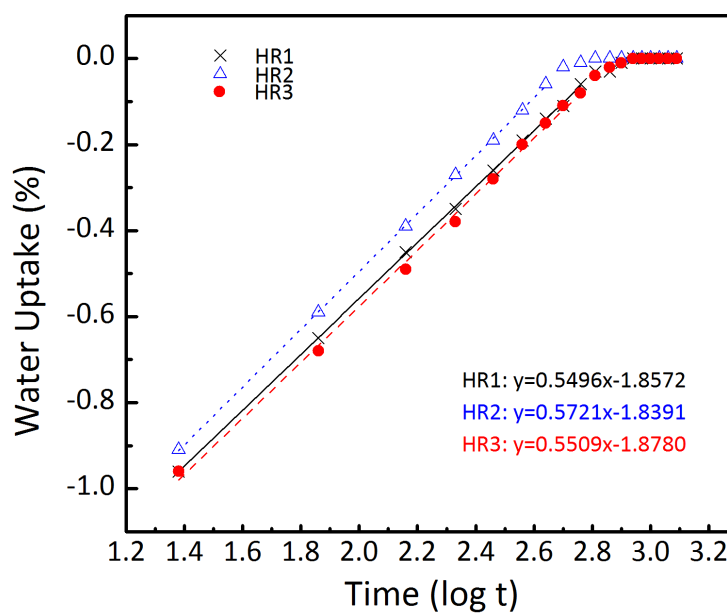
$$\log\left(\frac{w_t}{w_m}\right) = \log k + n \cdot \log t \quad (3-3)$$

which is derived from Eq. (3-2).

And the logarithmic curve is presented in Fig. 3-6. The values of the kinetic parameters  $n$  and  $k$  resulting from the linear fittings are summarized in Table 3-2. The values of  $n$  are close to 0.5, which shows that the process of water absorption is close to Fickian law in the case of these composites. The similar observations are reported in other natural-fiber-reinforced composites [64, 137, 138]. A. Retegi et al. [137] found that in the case of flax pulp/PP composites, with a value of  $n$  about 0.5, the sorption process shows a tendency to approach Fickian behavior. And the diffusion parameter  $k$  was found to have increasing tendency with the temperature. Ana Espert and co-workers [64] revealed that the absorption of water in natural fiber (sisal, coir and luffa sponge etc.) reinforced polypropylene composites approaches towards the Fickian diffusion case with values of  $n$  close to 0.5.

**Table 3-2 Diffusion kinetic parameters.**

Ageing condition	n	k	D (m <sup>2</sup> /s)
HR1	0.5496	$5.97 \times 10^{-5}$	$2.98 \times 10^{-13}$
HR2	0.5721	$7.53 \times 10^{-5}$	$3.90 \times 10^{-13}$
HR3	0.5509	$6.07 \times 10^{-5}$	$2.86 \times 10^{-13}$

**Fig. 3-6 Diffusion case fitting plots for PP/hemp composites.**

### 3.2.3.3 Fickian diffusion model

As the composites are thin plates, and the water diffusion can be simplified to a model of unidirectional diffusion along axis-x, and the diffusion coefficient is constant inside the material, the principle of mass conservation involve the following equation :

$$\frac{\partial c}{\partial t} = D_x \frac{\partial^2 c}{\partial x^2} \quad (3-4)$$

where  $C$  is the water concentration, and  $D$  is the diffusion coefficient in direction  $x$ .

The solution of Eq. (3-4) is:

$$\frac{w_t}{w_\infty} = 1 - \frac{8}{\pi^2} \sum_{i=0}^{\infty} \frac{1}{(2i+1)^2} \exp \left[ -(2i+1)^2 \pi^2 \left( \frac{D_x t}{h^2} \right) \right] \quad (3-5)$$

The diffusion coefficient is the most important parameter of the Fick's model, as it shows the ability of solvent molecules to penetrate into the composite structure. The water diffusion can be described by Fick's law diffusion model. According to Chi-Hung Shen and George S. Springer [139], the equation of Fick's law has been simplified to show the initial absorption (for values  $w_t/w_m$  lower than 0.5) :

$$\frac{w_t}{w_m} = \frac{4}{h} \left( \frac{D}{\pi} \right)^{\frac{1}{2}} t^{\frac{1}{2}} \quad (3-6)$$

where  $w_t$  is the percentage of water gain at time  $t$ ,  $w_m$  is the maximum percentage of water absorbed at saturation,  $h$  is the thickness of the samples,  $D$  is the diffusion coefficient, and  $t$  is the time.

By considering the slope of the first part of the water uptake curve, the diffusion properties of the composites can be evaluated. The coefficient of diffusion ( $D$ ) is defined as the slope of the normalized mass gain against  $t^{1/2}$ :

$$D = \pi \left( \frac{kh}{4w_m} \right)^2 \quad (3-7)$$

where  $D$  is the coefficient of diffusion,  $k$  is the initial slope of the water uptake plot ( $w_t$  versus  $t^{1/2}/h$ ),  $h$  is the thickness of composite,  $w_m$  is the maximum percentage of water absorbed at saturation.

The values of the water diffusion coefficients obtained for the fitting of the linear part to Eq. (3-2) are shown in Table 3-2. From the results, the increase in

fiber volume fraction led to higher values of the diffusion coefficients of the PP/hemp composites. The hydrophilic nature of natural fibers contributed to the water molecules to diffuse into the composite materials, as demonstrated by the kinetics of the diffusion processes. With better adhesion between matrices and fibers, the diffusion efficiency decreases since better interfacial adhesion involves less gaps, spaces, microcracks and also more hydrophilic groups are blocked by the matrix.

### 3.2.3.4 Dimension stability

The dimensional stability of a composite is referred to the water absorption behavior. The elementary fiber radius swelling could be expressed as the following equations [140] :

$$r_t^f (\%) = \frac{r_t^f - r_0^f}{r_0^f} \times 100\% \quad (3-8)$$

$$v_t^f (\%) = \frac{V_t^f - V_0^f}{V_0^f} = \frac{V_{H_2O}^f}{V_0^f} \times 100\% \quad (3-9)$$

$$W_t^f (\%) = \frac{M_t^f - M_0^f}{M_0^f} \times 100\% \quad (3-10)$$

$$r_t^f (\%) = \frac{\rho_f}{\rho_{H_2O}} \times W_t^f \quad (3-11)$$

where  $r_t^f$  (%) is the radial swelling ratio of elementary fiber.  $r$  is the radius elementary fiber.  $v_t^f$  (%) is the increase ratio of elementary fiber volume.  $V$  is the fiber volume.  $W_t^f$  (%) is the weight gains of elementary fiber.  $M$  is the weight of fiber bundle.  $\rho_f$  (1.48 g/cm<sup>3</sup>),  $\rho_{H_2O}$  (1.00 g/cm<sup>3</sup>) are the density of hemp fiber and water, respectively. The superscript  $f$  is fiber, the subscript 0 indicates the initial state of fibers, and  $t$  signifies the state of fibers after humidity ageing of  $t$

time.

Based on the previous studies, the fiber mainly swells in fiber radial direction [141]. Based on the hypothesis that there is no void in the composites, the composite swelling can be represented by [140] :

$$s_t^c (\%) = v_t^c (\%) = \frac{V_t^c - V_0^c}{V_0^c} = \frac{V_{H_2O}^c}{V_0^c} \times 100\% \quad (3-12)$$

$$s_t^c (\%) = W_t(\%) \times \frac{1}{\rho_{H_2O}} \times \frac{M_0^c}{V_0^c} \quad (3-13)$$

$$M_0^c = M_m + M_f \quad (3-14)$$

$$V_0^c = \frac{M_m}{\rho_m} + \frac{M_f}{\rho_f} \quad (3-15)$$

where  $s_t^c (\%)$  is the cross-section area increase of specimens,  $v_t^c (\%)$  is the volume increase of specimens,  $V_{H_2O}^c$  is the volume of absorbed water,  $W_t(\%)$  is the water content of the composite. V is volume, M is mass, the superscript c indicates the composite, the subscripts t, m, f are ageing time, matrix and fiber. Subscript 0 signifies the initial state of the composite.

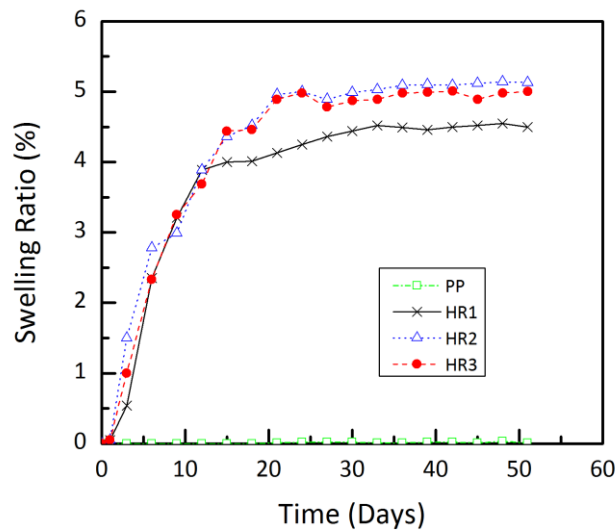


Fig. 3-7 Swelling ration of humidity-aged PP/hemp composites.

Fig. 3-7 shows the thickness swelling ratio of pure PP and humidity aged PP/hemp composites. These curves show an initial rapid increase, with a decreased rate of increase, finally a plateau region. The dimensions changed with changing moisture content. Because natural fibers contain hydroxyl groups and other groups which attract water molecules. Composites exposed or immersed in water will swell, the fibers expand until the water content reaches saturation.

### 3.3 UV ageing

Degradation exists not only in humid environment, but also under radiation. The main reason is the UV light transparency of the PP and the reactivity of the fibers to UV light, particularly lignin absorbs the radiation relatively strongly. The changes of properties of hemp reinforced PP composites under ultra-violet ageing were also studied in this part.

#### 3.3.1 Experimental methods

##### 3.3.1.1 UV ageing

Ultra-Violet ageing was performed in ATLAS SUNTEST XXL/XXL+, as is shown in Fig. 3-2. It is equipped with a source of xenon lamp. The samples were preserved in the chamber up to 8 weeks. The UV ageing parameters were controlled according to the standard ISO 4892-2: 2006, as shown in Table 3-3.

**Table 3-3 Exposure parameters of UV ageing of PP/hemp composites**

Exposure period	Irradiance (W/m <sup>2</sup> )	Black-standard temperature (oC)	Chamber temperature (oC)	Relative humidity (%)
Continuously dry	50 ±2	65 ±3	38 ±3	50 ±10

### **3.3.1.2 Tensile tests**

The tensile tests were performed in a static tension machine Instron 4484 at room temperature with a displacement rate of 2 mm/min. An extensometer with a 12.5 mm initial opening length was placed at the center of the specimens to measure the deformation. The tensile test was based on the standard test method ASTM D 3039/D 3039M – 08 (ASTM\_International 2008).

### **3.3.1.3 Numerical microscopy**

The hemp fiber fabric was observed under a numerical microscope, KEYENCE VHX-S15, assembled with an objective (magnification 100×~1000×). To observe the morphology and the dimension of one yarn of the hemp fiber fabric, the fibers were pulled tightly.

### **3.3.1.4 Scanning electron microscopy (SEM)**

The fiber surface morphology and the fracture topography were scanned by SEM. The hemp fibers were stuck to a paper, and coated with carbon with a SEM coater CC7650 to facilitate the electron beam incident. The composite samples were observed using a HITACHI S 3500 N or a HITACHI SU 8030 microscope.

## **3.3.2 Results and discussion**

### **3.3.2.1 Tensile test results**

Fig. 3-8 shows the mechanical properties of PP/hemp composites subjected to UV ageing from 0 to 8 weeks. From the figures, it is observed that the tensile strength, Young's modulus and fracture strain decreased during the ageing period. In the first two weeks, the Young's modulus and tensile strength did not reduce much more for all kinds of composites. But after 4 weeks' UV radiation, a sharp reduction occurred. The tensile strength decreased 25.8%, 28.8% and 27.0% for composites HR1, HR2 and HR3, respectively. At the end of 8 weeks' UV ageing, a decrease of more than 40% of the tensile strength happened to all the composites.

As for the fracture strain, the composites showed a decreasing tendency. But in the first two weeks, a slight increase occurred for composite HR3.

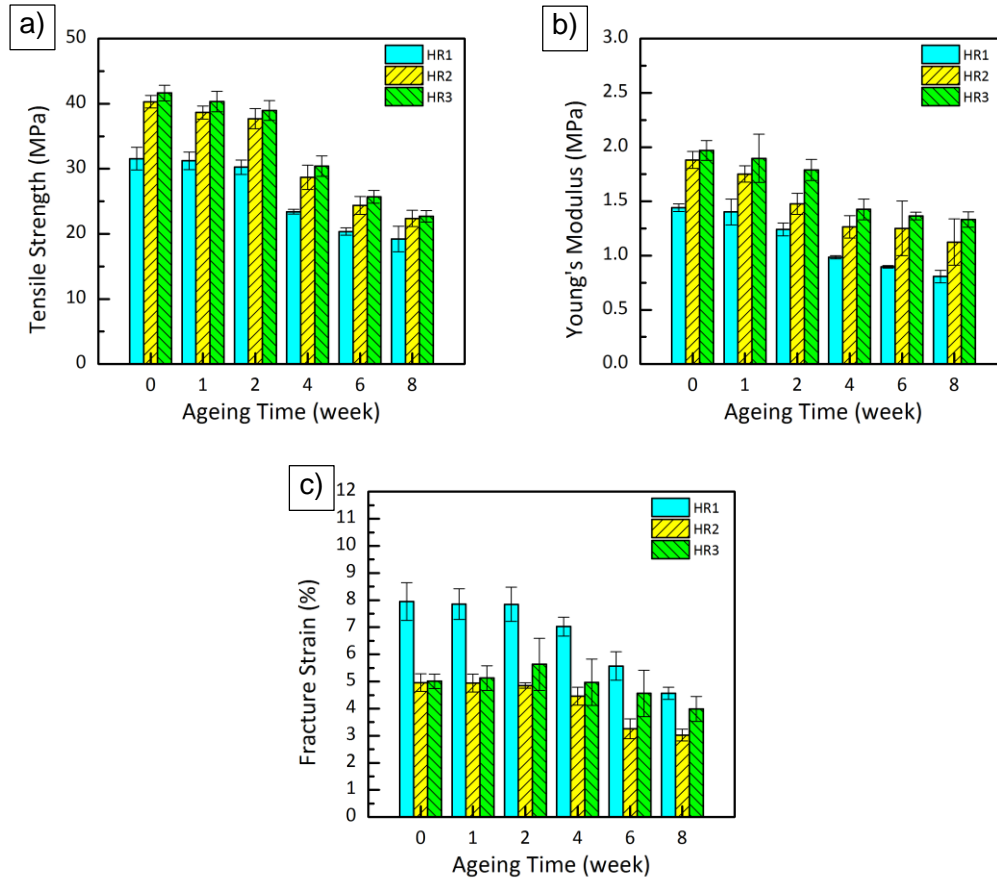


**Fig. 3-8 Mechanical properties of UV-aged PP/hemp composites under different conditions: 190 °C/0.4MPa/11%hemp; 190 °C/0.4MPa/19%hemp; 190 °C/0.6MPa/19%hemp, a) Tensile Strength; b) Young's Modulus; c) Fracture Strain**

### 3.3.2.2 UV ageing of PP/hemp composites

Fig. 3-9, Fig. 3-10 and Fig. 3-11 show the photos of PP/hemp composites HR1, HR2 and HR3 subjected to UV ageing from 1 to 8 weeks. The color of all the specimens under UV radiation altered from brown to white. During the first two weeks, the color of the composite surface did not change at all. After 4 weeks, the surface of the samples whitened rapidly, until it totally whitened. After 8-week's UV ageing, there were even macroscopic cracks occurred on the surface of some specimens.

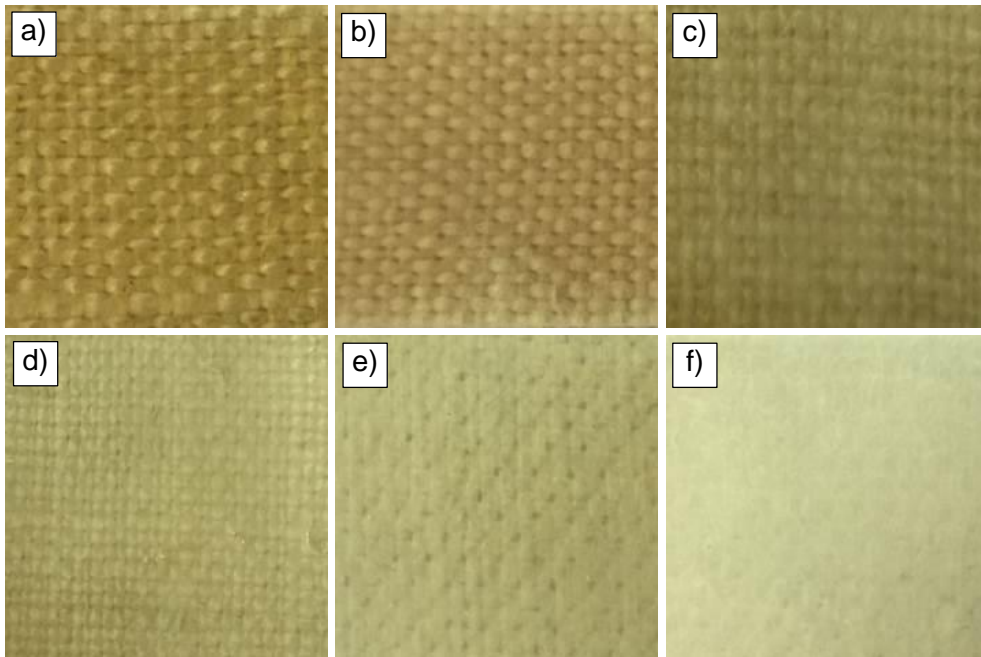


**Fig. 3-9** Photos of PP/hemp composite HR1 after UV ageing of a) 0; b) 1; c) 2; d) 4; e) 6; and f) 8 weeks

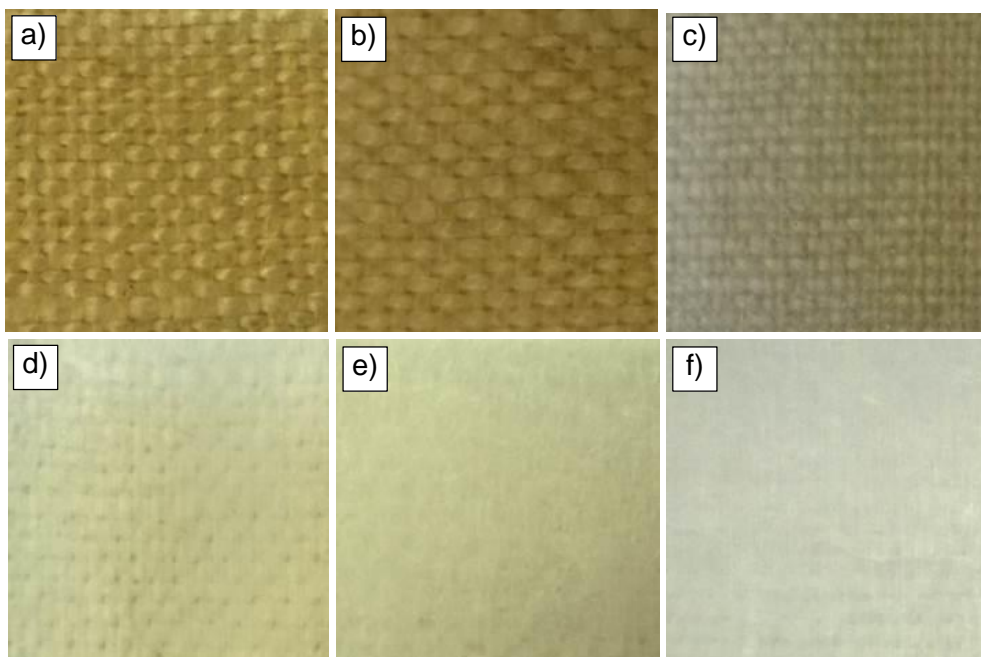


**Fig. 3-10** Photos of PP/hemp composite HR2 after UV ageing of a) 0; b) 1; c) 2; d) 4; e) 6; and f) 8 weeks

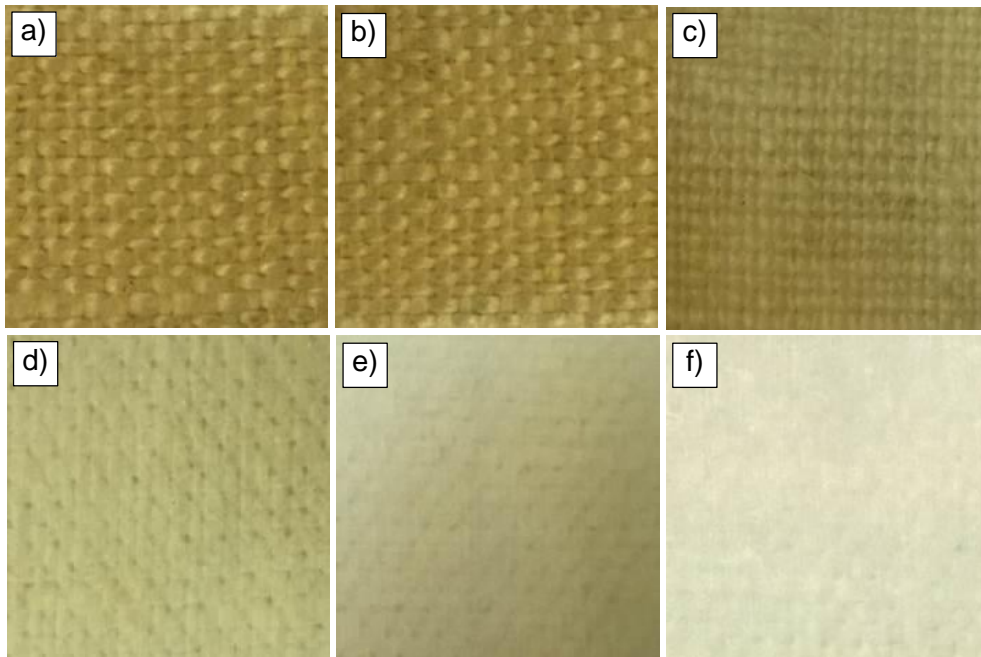


**Fig. 3-11** Photos of PP/hemp composite HR3 after UV ageing of a) 0; b) 1; c) 2; d) 4; e) 6; and f) 8 weeks

### 3.3.2.3 Fracture observation

Fig. 3-12 shows the fracture morphology of the composites after UV ageing. It is observed that the hemp fibers were pulled out directly from the matrix, and there were gaps between fiber and matrix. The poor matrix/fiber interfacial adhesion facilitates the separation of fiber/matrix interface. Thus the mechanical properties of the composites were affected, decreased.

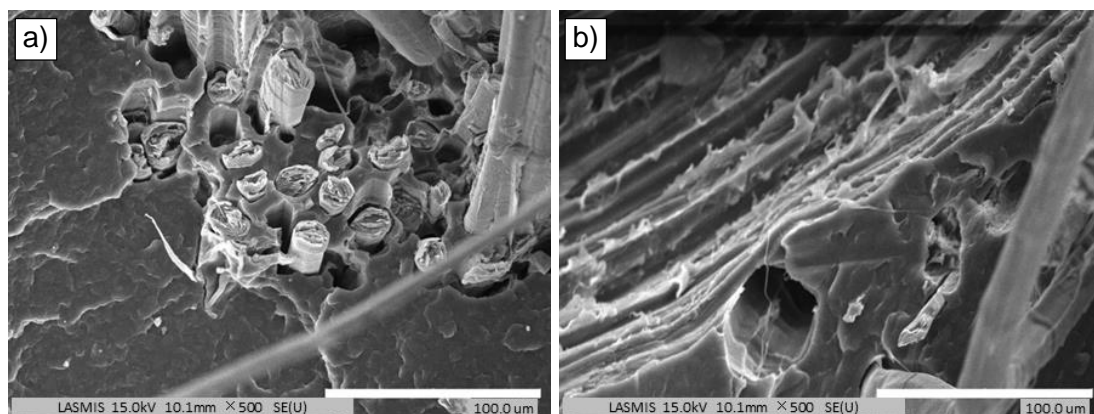


**Fig. 3-12** SEM images of fracture morphology of aged composites after UV ageing.

### 3.3.2.4 UV ageing of pure PP

We try to explain the phenomena of the UV-aged composites by several other experiments. Firstly, the surface appearances of the composites were checked. Fig. 3-13 illustrates the micrographic photos of pure PP after 8 weeks of UV ageing. It is observed from Fig. 3-13 that there are microcracks on PP surface and these cracks distribute in random directions. Surface cracks formed spontaneously from the first week of the UV ageing. Beginning from the fourth week, a network of microcracks without evident patterns formed. As time proceeded, the network of microcracks thickened. Even after 8 weeks, there were severe cracks formed because of the crack propagation. This phenomenon will definitely affect the mechanical properties of the composites. The crack growth cannot be generalized described because the formed patterns and the concentration of the cracks depend on the type and the ageing conditions of the elaborating processes and the geometry of the samples [142]. Regular cracks were observed in injection moulding samples [140, 142]. These regular cracks were perpendicular to the flow-lines.

Photodegradation is governed by the diffusion of O<sub>2</sub> in the polymers, and it irreversibly changes the structure and the behavior of the correspond materials. The photo-oxidation process involves the absorption of a photon by the molecule of polypropylene. After being absorbed, the PP molecules are in an excited electronic state with a relatively higher potential energy. The energy of the firstly excited molecules can transfer to the other ones. This photo-oxidation process can be described by the following chemical reactions:

- Polymer (POOH) +  $h\nu$  → P<sup>•</sup>
- P<sup>•</sup> + O<sub>2</sub> → PO<sub>2</sub><sup>•</sup>
- PO<sub>2</sub><sup>•</sup> + PH → POOH + P<sup>•</sup>

The consequences of these irreversible reactions can be divided to 3

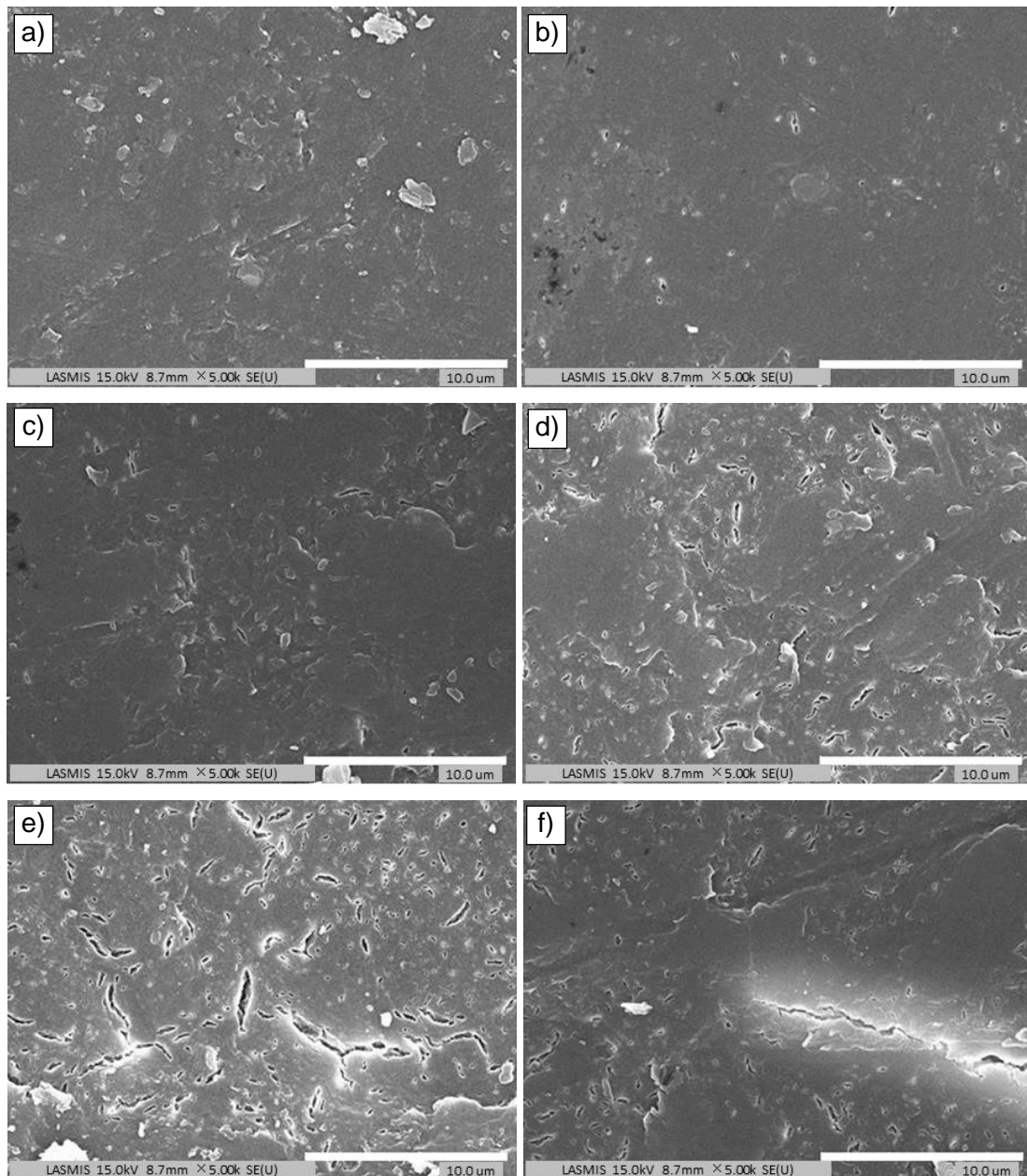


**Fig. 3-13 Development of cracks on PP surfaces during UV ageing: a) non-aged; b) 1 week; c) 2 weeks; d) 4 weeks; e) 6 weeks; f) 8 weeks.**

phenomena:

- Photo-oxidation and hydrolysis : chain break, loss of mechanical
- properties (embrittlement, separation)
- Photolysis : yellowing products, chalking and discoloration, appearance alteration (fading)

- Transformation of additives : modified functionality, acceleration of the loss of mechanical properties (stabilizers)

Hongchang HAN [140] detailedly studied the UV ageing of pure PP, manufactured by injection moulding. The tensile test results of PP are shown in Fig. 3-14 [140]. The Young's Modulus and Fracture Stress increased after 6 weeks UV ageing, and remarkably decreased after 8 weeks. And the embrittlement of PP remarkably induced the Fracture Strain after ageing. There are two main factors which affect the tensile properties of PP: surface cracking and crystallinity. Iryna Yakimets et al. have employed the linear elastic fracture mechanics to study the separate effects of surface cracking and chemical ageing on the Young's Modulus of the composites.

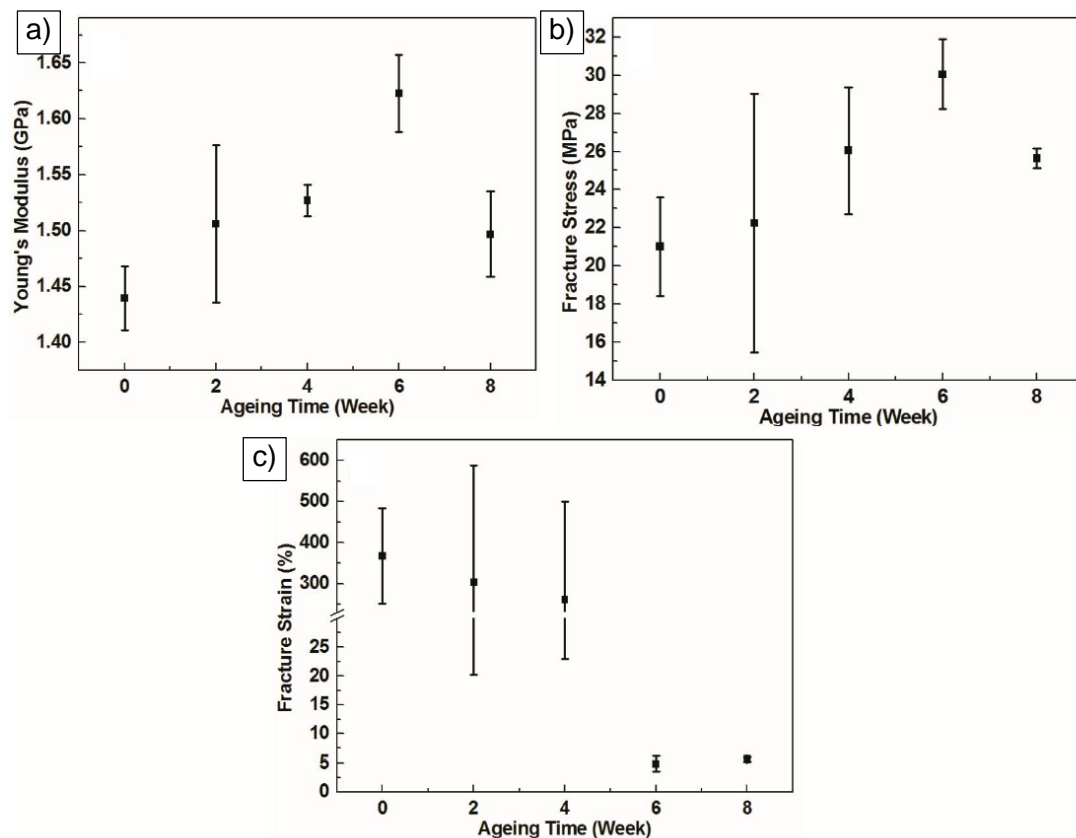


**Fig. 3-14 Tensile test results of PP subjected up to 8 weeks of UV ageing: a) Young's Modulus; b) Fracture Stress; c) Fracture Strain [140].**

Fig. 3-15 [140] shows the XRD patterns of PP without UV ageing and after 8 weeks of UV ageing. The position of the diffraction peak of PP remains the same after UV ageing, but the intensity of peaks and the amorphous background altered. Most of the crystalline peaks increased after ageing, indicating that the UV degradation of PP happened to be concentrated in the amorphous regions. The macromolecules of PP break to smaller molecules which facilitate crystallization, accompanied by an enhancement of crystallinity.

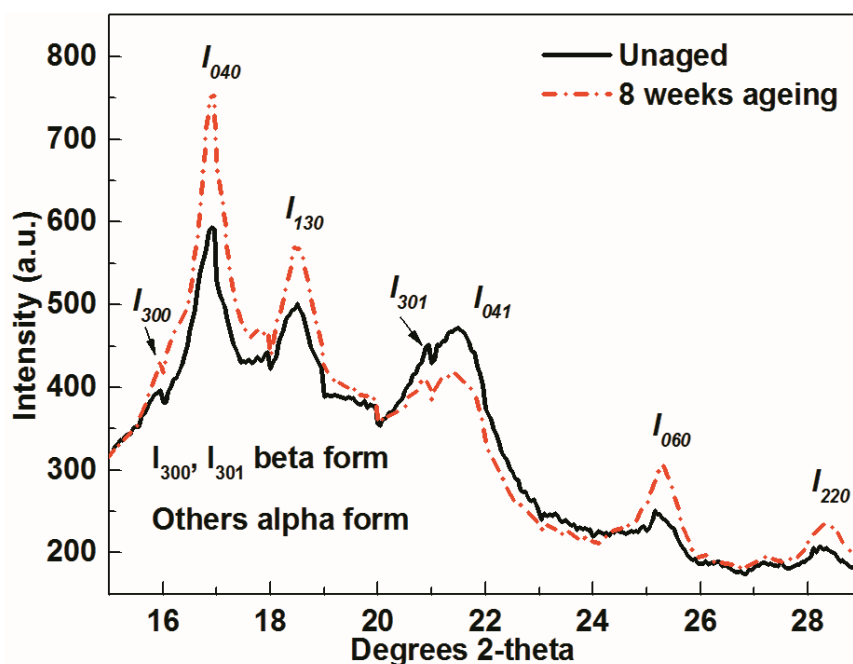


Fig. 3-15 XRD patterns of PP after UV ageing of 0 and 8 weeks [14].

### 3.3.2.5 Degradation of lignin

Of the main compositions of cellulose fibers, only lignin absorbs relatively strongly in the UV/visible region (as shown in Fig. 3-16). Lignin is a highly branched polymer. The mechanism of lignin photodegradation is very complex. Two chromophoric groups A and B [98] are shown to be responsible to absorb UV light and undergo different steps of the photodegradation mechanism. Free phenoxy radicals forming through different pathways lead to chain cleavage and yellowing. A guaiacoxy radical is one of the main phenoxy radicals, as shown in

Fig. 3-17 [143]. The transformations of these radicals are responsible to the yellowing of the surface of cellulose fibers.

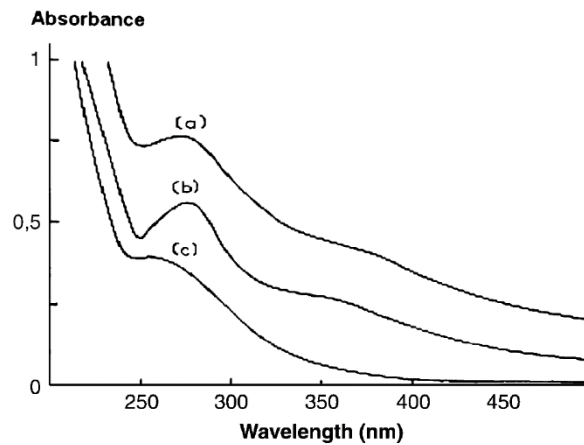


Fig. 3-16 Refection spectra of a) wood; b) lignin and c) cellulose [98].

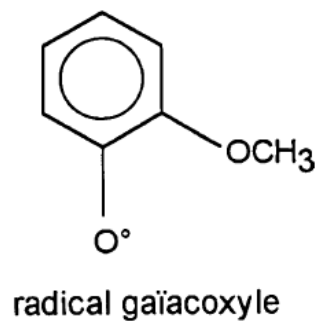


Fig. 3-17 Guaiacoxy radical from irradiated softwood lignin [143].

## 3.4 Conclusion

In this chapter, the effects of relative humidity on the PP/hemp composites were investigated firstly. When exposed to humid environment, because of their hydrophilicity, natural fibers will absorb water molecules. Consequently, decreases of mechanical properties of the PP/composites occurred according to the experimental results.

The moisture absorption of the composites reached saturation after 4 weeks immersion in water. The saturation level of water was related to the fiber loading

and matrix/fiber interfacial adhesion. Lower fiber loading and good matrix/fiber interfacial adhesion restrain the moisture absorption. Diffusion is the most important mechanism in moisture absorption. The kinetics of water diffusion in PP/hemp composites was verified to apply to Fickian diffusion law. The kinetic parameters were figured out by fittings of the absorption data. Higher fiber loading and poor matrix/fiber interfacial adhesion facilitates the water diffusion.

Swelling is a resulted phenomenon after moisture absorption. The dimension stability of the samples was taken into consideration. The thickness of the samples were measured and recorded. The thickness of the samples increased rapidly at the early stage, and then slowed down, until a plateau region was achieved. Higher fiber loading led to higher swelling ratio.

In the second part, the effects of Ultra-violet ageing on the composites were studied. In the first two weeks, the composites were not much affected. After 4 weeks, the mechanical properties of the composites showed a remarkable decrease. The fracture of the composites showed that the fibers were pulled out from the matrix, indicating poor matrix/fiber interfacial adhesion.

From the observation of the surface appearances of the composites, the composites were found to be more and more whitened until 8 weeks' UV ageing. After UV radiation, the PP surface appeared micro-cracks. As the UV ageing proceeded, the cracks propagated much longer and thicker after 8 weeks, even a successive crack formed. This reflected in the decrease of the mechanical properties. Crack propagation, chemical-crystallization and lignin degradation affect the total degradation of the composites.



## **Chapter 4.**

# **Residual Stress and Its Influence On the Mechanical Properties of Composites**

## **Chapter 4. Residual Stress and Its Influence On the Composites**

4.1	Introduction.....	99
4.2	The hole drilling method.....	99
4.2.1	History of the hole drilling method.....	99
4.2.2	Incremental hole drilling method.....	103
4.3	Determination of the coefficients of calibration .....	109
4.4	The drilling process.....	113
4.4.1	Strain-gage rosette .....	113
4.4.2	Drilling dispositions.....	115
4.4.3	The hole drilling process.....	115
4.5	Residual stresses in the composites .....	116
4.5.1	Strains measured in the composites .....	117
4.5.2	Residual stresses in the composites .....	117
4.5.2.1	Influence of temperature .....	117
4.5.2.2	Influence of cooling rate .....	119
4.5.2.3	Influence of humidity ageing.....	120
4.6	Conclusion .....	122

## **4.1 Introduction**

In the last chapter, the composites under different environmental ageing are analyzed. Because of the mismatch of thermal expansion coefficients of fibers and matrices during curing from a high temperature, or of the different performances under ageing conditions, fibers and matrices would show great differences of all kinds. In this chapter, the residual stresses in the composites will be investigated. And the influence of the residual stress on the mechanical properties will be discussed.

In the manufacturing process of composites, thermal residual stresses emerge on account to the shrinkage and mismatch of thermal expansion coefficients between the fibers and matrices, between the plies with different orientations for composite laminates. Since residual stresses exist in almost all composite materials, influence and even deteriorate the properties of composites, leading to the failure of a component below the design load or prior to its design service life under fatigue load. It is of great importance to identify, determine the residual stresses and take them into consideration during composite component design and modelling.

## **4.2 The hole drilling method**

### **4.2.1 History of the hole drilling method**

The hole drilling method in order to measure the residual stresses dates from the 1930s. Josef Mathar et al. [144] invented a method is based on a disturbance of the equilibrium of forces. It is assumed that the hole is very small, and the stress is uniform ignoring the thickness effect. This method is limited to the macroscopically homogeneous and isotropic materials. Attention should be paid during the hole drilling, the installation of the gage and the strain-gage readings.

In 1966, N. J. Rendler and I. Vigness [108] improved this method by eliminating the necessity of the calibration for every material. They obtained the magnitudes and principal directions of residual stresses at the hole location by this method. When the hole is drilled, an empirically relation between the magnitudes and directions of the principal stresses and the strain relaxation about the hole is employed for a non-dimensional model. In a uniaxial-stressed material, to drill a hole will change the strain distribution around the hole in the surface. As shown in Fig. 4-1 [108], the change of strain from a depth  $z$  to a depth of  $z+\Delta z$  is:

$$\Delta\varepsilon_z(\alpha) = K_z(\alpha)\sigma_z\Delta z \quad (4-1)$$

where  $\Delta\varepsilon_z(\alpha)$ : the change of strain in the surface;

$\alpha$ : angle between the stress axis and a supposed radical direction;

$K_z(\alpha)$ : a parameter related to  $z$ ,  $\Delta z$  and  $\alpha$ ;

$\sigma_z$ : residual stress at depth  $z$ .

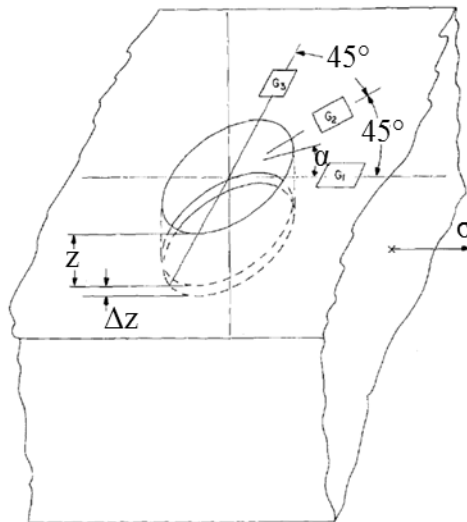


**Fig. 4-1 Hole-gage assembly in a stressed plate [108]**

For calculation simplicity, we will consider the case in which the full depth ( $z$ ) of the hole is drilled, and:

$$\varepsilon(\alpha) = K(\alpha)\sigma \tag{4-2}$$

If we consider two principal stresses in a plane parallel to the material surface, and orthometric to each other, the formulation gives as:

$$\varepsilon(\alpha) = K(\alpha)\sigma_1 + K\left(\alpha + \frac{\pi}{2}\right)\sigma_2 \tag{4-3}$$

where  $\alpha$  is measured from the direction of the maximum stress  $\sigma_{\max}$ .

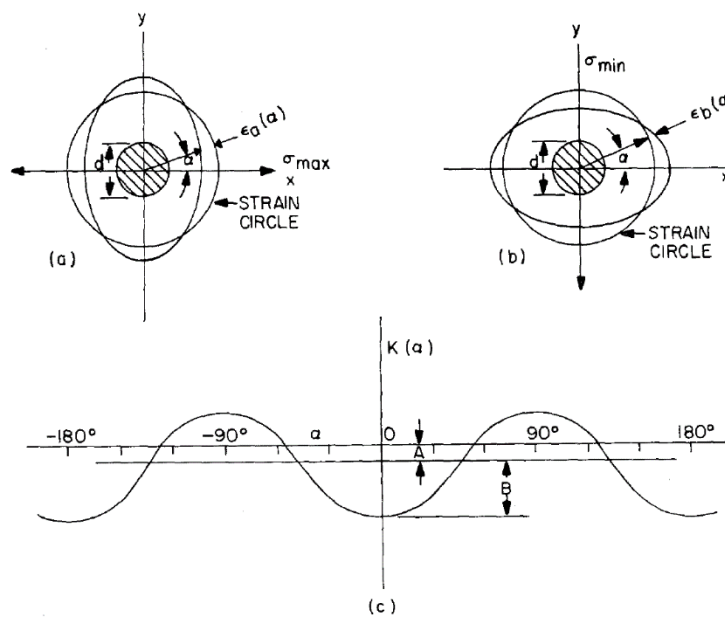


**Fig. 4-2 Strain as the radial distance between gage circle and ellipse is shown for uniaxial stress along a) axis x, b) axis y. c) the strain (in rectangular coordinates, proportional to  $K(\alpha)$ ) [108].**

The radial strain caused by drilling a hole of diameter (d) at a fixed distance from the hole is shown in the polar diagram in Fig. 4-2 [108]. In the two respective cases, there exist uniaxial stresses in the x and y directions. So  $K(\alpha)$  is an even function, it can be represented by:

$$K(\alpha) = \sum_n A_n \cos 2n\alpha , n = 0, 1, 2, 3 \dots \tag{4-4}$$

In an approximate way, only retain the first two terms, thus:

$$K(\alpha) = A + B \cos 2\alpha \quad (4-5)$$

With substitution, Eq. (4-3) becomes:

$$\begin{aligned} \varepsilon(\alpha) = [A + B \cos 2(\theta - \beta)]\sigma_1 + \\ \left[ A + B \cos 2\left(\theta - \beta + \frac{\pi}{2}\right) \right] \sigma_2 \end{aligned} \quad (4-6)$$

where  $\beta$ : angle between the x-axis and the direction of  $\sigma_1$ ;

$\theta$ : angle between x-axis and a radial direction;

$\alpha$ :  $\alpha = \theta - \beta$ , angle between the radial direction and  $\sigma_1$ .

There are 3 unknowns in Eq. (4-6),  $\alpha$ ,  $\sigma_1$  and  $\sigma_2$ . It is possible to get the solution of the two principle stresses and the angle  $\alpha$  by applying known stresses and measuring the strain. It is convenient to let  $\theta = 0, \frac{\pi}{4}, \frac{\pi}{2}$ . The principal stresses and their directions can thus be determined as:

$$\begin{cases} \sigma_1 = \frac{(A+B \sin \gamma)\varepsilon_1 - (A-B \cos \gamma)\varepsilon_2}{2AB(\sin \gamma + \cos \gamma)} \\ \sigma_2 = \frac{(A+B \cos \gamma)\varepsilon_1 - (A-B \sin \gamma)\varepsilon_2}{2AB(\sin \gamma + \cos \gamma)} \\ \gamma = \tan^{-1} \left( \frac{\varepsilon_1 - 2\varepsilon_2 + \varepsilon_3}{\varepsilon_1 - \varepsilon_3} \right) \end{cases} \quad (4-7)$$

where,  $\gamma = -2\beta$ .

Although this method facilitates the determination of the residual stresses, there are still obvious limitations. It can only be applied to elastic, isotropic materials. In 1968, Charles W. Bert and Gary L. Thompson [145] developed a method for determining the principal residual stresses and directions in rectangularly orthotropic materials. A third constant C was brought into their theory.

A material is stressed in a generalized-plane-stress field ( $\sigma_{11}, \sigma_{22}, \sigma_{12}$ ). The change of strain which occurs at any location at a fixed radial distance from the

hole center can be expressed as:

$$\varepsilon(\alpha) = K(\alpha)\sigma_{11} + K\left(\alpha + \frac{\pi}{2}\right)\sigma_{22} + L(\alpha)\sigma_{12} \quad (4-8)$$

where,  $\alpha$ : angle between the radial direction and  $\sigma_{11}$ ;

$\varepsilon(\alpha)$ : the change of strain at angle  $\alpha$ ;

$K(\alpha)$ ,  $L(\alpha)$ : strain distribution functions dependent on the angle  $\alpha$ .

Over the following time, many researchers have made much effort to complete this method. N.K. Naik and R.D. Sahani [146] studied the residual stress of glass fabric reinforced composite by hole drilling method. Jia-yong Wang [147] investigated the influence of the hole position on the final stresses, and proposed a solution available for the center or off-center hole-drilling cases and for the case of which the array of gages is arbitrary. C.B. Prasad et al. [148, 149] have tried to obtain the hole-drilling calibration constants for thin isotropic orthotropic composite materials, by employing Savin's complex stress function approach. G.S. Schajer and L. Yang [150] described a new stress-calculation method based on the analytical solution for the displacement field around a hole in a stressed orthotropic plate with assessed validity through experimental measurements. M.M. Shokrieh and A.R. Ghasemi K. [151] presented a new method for calculating the calibration factors for orthotropic materials, and made comparison with theoretical values.

### **4.2.2 Incremental hole drilling method**

In the hole drilling method, a fundamental problem is to find a relation between the strains in material surface and the internal residual stresses of this material. In spite of the further development of this method, its limitations for determining uniform stresses along the depth of the hole cannot be neglected. In our study, we are interested in the distribution of the residual stresses in the composite laminates. The stress distribution along the thickness of the material is

not uniform. It's necessary for us to employ the incremental hole drilling method. The incremental hole drilling method was utilized by O. Sicot and X.L. Gong [152, 153] to determine and analyze the residual stresses in composite laminates. We applied a new approach developed by Wen [154] to build the relation between the strains in surface and the internal residual stresses.

The assumptions are as follows: the material is elastic and orthotropic; the stress component ( $\sigma_{zz}$ ) perpendicular to the surface plane is very small and can be neglected [152]. So the residual stresses in the composites are in a plane-stress state. We define a global Cartesian coordinate system for the plate, where the direction 'x' represents the direction of the direction of the fiber. There is an angle  $\beta$  between the principal stress direction 'X' and the direction 'x'. The measured strain is supposed to be at an angle  $\theta$  from the reference axis 'x', as shown in Fig. 4-3.

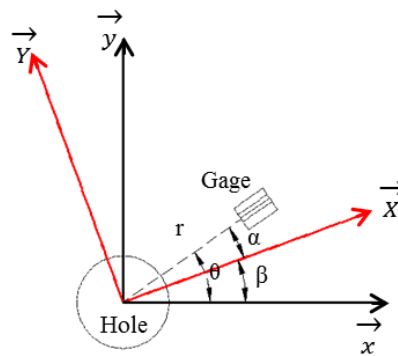


**Fig. 4-3 Coordinate system diagram, the stress component and the location of strain-gage**

The stress tensor can be formulated after conversion to cylindrical coordinate:

$$\sigma_{(0,r,\theta)} = \begin{bmatrix} \sigma_r & \tau_{r\theta} \\ \tau_{r\theta} & \sigma_\theta \end{bmatrix} \quad (4-9)$$

and

$$\begin{cases} \sigma_r = \frac{\sigma_x + \sigma_y}{2} + \frac{\sigma_x - \sigma_y}{2} \cos 2\theta + \tau_{xy} \sin 2\theta \\ \sigma_\theta = \frac{\sigma_x + \sigma_y}{2} - \frac{\sigma_x - \sigma_y}{2} \cos 2\theta - \tau_{xy} \sin 2\theta \\ \tau_{r\theta} = -\frac{\sigma_x - \sigma_y}{2} \sin 2\theta + \tau_{xy} \cos 2\theta \end{cases} \quad (4-10)$$

$$\begin{cases} \sigma_x = \frac{1}{2}X - \frac{1}{2}Y \cos 2\beta \\ \sigma_y = \frac{1}{2}X + \frac{1}{2}Y \cos 2\beta \\ \tau_{xy} = \frac{1}{2}Y \sin 2\beta \\ X = \sigma_1 + \sigma_2 \\ X = \sigma_1 - \sigma_2 \end{cases} \quad (4-11)$$

According to the elastic theory of anisotropic materials, the Hooke's law for materials without the drilled hole is:

$$\begin{pmatrix} \epsilon_r \\ \epsilon_\theta \\ \epsilon_{r\theta} \end{pmatrix} = C \begin{pmatrix} \sigma_r \\ \sigma_\theta \\ \sigma_{r\theta} \end{pmatrix} \quad (4-12)$$

where, C is the compliance tensor:

$$C = \begin{bmatrix} C_{xx} & C_{xy} & C_{xs} \\ Z & Z & Z \\ Z & Z & Z \end{bmatrix} \quad (4-13)$$

The above relation doesn't apply to the drilled hole. We introduce three unknowns ( $f_1, f_2, f_3$ ) depending on the hole and the material, so Eq. (4-13) becomes:

$$\begin{pmatrix} \epsilon_r \\ \epsilon_\theta \\ \epsilon_{r\theta} \end{pmatrix} = \begin{bmatrix} C_{xx}f_1 & C_{xy}f_2 & C_{xs}f_3 \\ Z' & Z' & Z' \\ Z' & Z' & Z' \end{bmatrix} \begin{pmatrix} \sigma_r \\ \sigma_\theta \\ \sigma_{r\theta} \end{pmatrix} \quad (4-14)$$

Then, by employing the above equations, the radial strain around the hole is:

$$\epsilon_r = \frac{C_{xx}f_1 + C_{xy}f_2}{2} X + \frac{C_{xx}f_1 - C_{xy}f_2}{2} Y \cos 2(\theta - \beta) + C_{xs}f_3 Y \sin 2(\beta - \theta) \quad (4-15)$$

If we define  $A = \frac{C_{xx}f_1 + C_{xy}f_2}{2}$ ,  $B = \frac{C_{xx}f_1 - C_{xy}f_2}{2}$  and  $C = C_{xs}f_3$ , then:

$$\varepsilon_r = AX + BY \cos 2(\theta - \beta) + CY \sin 2(\beta - \theta) \quad (4-16)$$

If the strain-gage rosette is configured as shown in Fig. 4-4, the strains  $\varepsilon_1$ ,  $\varepsilon_2$ ,  $\varepsilon_3$  correspond to  $\theta=0$ ,  $-\frac{3}{4}\pi$ ,  $\frac{1}{2}\pi$ , respectively. The strains are:

$$\begin{cases} \varepsilon_1 = \varepsilon_0 = AX + BY \cos 2(0 - \beta) + CY \sin 2(\beta - 0) \\ \varepsilon_2 = \varepsilon_{-\frac{3}{4}\pi} = AX + BY \cos 2\left(-\frac{3}{4}\pi - \beta\right) + CY \sin 2\left(\beta + \frac{3}{4}\pi\right) \\ \varepsilon_3 = \varepsilon_{\frac{1}{2}\pi} = AX + BY \cos 2\left(\frac{1}{2}\pi - \beta\right) + CY \sin 2\left(\beta - \frac{1}{2}\pi\right) \end{cases} \quad (4-17)$$

and,

$$\begin{cases} \sigma_1 = \frac{(A - B \sin \varphi + C \cos \varphi) \varepsilon_1 - (A - B \cos \varphi - C \sin \varphi) \varepsilon_2}{2A[B(\cos \varphi - \sin \varphi) + C(\cos \varphi + \sin \varphi)]} \\ \sigma_2 = -\frac{(A + B \sin \varphi - C \cos \varphi) \varepsilon_1 - (A + B \cos \varphi + C \sin \varphi) \varepsilon_2}{2A[B(\cos \varphi - \sin \varphi) + C(\cos \varphi + \sin \varphi)]} \\ \tan \varphi = \frac{B(\varepsilon_3 + \varepsilon_1 - 2\varepsilon_2) - C(\varepsilon_1 - \varepsilon_3)}{C(2\varepsilon_2 - \varepsilon_1 - \varepsilon_3) - B(\varepsilon_1 - \varepsilon_3)}, \quad \varphi = 2\beta \end{cases} \quad (4-18)$$

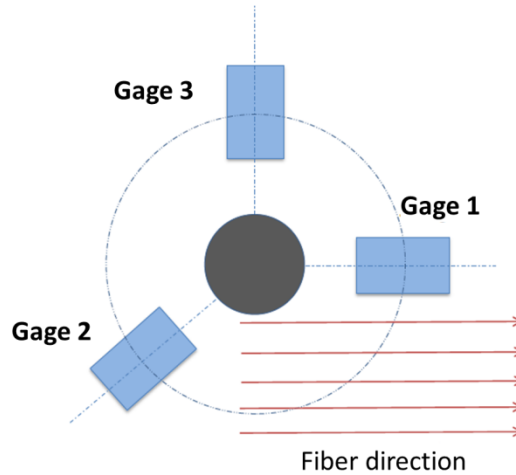


**Fig. 4-4 The configuration of the strain-gage rosette**

When adapting the incremental hole drilling method, we consider that the model is valid for a thin layer of thickness  $h_i$ , and that the residual stresses are constant along the depth of this layer. After each drilling increment, the strains

change is induced by the change of the hole geometry and the redistribution of the stresses. After the  $n^{\text{th}}$  increment, the residual stress in the  $i^{\text{th}}$  layer ( $i < n$ ) is already known as  $\sigma_{1i}$ ,  $\sigma_{2i}$ ,  $\beta_i$ . The induced strain in this layer is:

$$\begin{aligned} \varepsilon_{in} = & A_{in}(\sigma_{1i} + \sigma_{2i}) + B_{in}(\sigma_{1i} - \sigma_{2i})\cos 2(\theta - \beta_i) + \\ & C_{in}(\sigma_{1i} - \sigma_{2i})\sin 2(\beta_i - \theta) \end{aligned} \quad (4-19)$$

where,

$\sigma_{1i}$ ,  $\sigma_{2i}$ : principal residual stresses of the  $i^{\text{th}}$  layer;

$\varepsilon_{in}$ : contribution of the  $i^{\text{th}}$  increment to the total strain of the  $n^{\text{th}}$  increment;

$A_{in}$ ,  $B_{in}$ ,  $C_{in}$ : coefficients of calibrations in the  $i^{\text{th}}$  layer of the  $n^{\text{th}}$  increment;

$\beta_i$ : angle between the direction of principal residual stresses in the  $i^{\text{th}}$  layer and the supposed direction  $\vec{x}$ ;

$\theta$ : angle between strain-gage and the supposed direction  $\vec{x}$ .

In fact, each removed layer previously affects the total strain measured in the surface, so the change of the hole geometry should be taken in account. According to previous research [152-154], the strain due to the remove of the last layer is:

$$\varepsilon_{nn} = \varepsilon_{tn} - \sum_{i=1}^{n-1} \varepsilon_{in} \quad (4-20)$$

where,  $\varepsilon_{tn}$  is the strain measured right after the  $n^{\text{th}}$  increment.

An example is presented for better understanding the incremental analysis: a model of three increments,  $n=3$ , as shown in Fig. 4-5.

In the first step of the incremental drilling method,  $h_i=h_1$ , one layer is drilled. The measured strain in surface ( $\varepsilon_{t1}^1$ ) is the strain ( $\varepsilon_{11}^1$ ) induced by the relaxation of the residual stresses in the first layer. We get the following equations:

$$\begin{aligned}
 \varepsilon_{t1}^1 &= \varepsilon_{11}^1 = A_{11}(\sigma_{11} + \sigma_{21}) + B_{11}(\sigma_{11} - \sigma_{21}) \cdot \cos 2(\theta^1 - \beta_1) + C_{11}(\sigma_{11} - \sigma_{21}) \\
 &\quad \cdot \sin 2(\beta_1 - \theta^1) \\
 \varepsilon_{t1}^2 &= \varepsilon_{11}^2 = A_{11}(\sigma_{11} + \sigma_{21}) + B_{11}(\sigma_{11} - \sigma_{21}) \cdot \cos 2(\theta^2 - \beta_1) + C_{11}(\sigma_{11} - \sigma_{21}) \\
 &\quad \cdot \sin 2(\beta_1 - \theta^2) \\
 \varepsilon_{t1}^3 &= \varepsilon_{11}^3 = A_{11}(\sigma_{11} + \sigma_{21}) + B_{11}(\sigma_{11} - \sigma_{21}) \cdot \cos 2(\theta^3 - \beta_1) + C_{11}(\sigma_{11} - \sigma_{21}) \\
 &\quad \cdot \sin 2(\beta_1 - \theta^3)
 \end{aligned}
 \tag{4-21}$$

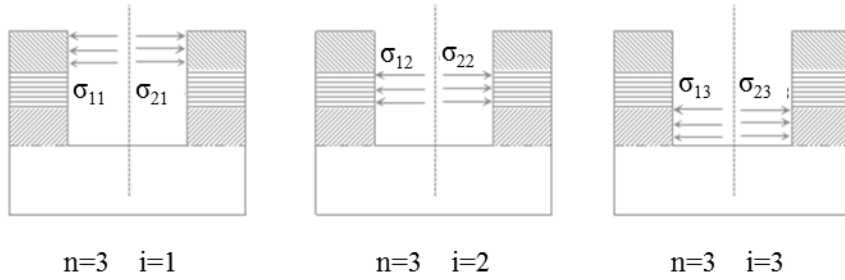


**Fig. 4-5 An example of the incremental analysis**

In the second step, a second layer is removed,  $h_i=h_2$ . That the strain induced by the residual stresses in the  $n^{\text{th}}$  layer, for each increment, is the difference between the total strain measured in the surface and the strain induced by the residual stresses in all the preceding layers. The strain ( $\varepsilon_{22}^1$ ) induced by the relaxation of the residual stresses in the second layer is:

$$\varepsilon_{22}^1 = \varepsilon_{t2}^1 - \varepsilon_{12}^1$$

$$\begin{aligned}
 \varepsilon_{12}^1 &= A_{12}(\sigma_{11} + \sigma_{21}) + B_{12}(\sigma_{11} - \sigma_{21}) \cdot \cos 2(\theta^1 - \beta_1) + C_{12}(\sigma_{11} - \sigma_{21}) \\
 &\quad \cdot \sin 2(\beta_1 - \theta^1)
 \end{aligned}
 \tag{4-22}$$

In the same way, we can get the strain in the third layer by applying the Eq. (4-19),

$$\varepsilon_{33}^1 = \varepsilon_{t3}^1 - \sum_{i=1}^2 \varepsilon_{i3}^1 = \varepsilon_{t3}^1 - \varepsilon_{13}^1 - \varepsilon_{23}^1$$

$$\begin{aligned}
 \varepsilon_{13}^1 &= A_{13}(\sigma_{11} + \sigma_{21}) + B_{13}(\sigma_{11} - \sigma_{21}) \cdot \cos 2(\theta^1 - \beta_1) + C_{13}(\sigma_{11} - \sigma_{21}) \\
 &\quad \cdot \sin 2(\beta_1 - \theta^1) \\
 \varepsilon_{23}^1 &= A_{23}(\sigma_{12} + \sigma_{22}) + B_{23}(\sigma_{12} - \sigma_{22}) \cdot \cos 2(\theta^1 - \beta_1) + C_{23}(\sigma_{12} - \sigma_{22}) \\
 &\quad \cdot \sin 2(\beta_1 - \theta^1) \\
 \varepsilon_{33}^1 &= A_{33}(\sigma_{13} + \sigma_{23}) + B_{12}(\sigma_{13} - \sigma_{23}) \cdot \cos 2(\theta^1 - \beta_1) + C_{12}(\sigma_{13} - \sigma_{23}) \\
 &\quad \cdot \sin 2(\beta_1 - \theta^1)
 \end{aligned}
 \tag{4-23}$$

Also, the strain induced by the residual stresses in the 3<sup>rd</sup> layer for strain-gages 2 and 3 can be obtained in the same way,  $\varepsilon_{33}^2$  and  $\varepsilon_{33}^3$ .

If the strain-gage rosette is placed on the surface of the samples in the three directions:  $\theta^1 = 0$ ,  $\theta^2 = -\frac{3}{4}\pi$ ,  $\theta^3 = \frac{1}{2}\pi$ , the residual stresses in the third layer are determined as:

$$\left\{ \begin{aligned}
 \sigma_{13} &= \frac{(C_{33} \cos \varphi_3 + A_{33} - B_{33} \sin \varphi_3) \varepsilon_{33}^1 + (B_{33} \cos \varphi_3 + C_{33} \sin \varphi_3 - A_{33}) \varepsilon_{33}^2}{2A_{33}[B_{33}(\cos \varphi_3 - \sin \varphi_3) + C_{33}(\cos \varphi_3 + \sin \varphi_3)]} \\
 \sigma_{23} &= \frac{(C_{33} \cos \varphi_3 - A_{33} - B_{33} \sin \varphi_3) \varepsilon_{33}^1 + (B_{33} \cos \varphi_3 + C_{33} \sin \varphi_3 + A_{33}) \varepsilon_{33}^2}{2A_{33}[B_{33}(\cos \varphi_3 - \sin \varphi_3) + C_{33}(\cos \varphi_3 + \sin \varphi_3)]} \\
 \tan \varphi_3 &= \frac{B_{33}(\varepsilon_{33}^1 + \varepsilon_{33}^3 - 2\varepsilon_{33}^2) + C_{33}(\varepsilon_{33}^3 - \varepsilon_{33}^1)}{C_{33}(2\varepsilon_{33}^2 - \varepsilon_{33}^1 - \varepsilon_{33}^3) + B_{33}(\varepsilon_{33}^3 - \varepsilon_{33}^1)}, \varphi_3 = 2\beta_3
 \end{aligned} \right.
 \tag{4-24}$$

In this way, it allows us to associate the strains in the surface and the residual stresses in the composites. This new approach is appropriate for our application, according to the above analysis.

### 4.3 Determination of the coefficients of calibration

After established the relationship between the stresses and deformations, the

following step is to determine the calibration coefficients ( $A_{in}$ ,  $B_{in}$  and  $C_{in}$ ) in the solution and to measure the deformations in the sample surface. The finite element method was developed to determine those coefficients of calibration.

The principle of simulation involves the incremental hole drilling, applying different known loads, measuring the displacements on the surface of the simulated plate, at last calculating the coefficients through the suitable equations. So a computational method based on finite element analysis was developed. ABAQUS/Standard was utilized to accomplish model building and computation. With our program, we could figure out the calibration coefficients by considering the plate geometry, the position of the strain gage rosette, the configuration of the composites and the elastic constants of the materials and so on.

A model is created by the software ABAQUS and program language Python. The data bases are the materials constants (Young's modulus, shear modulus, etc.), the structure parameters of the materials (number of layers, thickness of layers, etc.) and the configuration of the strain gages (their positions and geometries, etc.). The model is assigned with finite elements of type C3D8 and C3D6. In order to apply the incremental method, we define the sets which represent the elements at the position of the hole. While we go forward every time, we remove the corresponding sets. The Fig. 4-6 shows the finite element model built in Abaqus.

When conduct the determination of the coefficients it's necessary to keep in mind that the cylindrical loads should be in the opposite directions with respect to the supposed residual stresses. For  $A_{in}$ , we suppose an equi-biaxial stress state ( $\sigma_{1i}=\sigma_{2i}=\sigma$ ,  $\beta_i=0$ ) at the hole inside of the model, as shown in Fig. 4-7. In the cylindrical coordinates, it becomes:  $\sigma_{ri}=-\sigma$  and  $\sigma_{r\theta i}=0$ , which is equivalent to an uniform pressure  $p=\sigma$  on the lateral surface of the  $i^{\text{th}}$  layer, as shown in . Thus, the Eq. (4-19) becomes:

$$\varepsilon_{in} = 2\sigma A_{in} \quad (4-25)$$

$$A_{in} = \varepsilon_{in}/2\sigma \quad (4-26)$$

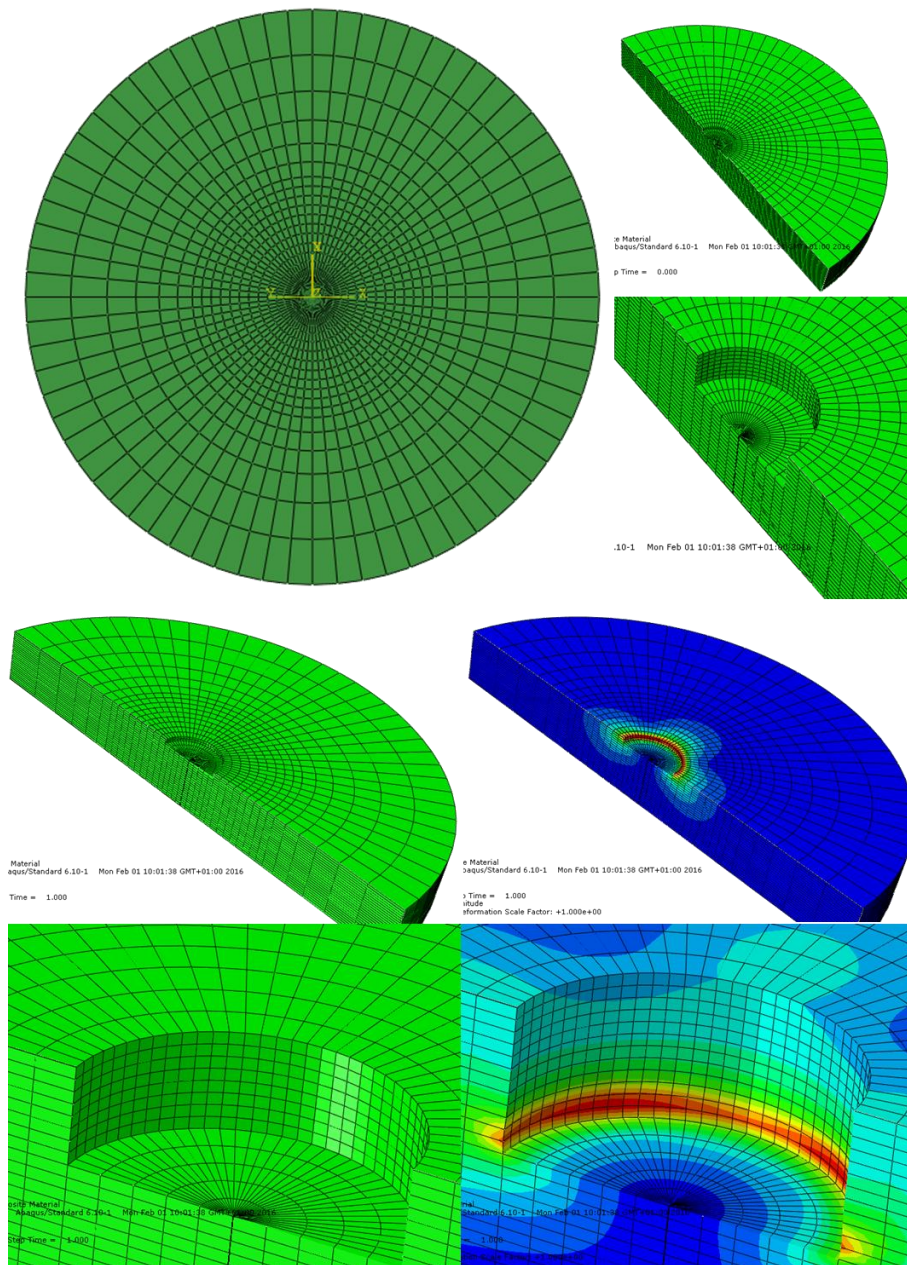


Fig. 4-6 The finite element model

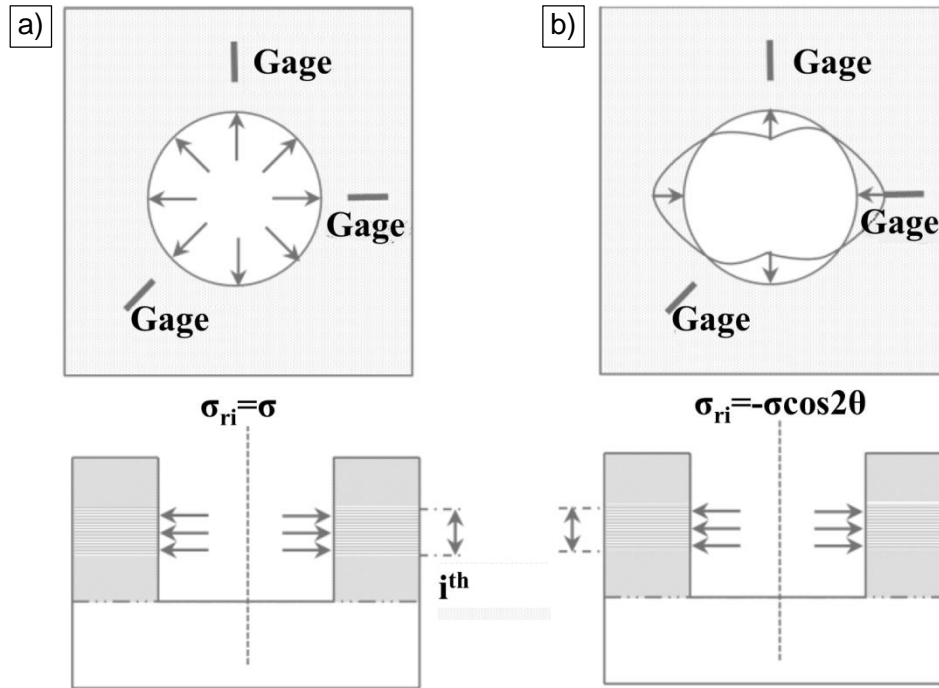


Fig. 4-7 Two types of applied loadings during the determination of the coefficients of calibration

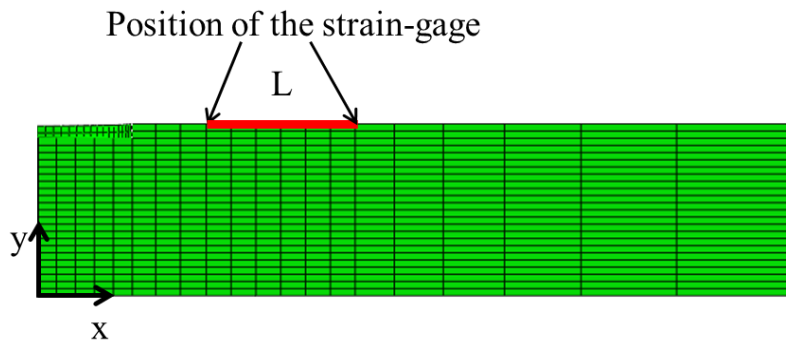


Fig. 4-8 Position of the strain-gage attached on the composites

The coefficients  $B_{in}$  and  $C_{in}$  can be determined in the same way by applying a stress state:  $\sigma_{1i} = -\sigma_{2i} = \sigma$  and  $\beta_i = 0$ . It can be regarded as a radial stress  $\sigma_{ri} = -\sigma \cos(2\theta)$  and  $\sigma_{r\theta i} = \sigma \sin(2\theta)$ , as shown in Fig. 4-7. Thus, the Eq. (4-19) becomes:

$$\varepsilon_{in} = 2\sigma B_{in} \cos 2\theta - 2\sigma C_{in} \sin 2\theta \quad (4-27)$$

If we know the strain  $\varepsilon_{in}(\theta=0)$ , and  $\varepsilon_{in}(\theta=\pi/2)$ , then:

$$\begin{cases} B_{in} = \varepsilon_{in}(\theta = 0)/2\sigma \\ B_{in} = -\varepsilon_{in}(\theta = \pi/2)/2\sigma \end{cases} \quad (4-28)$$

The radial strain can be determined from the radial displacement  $U(r, \theta)$ , where  $r$  and  $\theta$  indicate the displacement position in the model (in Fig. 4-8) :

$$\varepsilon_{in}(\theta) = \frac{U_{in}(r_2, \theta) - U_{in}(r_1, \theta)}{L} \quad (4-29)$$

where,  $U_{in}(r_1, \theta)$  and  $U_{in}(r_2, \theta)$  are the displacements at position  $r_1$  and  $r_2$  in the direction  $\theta$ ; and  $L=r_2-r_1$  is the distance between  $r_1$  and  $r_2$ .

Then we get all the three coefficients as:

$$\begin{cases} A_{in} = \frac{U_{in}(r_2, 0) - U_{in}(r_1, 0)}{2\sigma L} \\ B_{in} = \frac{U_{in}(r_2, 0) - U_{in}(r_1, 0)}{2\sigma L} \\ C_{in} = \frac{U_{in}(r_2, \frac{\pi}{4}) - U_{in}(r_1, \frac{\pi}{4})}{2\sigma L} \end{cases}, \quad \sigma_{1i} = \sigma_{2i} = \sigma, \quad \beta_i = 0 \quad (4-30)$$

Finally, all the coefficients of calibration are thus determined. It is necessary to repeat this process for all the previous increments. In this simulation, the coefficients of calibration depend on the parameters of the drill, the hole geometry, the strain-gage type, the strain-gage position and the material properties. As a consequent, every time the experimental parameters are changed, the model of calibration should also be modified to figure the corresponding coefficients of calibration.

## 4.4 The drilling process

The incremental hole drilling method has been presented in previous sections; the strains will be measured in the next step. In this part, we introduced the strain-gage rosette and the drilling process.

### 4.4.1 Strain-gage rosette

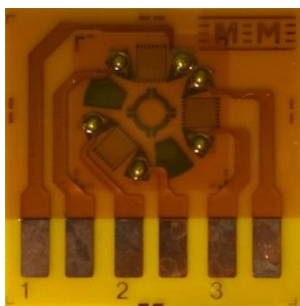
For measuring the strains, the strain-gage rosette is the most important. A hole was milled in the center of the strain-gage rosette with the allowed tolerance on the diameter, so it is very important to choose an appropriate gage rosette.

According to the research of [152], the parameters of the gages have a pronounced influence on the sensibility of measuring during the practice of the method. The relative position between the gages and the hole is a fundamental factor in the method. The gage geometry has less influence over the measuring precision. The gages shouldn't be too close to the hole to avoid the unexpected interactions with the hole zone, and not be too far away from the hole resulting in loss of information of the strains. Thus the evolution of the deformation on surface can be correctly recorded during the hole drilling process.

The type of gages utilized in our study for the determination of the residual stresses was provided by the company Vishay Precision Group Micro-Measurement® 'TEA-06-062RK-120'. The parameters of this gage are presented in the following Table 4-1. These parameters were used during the determination of the coefficients of calibration.

**Table 4-1 The parameters of the strain gages**

Designation	Dimensions (mm)			
	Gage length	Diameter of gage center circle	Hole diameter	
min			max	
TEA-06-062RK-120	1.57	5.13	1.5	2.0



Before gluing the gages to the surface of the test samples, we cleaned the contacting surfaces of the samples and the gage rosette. Exclusive attention is necessary during the bonding, and the bonding layer is better as thin as possible. Different wires were welded to the corresponding welding spots of the gages. Then the gages are connected with an instrument and a computer through cables of data-acquisition. As long as the samples are prepared, they are fixed onto a holder in order to conduct the experiments and measurements.

## 4.4.2 Drilling dispositions

When applying the incremental hole drilling method, the parameters of the drilling process can affect the hole quality and the hole geometry, and finally the residual stresses. These parameters can be the type of the drill, drill feeding speed, drill rotation speed, incremental depth and the hole diameter, and so on.

The direct factor is the abrasion between the drill and the materials. For laminate materials, the common problems are delaminating. An example of the comparison of the hole quality is shown in Fig. 4-9. Fig. 4-9 a) shows a hole drilled with high quality, but b) and c) are those with defects and flaws around the hole or the wall. These problems may occur during the drilling process, so it is necessary to choose suitable the drill feeding and rotation speed. The other parameters are determined beforehand by the strain gages and the readymade devices.



**Fig. 4-9 Comparison of the hole quality**

The drilling systems (Fig. 4-10) including the drill devices and the holder are supported by an air cushion table, so as to avoid the influences of vibrations. The drilling device of micrometric displacement is controlled by computer commands, it can move to any positions. The drill works under the help of a driver screw with a displacement resolution of 1  $\mu\text{m}$ .

## 4.4.3 The hole drilling process

The experiments of the incremental hole drilling method were carried out on the samples with the chosen parameters. We have drilled the holes until a depth of

900  $\mu\text{m}$ , half of the thickness of the composite plates. It was carried out in 6 steps, the first step to a depth of 150  $\mu\text{m}$ , retreat of the drill outside of the hole and measurements of the strains in the three positions of gages; and then the second step..., until completing the drilling process.

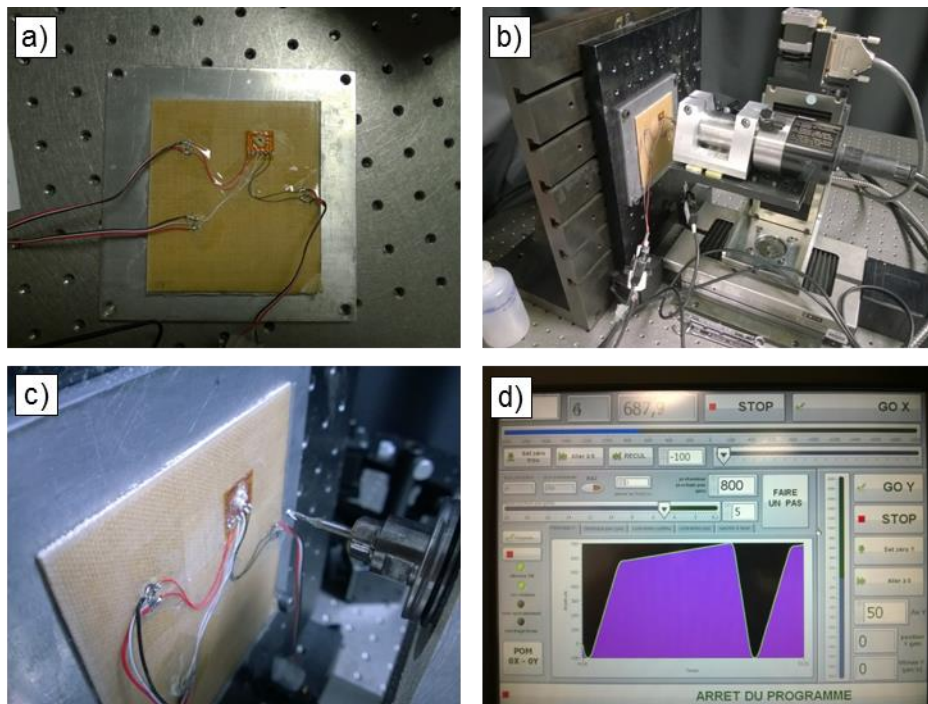


Fig. 4-10 Configurations of the drilling devices

## 4.5 Residual stresses in the composites

Stresses may occur, due to temperature differentials and moisture absorption, the intrinsic heterogeneous nature of composite materials, the different thermal and hygroscopic swelling of the components (fibers and matrices) and the adjacent plies, the cooling from the manufacturing temperature to room temperature. So the stresses occurred in composites should be assessed. We carried out several different experiments under different conditions to analyse and assess the residual stresses in the composites.

## 4.5.1 Strains measured in the composites

The strains induced by the relaxation of the residual stresses were measured by the strain gages fixed around the drilled hole. The incremental hole drilling method was firstly employed to the unaged PP/hemp composites. The tendency of the strains measured for different composites showed to be similar. So a following typical diagram is presented. The typical measured strains are shown in Fig. 4-11.

The tendency of the strain curves for all the composites are similar. It is observed that the measured strains of gage 1 elevate firstly until around the interface of the polypropylene layer and the hemp layer. Then the measured strains of Gage 1 alleviate until the end of the hole. For the gage 2, the values are always negative. The strains of gage 2 increase until the end of the hole. As for the gage 3, we find the similar tendency as gage 2.

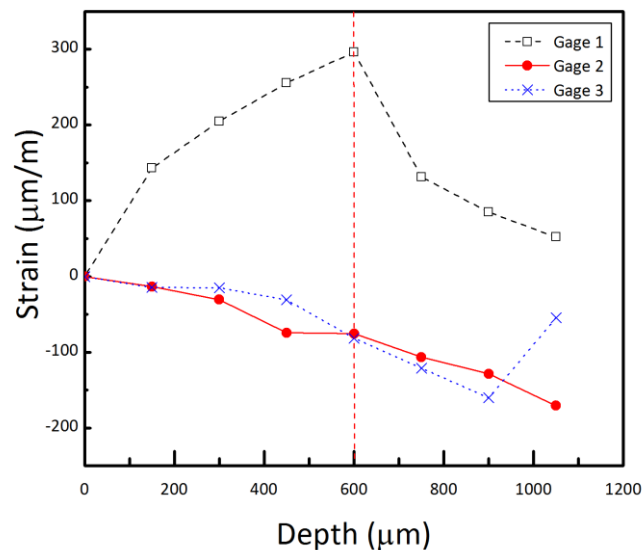


Fig. 4-11 Measured strains of PP/hemp composites by the strain gages

## 4.5.2 Residual stresses in the composites

### 4.5.2.1 Influence of temperature

It isn't easy to predict the residual stresses with the strain information around

the drilled hole. We can get the results of the residual stresses by using the previous work and analysis. The residual stresses in the composites under different manufacturing temperatures are presented in Fig. 4-12 and Fig. 4-13.

We can get several interesting information from the residual stresses of the composites. The residual stresses are divided into two parts: before the interface and after the interface (red line). For the residual stress  $\sigma_x$ , the negative values indicate that the PP layer suffers a compressive stress state (about -5.5 MPa); in the contrary way, the hemp layer suffers a tensile stress state (about 14.5 MPa). The stress  $\sigma_y$  shows almost the same magnitude in the PP layer (5 MPa), but in the hemp layer, it shows different values. The values at 900  $\mu\text{m}$  are very small, where it may be due to the hemp layer interface.

The temperature doesn't show a remarkable influence on the residual stresses of the composites. But for the residual stress in hemp layer, the stress increase with the increasing temperatures. According to our previous study in section 2.5.1.3, the hemp showed a decreased tendency in mechanical properties. The high temperature perhaps affected the hemp, and then affected the residual stresses.

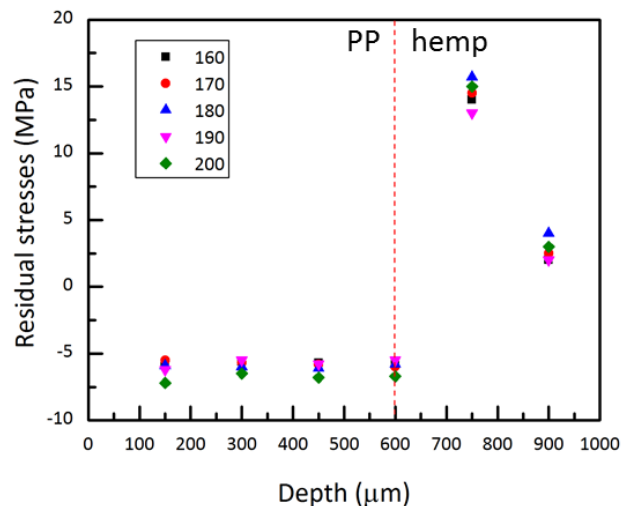


**Fig. 4-12 Residual stress  $\sigma_x$  under different temperatures**

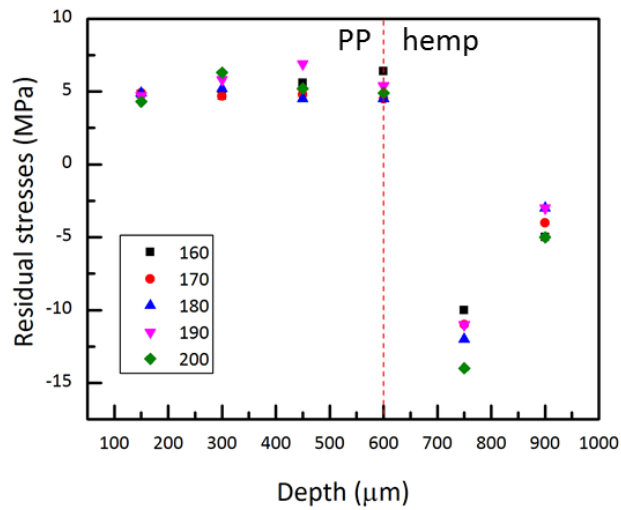


Fig. 4-13 Residual stress  $\sigma_y$  under different temperatures

#### 4.5.2.2 Influence of cooling rate

The incremental hole drilling method was carried out for the PP/hemp composites under different cooling rates (Fig. 4-14 and Fig. 4-15). The composites are cooled in the compression molding machine (slow), within the molds in air under the environmental temperature (medium) and being kept in the molds for 2h, then being demold to cool down in the air (fast).

The residual stresses in the composites show a similar tendency as the previous ones. The cooling rate has an important effect on the residual stresses. The stresses increase with the cooling rate. In the case of  $\sigma_x$ , the PP layer is under compression whereas the hemp layer is under traction and vice versa for  $\sigma_y$ .

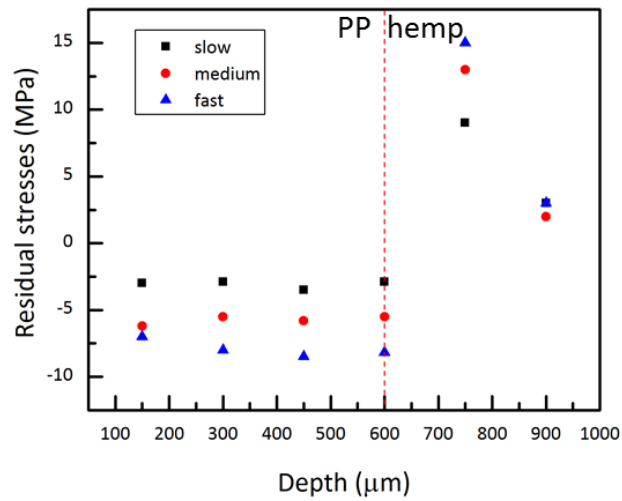


Fig. 4-14 Residual stress  $\sigma_x$  under different cooling rates

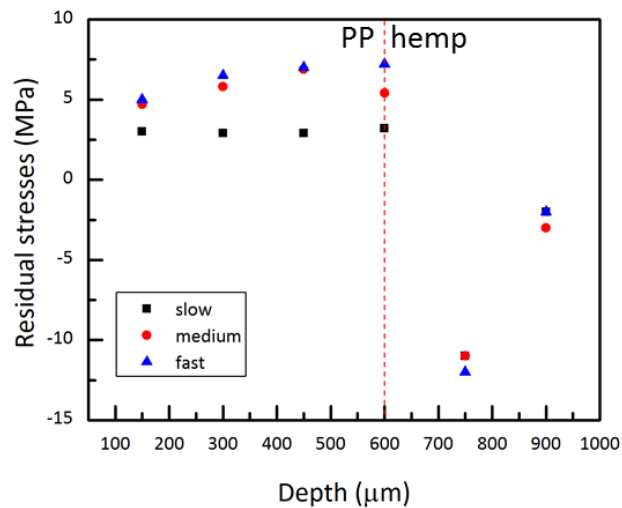


Fig. 4-15 Residual stress  $\sigma_y$  under different cooling rates

### 4.5.2.3 Influence of humidity ageing

Due to their intrinsic heterogeneity, emerging at the microscopic and at the macroscopic scale and related to the difference in hygrothermo-elastic properties of the adjacent fibers and matrices, fibers with different orientations, composites are very sensitive to hygrothermo-elastic influences.

Gigliotti M. et al. [155, 156] considered the water absorption as the origin of the interne stresses in composite laminates, and devoted to the modelling and the

simulation of hygrothermo-elastic stresses in composite laminated plates. So a relaxation of the residual stresses in composites may occur following the hygrothermal ageing process. We have measured and analyzed the mechanical properties of the PP/hemp composites after long-term humidity ageing. And its influence on the distribution of the residual stresses was then assessed.

The residual stresses of the hemp reinforced polypropylene composites were determined by incremental hole drilling method. The results are presented in Fig. 4-16 and Fig. 4-17. According to the results, the distribution of the residual stresses (both  $\sigma_x$  and  $\sigma_y$ ) was pronouncedly affected by the ageing condition. Before 2 weeks, the level of the stresses didn't change much; but after 2 weeks, it began to decrease about 30%-40%. After 4 weeks, the values of the residual stresses reduced almost to 0. It means that for our composites, the 4-week humidity ageing can eliminate the residual stresses in the composites.

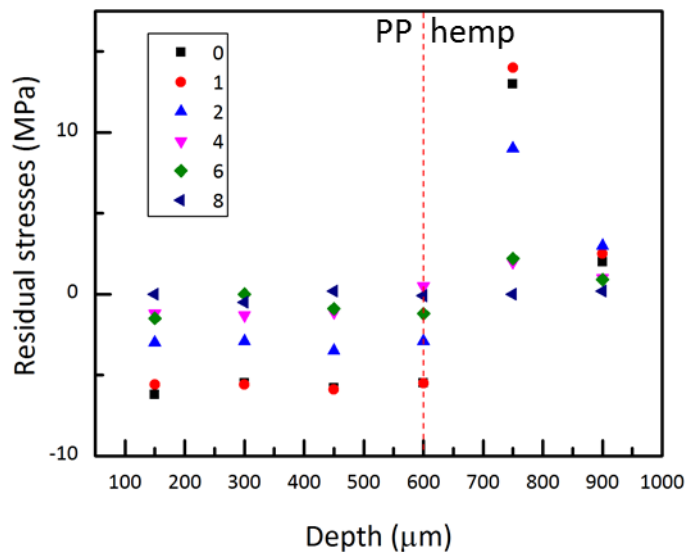


Fig. 4-16 Residual stress  $\sigma_x$  under different ageing time

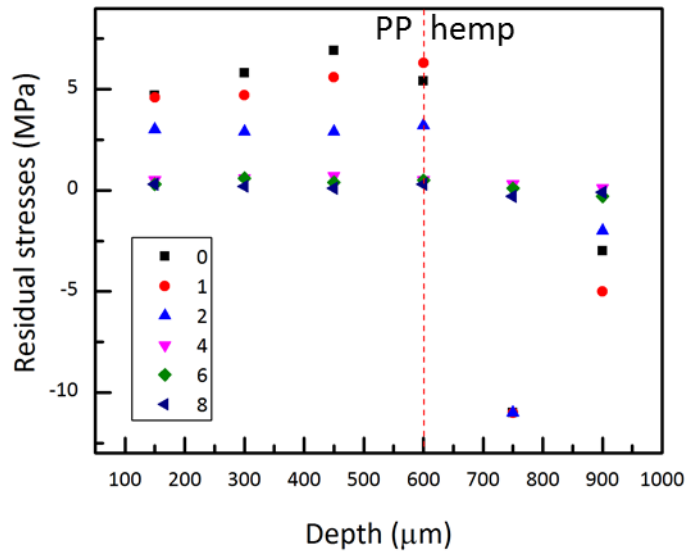


Fig. 4-17 Residual stress  $\sigma_y$  under different ageing time

## 4.6 Conclusion

In this chapter, the residual stresses in the composites were assessed; some information can be concluded as following:

A new approach was proposed to determine the residual stresses in the hemp reinforced polypropylene composites by incremental hole drilling method. This method has practical advantage. The determination of the coefficients of calibration was realized by ABAQUS modelling.

The residual stresses in the composites were determined by this method. The distribution of the residual stresses in the composites was not uniform. The residual stresses in the PP layer reached -5.5 MPa ( $\sigma_x$ ), 5MPa ( $\sigma_y$ ) and 14.5 MPa ( $\sigma_x$ ), -15 MPa ( $\sigma_y$ ), respectively.

The influence of the cooling rate on the residual stresses was determined. It was found that the level of the residual stresses increased with the increasing cooling rate.

The effects of the humidity ageing up to 8 weeks on the residual stresses were

analyzed. After 1 week ageing, the level of residual stresses wasn't affected very much, but after 2 weeks, it decreased 30%. And the subsequent ageing almost eliminated the residual stresses in the composites.



**Chapter 5.**  
**General Conclusions**  
**and Perspectives**

## Chapter 5. Conclusions and Perspectives

### 5.1 Conclusions

This study was accomplished on hemp fabric fiber reinforced polypropylene composites. Our work was aimed at the following objectives: to manufacture the PP/hemp plates by utilizing the compression molding; determine the mechanical properties of the composites under different parameters; to carry out the influence of ageing condition on the composites; and to determine the residual stresses in the composites.

The mechanical properties of the hemp fibers are interesting according to our study. The hemp fibers show elevated tensile properties in the longitudinal direction than those in the transversal direction. The spiral angle of the hemp yarns was responsible for the difference of the tensile properties of the hemp fibers.

The hemp/PP composites were manufactured through compression molding method under different parameters. The parameters have an influence over the mechanical properties of the composites. Composites manufactured at 190 °C show higher performances than the others. The hemp fibers were affected by the temperature according to the DSC analysis, color appearance and the tensile properties results. When the temperature goes higher, the PP will be more easily penetrates into the space between the hemp yarns, and the hemp fibers' thin branches result in more surface contact with the polypropylene matrix. When the temperature is higher than 200 °C, the strength decreases markedly.

The effects of relative humidity on the PP/hemp composites were investigated. The moisture absorption of the composites reached saturation after 4 weeks immersion in water. The saturation level of water was related to the fiber loading and matrix/fiber interfacial adhesion. Lower fiber loading and good matrix/fiber interfacial adhesion restrain the moisture absorption. Diffusion is the most important mechanism in moisture absorption. The kinetics of water diffusion in PP/hemp composites was verified to apply to Fickian diffusion law. The kinetic

parameters were figured out by fittings of the absorption data. Higher fiber loading and poor matrix/fiber interfacial adhesion facilitates the water diffusion.

Swelling is a resulted phenomenon after moisture absorption. The dimension stability of the samples was taken into consideration. The thickness of the samples were measured and recorded. The thickness of the samples increased rapidly at the early stage, and then slowed down, until a plateau region was achieved. Higher fiber loading led to higher swelling ratio.

The effects of Ultra-violet ageing on the composites were studied. In the first two weeks, the composites were not much affected. After 4 weeks, the mechanical properties of the composites showed a remarkable decrease. The fracture of the composites showed that the fibers were pulled out from the matrix, indicating poor matrix/fiber interfacial adhesion.

From the observation of the surface appearances of the composites, the composites were found to be more and more whitened until 8 weeks' UV ageing. After UV radiation, the PP surface appeared micro-cracks. As the UV ageing proceeded, the cracks propagated much longer and thicker after 8 weeks, even a successive crack formed. This reflected in the decrease of the mechanical properties. Crack propagation, chemical-crystallization and lignin degradation affect the total degradation of the composites.

A new approach was proposed to determine the residual stresses in the hemp reinforced polypropylene composites by incremental hole drilling method. This method has practical advantage. The determination of the coefficients of calibration was realized by ABAQUS modelling.

The residual stresses in the composites were determined by this method. The distribution of the residual stresses in the composites was not uniform. The residual stresses in the PP layers reached -5.5 MPa ( $\sigma_x$ ), 5MPa ( $\sigma_y$ ) and in the he,p layers 14.5 MPa ( $\sigma_x$ ), -15 MPa ( $\sigma_y$ ), respectively.

The influence of the cooling rate on the residual stresses was determined. It

was found that the level of the residual stresses increased with the increasing cooling rate.

The effects of the humidity ageing up to 8 weeks on the residual stresses were analyzed. After 1-week ageing, the level of residual stresses wasn't affected very much, but after 2 weeks, it decreased 30%. And the subsequent ageing almost eliminated the residual stresses in the composites.

## 5.2 Perspectives

This work is focused on three parts, the elaboration of the composites, the behavior of the composites under environmental ageing conditions and the residual stresses in the composites. There are still some more works that can be carried out in the continuing research following this thesis:

1. Firstly, being restricted to the raw materials, the volumetric fraction of the fibers can only be adjusted by several specific values. Another approach may be found to manufacture the long fiber reinforced polymer composites with consecutive change of the volumetric fraction of the fibers.
2. Introduce interfacial treatment methods in order to improve the interfacial adhesion between the fibers and the matrices. According to the literature study, the surface treatment can have an obvious effect on the quality of the interface.
3. Carry out the simulation of the flowability of the polymer in the formation of the composites.

**Chapitre 6.**  
**Résumé en Français**

## Chapitre 6. Résumé en Français

6.1	Introduction.....	131
6.2	Élaboration et performance des composites .....	133
6.2.1	Caractérisation de la fibre chanvre .....	133
6.2.1.1	Essai de traction .....	133
6.2.1.2	Angle spiral.....	135
6.2.2	Élaboration des composites .....	136
6.2.3	Propriétés des composites .....	137
6.2.3.1	Influence de la température.....	137
6.2.3.2	Influence de la température sur chanvre .....	138
6.2.3.3	Observation microscopique .....	139
6.3	Effets du vieillissement.....	140
6.3.1	Vieillissement en humidité relative.....	140
6.3.1.1	Résultats des essais de traction .....	141
6.3.1.2	Absorption de l'eau.....	142
6.3.2	Vieillissement au UV .....	144
6.3.2.1	Résultats des essais de traction .....	144
6.3.2.2	Observation d'apparence .....	145
6.4	Contraintes résiduelles dans les composites .....	146
6.4.1	La méthode du trou incrémentale .....	147
6.4.2	Détermination des coefficients de calibration.....	150
6.4.3	Contraintes résiduelles .....	152
6.4.3.1	Influence de température .....	152
6.5	Conclusions .....	153

## 6.1 Introduction

Cette thèse se compose de trois parties : Elaboration et Caractérisation des agro-composites chanvre/polypropylène, Vieillessement et son influence sur le comportement mécanique d'agro-composites et Détermination des contraintes résiduelles dans les agro-composites stratifiés. Dans la matrice de base en polypropylène, un tissu de chanvre a été utilisé comme renfort dans des composites. Ces derniers sont élaborés par compression thermique avec différents paramètres d'élaboration comme : la température, la pression et le temps...etc. Les influences de ces paramètres sur la qualité physique-mécanique de ces matériaux sont analysées. Les résultats ont montré que la température a un effet significatif sur les propriétés mécaniques des composites. Le composite fabriqué sous 190°C présente de meilleures propriétés mécaniques que les autres composites. Nous avons ensuite étudié l'influence de deux types de vieillissement sur les propriétés du matériau : un vieillissement en Humidité Relative (RH) et puis un vieillissement aux Ultra-Violets (U.V). Enfin, nous avons développé la méthode du trou incrémental pour analyser les contraintes résiduelles générées lors du procédé de fabrication mais aussi générées pendant le vieillissement. Pour cela, des coefficients de calibration spécifiques à ces matériaux ont été déterminés par la méthode des éléments finis.

Un matériau composite peut être défini comme l'assemblage d'au moins deux matériaux non miscibles entre eux. Ce matériau présente des propriétés que les matériaux seuls ne possèdent pas. Plus précisément, un matériau composite permet de coupler les performances des deux matériaux.

Depuis quelques années les matériaux composites à base de fibres naturelles sont de plus en plus utilisés pour les nouvelles performances qu'ils proposent. C'est surtout au niveau des fibres naturelles que de nouvelles propriétés sont proposées. Tout d'abord ces fibres, constituées de cellulose et d'hémicellulose [6], ont un impact très faible sur l'environnement. Ensuite, mécaniquement, elles sont très résistantes et ont des modules équivalents aux modules des fibres de verre [27-33]. Enfin, ces fibres sont de très bons isolants thermiques et phoniques. De ce fait avoir un matériau qui couple l'ensemble de ces propriétés est un atout intéressant pour le

développement de composants dans le domaine du transport (maritime et automobile) mais aussi dans le domaine du sport, de l'ameublement ou de la construction.

Dans ce travail, nous nous sommes essentiellement intéressés aux fibres naturelles de chanvre. Ces fibres sont déjà fortement utilisées dans l'automobile et la construction. En Europe, ces fibres sont produites principalement en France et plus particulièrement dans l'Aube.

Actuellement ces fibres sont utilisées sous forme de fibres courtes dans des compounds qui sont ensuite injectés. Les agro-composites ainsi élaborés ont des propriétés mécaniques intéressantes. Pour augmenter ces propriétés et développer des agro-composites hautes performances, c'est sous la forme de fibres longues et de tissés que nous avons choisi d'orienter ce travail de thèse.

C'est la thermocompression que nous avons choisi pour élaborer des plaques avec des tissus de chanvre et une matrice en polypropylène (PP).

Ce travail se décompose en trois parties.

La première partie sera consacrée à la caractérisation mécanique des tissus de chanvre. Dans cette partie, nous développerons le mode opératoire pour élaborer les composites PP/chanvre. Puis nous regarderons les propriétés de ces composites et mettrons en évidence l'influence de la température d'élaboration sur le comportement [57, 64, 80-87].

La seconde partie orientera nos études sur l'effet du vieillissement sur le comportement mécanique de ces matériaux. En effet les agro-composites sont chimiquement sensibles aux vieillissements. La matrice et les fibres étant des matériaux polymères, ils peuvent se dégrader assez rapidement sous des sollicitations environnementales. Dans cette partie, nous regarderons le vieillissement à l'humidité relative (HR) et aux UVs.

Enfin la troisième partie sera consacrée à une analyse des contraintes résiduelles introduites dans ces matériaux. Les contraintes résiduelles jouent un rôle important sur la tenue, la durée de vie et le comportement des composants [99-101].

C'est la méthode du trou incrémental qui sera utilisée avec un développement particulier pour le calcul des coefficients de calibration. Ici aussi, nous regarderons l'effet de la température d'élaboration sur les contraintes résiduelles.

## 6.2 Élaboration et performance des composites

Dans cette partie, nous avons commencé par analyser le comportement mécanique en traction des tissus de chanvre.

Le procédé de fabrication étant directement lié aux performances du matériau, nous avons ensuite regardé l'effet de la température d'élaboration sur le comportement à la fois des tissus seuls puis des tissus insérés dans une matrice de PP. Plusieurs plaques d'agro-composites élaborés par thermocompression seront ici testés.

### 6.2.1 Caractérisation de la fibre chanvre

#### 6.2.1.1 Essai de traction

Les tissus de chanvre, Fig. 6-1 a ont été testés en traction uniaxiale. La première difficulté a été de déterminer la section réelle de nos éprouvettes. En effet, les espaces créés entre les mèches Fig. 6-1 b) ne doivent pas être pris en compte dans le calcul de la section. Ceci fausserait la détermination des contraintes. La section réelle des échantillons a donc été mesurée de deux manières différentes. Tout d'abord nous avons utilisé un simple pied à coulisse puis avons mesuré plus finement la section à l'aide d'un microscope numérique. A la suite de cette étude, nous avons pu mettre en évidence une relation entre la mesure avec le pied à coulisse et la mesure avec le microscope numérique. Cette relation (6-1) ci-dessous, permettra par la suite d'utiliser le pied à coulisse en toute confiance.

$$W_r = W_{NM} = \alpha \cdot W_{VC} \quad (6-1)$$

avec,  $W_r$  est la largeur réelle,  $W_{NM}$  est la largeur mesurée avec le microscope numérique,  $W_{VC}$  la largeur mesurée avec le pied à coulisse et  $\alpha$  est le coefficient

qui permet de relier ces deux types de mesure. Nous avons pu en déduire que ce coefficient était de 0.626.

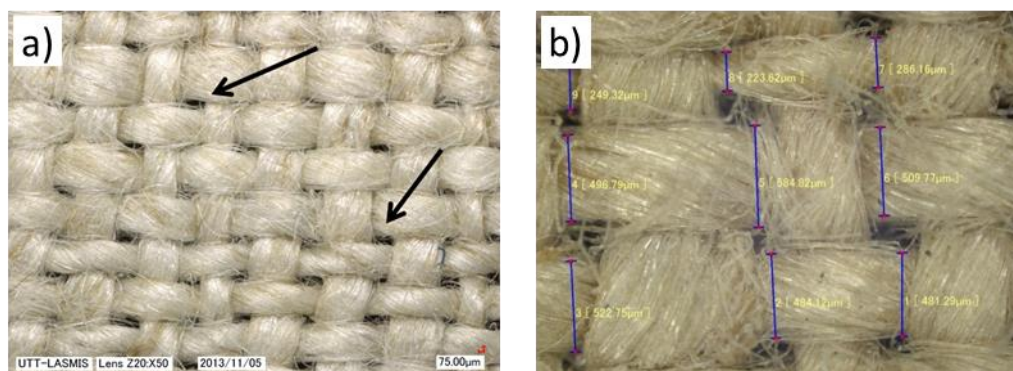


**Fig. 6-1 Photographie des tissus de chanvre au microscope numérique**

Les essais de traction ont été effectués avec une machine de traction Instron 4484 statique à température ambiante. Les essais ont été faits suivant la norme ASTM D3039/D3039M norme – 08 (ASTM International 2008). Les échantillons ont été découpés en bandes rectangulaires à la fois suivant le sens fil et suivant le sens trame. Les essais de traction ont été effectués suivant deux directions, longitudinale et transversale. Cinq échantillons ont été testés et la moyenne des cinq mesures est présentée sur la Fig. 6-2. La Fig. 6-2 présente les propriétés mécaniques des fibres de chanvre suivant les deux directions. Nous pouvons noter une forte différence de comportement suivant la direction de sollicitation. Cela est dû à l'orientation angulaire des mèches. La contrainte maximale dans la direction longitudinale est  $165.89 \pm 8.22$  MPa, qui est 63.8% plus élevée que suivant la direction transversale. Les modules d'Young sont très proches suivant les deux directions. La déformation à la rupture quant à elle est de  $11.35 \pm 0.68\%$  dans la direction longitudinale et plus importante dans la direction transversale.

A la suite de cette première étude, nous avons voulu mesurer l'orientation angulaire des mèches en mesurant l'angle spiral.

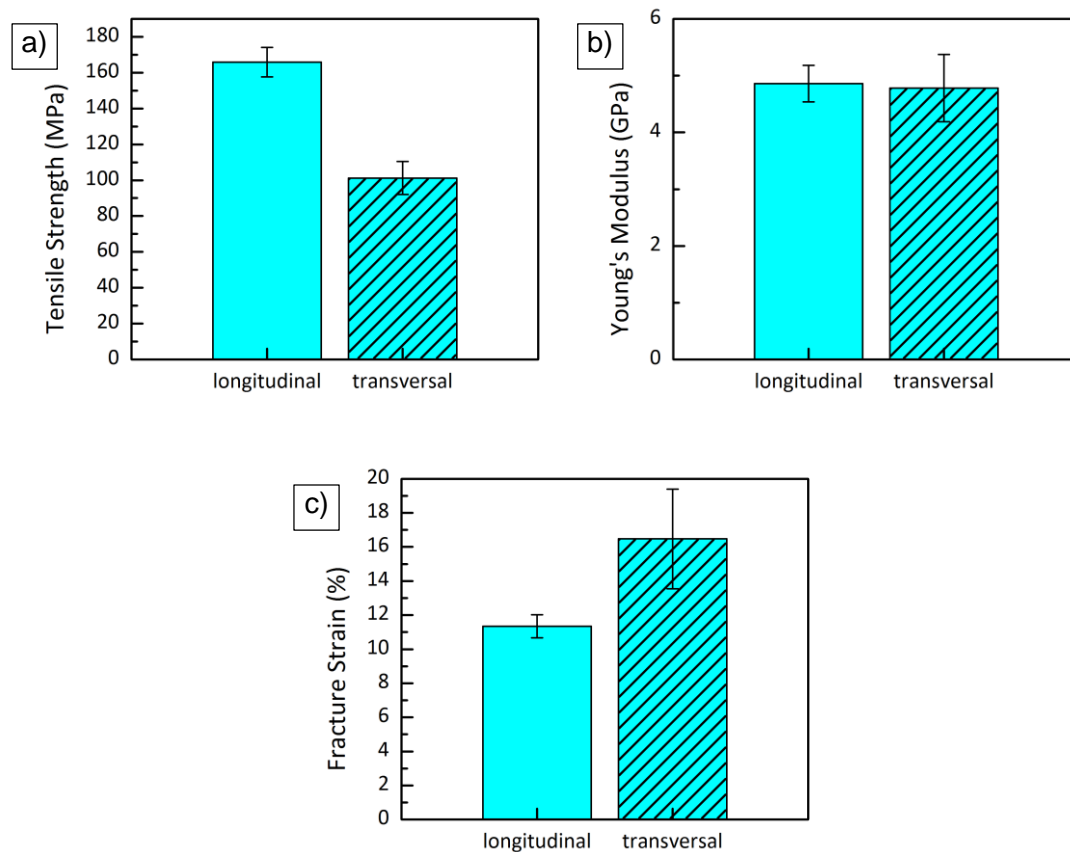


**Fig. 6-2 Propriétés mécaniques des chanvres, a) la contrainte maximale; b) Module d'Young; c) déformation à la rupture.**

### 6.2.1.2 Angle spiral

Pour expliquer les différences des propriétés mécaniques entre les deux directions, nous avons effectués des observations microscopiques des tissus et avons mesuré l'angle entre les mèches avant et après la sollicitation de traction. La Fig. 6-3 présente la mesure de l'angle spiral avec un microscope numérique dans les deux directions.

Dans la Fig. 6-3 b), montre que les angles diminuent suite à la traction. L'angle spiral dans la direction transversale est de  $28.37^\circ \pm 6.27$ , et de 24.7% dans direction longitudinale ( $21.36^\circ \pm 5.65$ ). Nous voyons surtout que cet angle diminue suite à la sollicitation et qu'il joue un rôle important sur la manière avec laquelle les tissus se comportent mécaniquement.

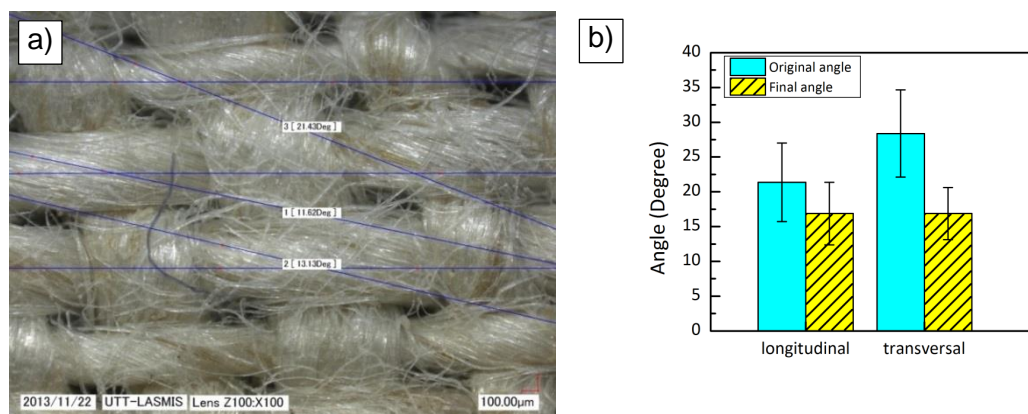


**Fig. 6-3 La mesure de l'angle spirale, a) la direction longitudinale; b) la direction transversale**

Ces études nous ont permis de comprendre un peu mieux le comportement des tissus que nous allons utiliser comme renfort dans les agro-composites. La partie suivante abordera la manière avec laquelle nous avons élaborées composites.

## 6.2.2 Élaboration des composites

Ci-dessous sont décrites succinctement les différentes étapes du processus d'élaboration. Cette procédure est relativement classique et peut se résumer en 5 étapes.

- (1) Préchauffer les fibres de chanvre pour éliminer l'humidité contenue dans les fibres, ce qui réduit l'influence de l'humidité.
- (2) Assembler les matériaux dans les moules, les fibres et les films de polypropylène ont été placés pli par pli dans un moule en aluminium spécialement usiné pour cette étude.
- (3) Chauffer le moule dans un four classique.
- (4) Compresser l'ensemble sous une presse chauffante
- (5) Refroidir les plaques de composites.

Cette procédure nous permet d'élaborer rapidement nos matériaux et de pouvoir faire varier certains paramètres. C'est surtout la température d'élaboration que nous avons fait varier pour analyser son effet sur le comportement mécanique

des agro-matériaux ainsi élaborés.

## 6.2.3 Propriétés des composites

### 6.2.3.1 Influence de la température

Dans un premier temps, nous avons étudié l'influence de la température d'élaboration sur les performances des composites. Nous avons imposé des températures de 160, 170, 180, 190 et 200 °C, quant à la pression imposée pour la compression, nous avons choisi 0.4 MPa. La fraction volumique  $V_f$  est de 19.70%. Les Fig. 6-4 présentent l'influence de la température d'élaboration sur les propriétés des composites.

Tout d'abord nous pouvons constater que la contrainte diminue légèrement lorsque la température d'élaboration augmente et qu'à 190°C celle-ci augmente à nouveau pour diminuer à nouveau. Ensuite le module d'Young croît légèrement jusque 190 °C puis chute au-delà de cette température.

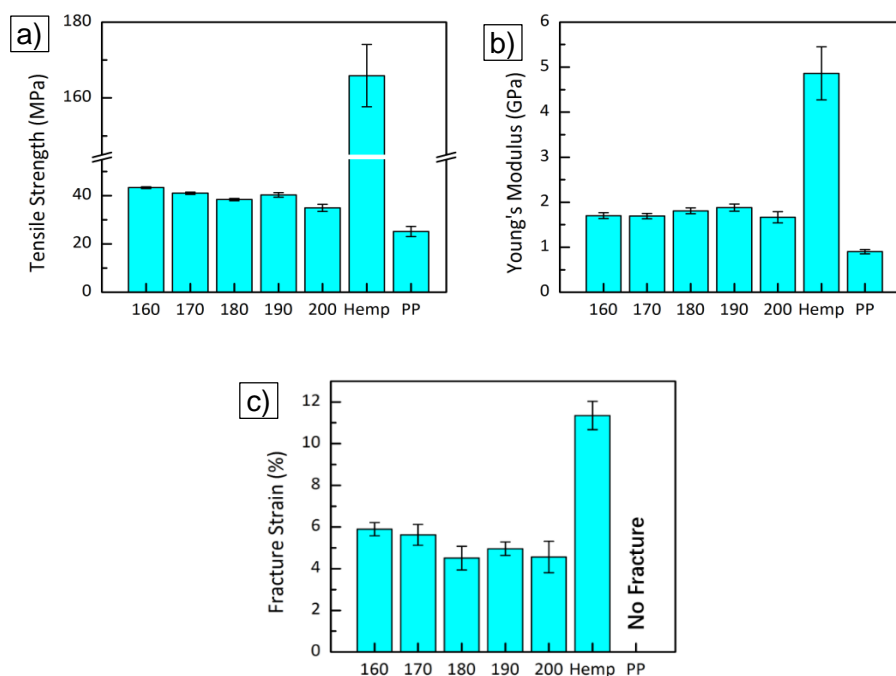


**Fig. 6-4 Propriétés mécaniques des composites, a) la contrainte maximale; b) le module d'Young; c) la déformation à la rupture.**

### 6.2.3.2 Influence de la température sur chanvre

Les fibres de chanvre ont été étudiées pour identifier les influences de la température. Les fibres ont été traitées dans un four pendant 120 minutes sous températures différentes, 160 °C, 180 °C, 200 °C, 220 °C, 240 °C, 260 °C, 280 °C. Elles sont comparées avec les fibres de chanvre non-traitées (Fig. 6-5 et Fig. 6-6).

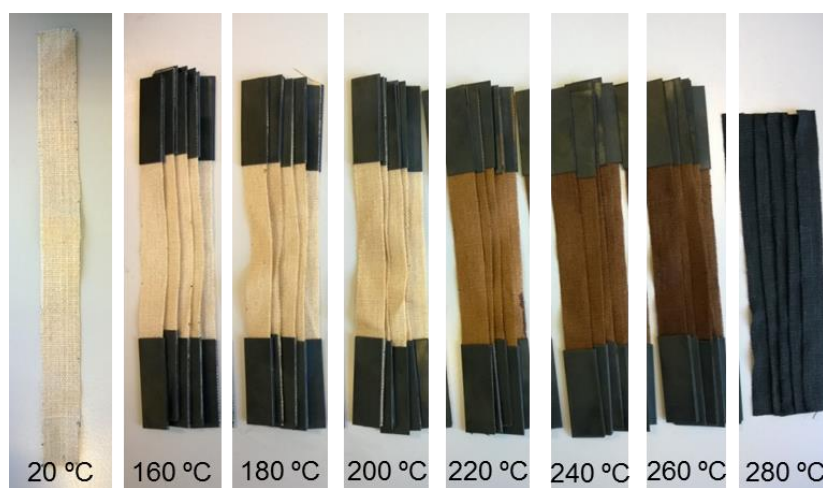


Fig. 6-5 Variation des couleurs des chanvres traités sous les températures différentes

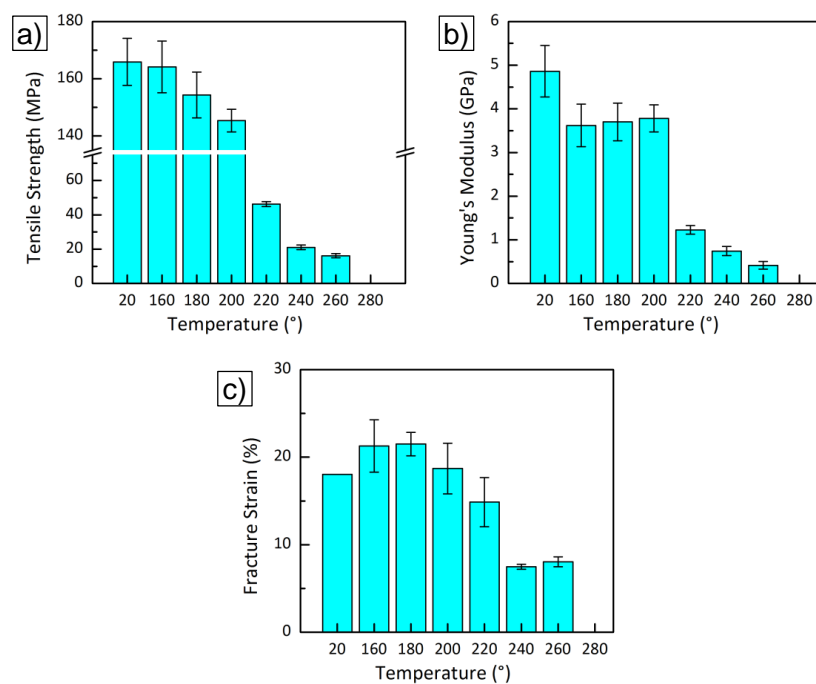


Fig. 6-6 Propriétés mécaniques des chanvres traités sous les températures différentes, a) la contrainte maximale, b) le module d'Young, c) la déformation à la rupture.

Sur la Fig. 6-5, nous pouvons constater que les fibres de chanvre traitées à 160 °C, 180 °C et 200 °C présentent presque la même couleur que les fibres de chanvres non-traitées. Cependant, au-dessus de 200 °C, la couleur du chanvre s'assombrit de plus en plus. À la fin, la fibre de chanvre devient noire à 280 °C. Sur la Fig. 6-6, la résistance ainsi que le module d'Young diminue avec l'augmentation de température. Cette diminution est due à la dégradation des lignines et des pectines puis à la dégradation de l'hémicellulose et de la cellulose. En effet ces constituants chimiques des fibres naturelles sont très sensibles aux variations de température et se dégradent irréversiblement à partir de certaines températures. Ces dégradations peuvent être observées de manière plus qualitative à l'aide d'un MEB.

### 6.2.3.3 Observation microscopique

Après les tests de traction et les analyses des propriétés mécaniques, les fibres de chanvre ont été observées à l'aide d'un MEB. La Fig. 6-7 montre les photographies de ces observations.

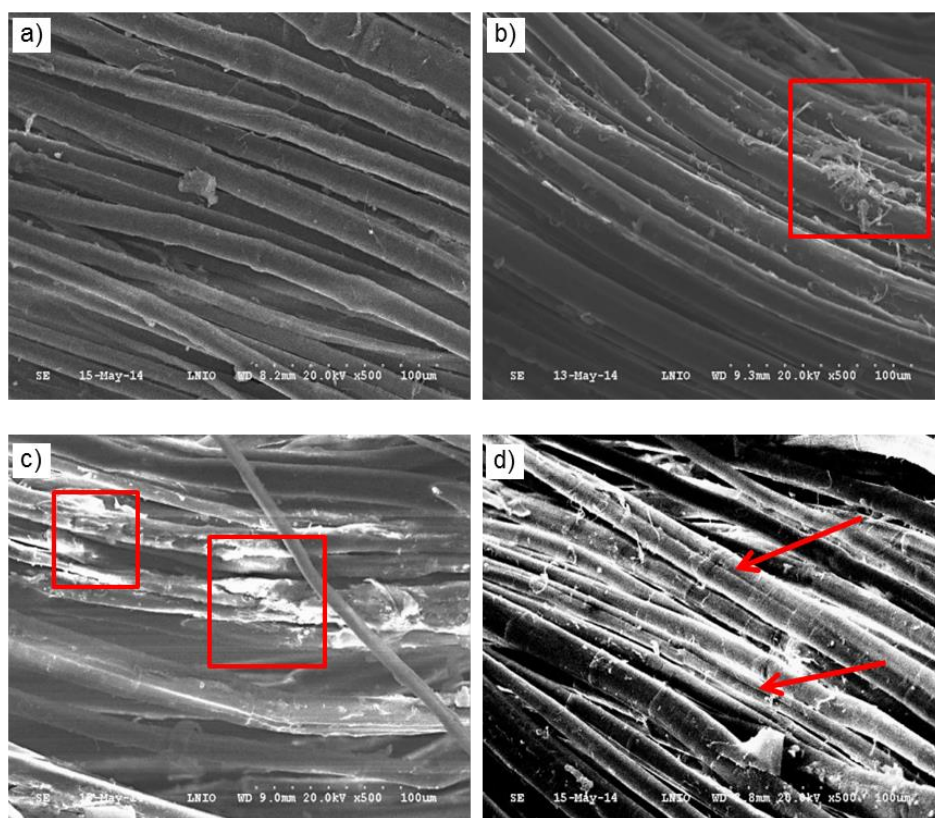


Fig. 6-7 Photographies MEB du chanvre traité a) 160 °C, b) à 180 °C, c) 200 °C, d) 240 °C.

À 160 °C, il n'y a presque pas de dégradation de la fibre, nous ne voyons pas de trace d'endommagement, pas de rupture des microfibrilles. A 180 °C, quelques traces apparaissent et nous pouvons aussi constater que quelques microfibrilles se sont endommagées par quelques ruptures très localisées.

Par contre après 200 °C, les surfaces de la fibre ont été endommagées plus gravement. A cette température, les fibres ont été brûlées et nous pouvons constater des ruptures assez importantes. A 240 °C, nous constatons les mêmes phénomènes d'endommagement mais beaucoup plus accentués.

Ces dégradations directement liées au processus d'élaboration jouent un rôle important sur la tenue mécanique des agro-composites. Aussi par la suite, nous avons fixée 190°C comme température de fabrication. A cette température, les fibres sont peu endommagées et le comportement mécanique est le meilleur.

Suite à cette étude, nous avons regardé l'effet du vieillissement aux UV et à l'humidité séparément des composites PP/chanvre décrit précédemment

## **6.3 Effets du vieillissement**

### **6.3.1 Vieillissement en humidité relative**

En premier lieu, c'est le vieillissement à l'humidité que nous avons regardé. Les éprouvettes sont exposées à l'humidité relative de manière cyclique dans une enceinte de vieillissement ATALAS SUNTEST XXL/XXL +. Plus précisément, l'humidité relative est fixée à 80 %( $\pm 5\%$ ), à 20 °C et à l'obscurité.

Pour bien comprendre le mécanisme de dégradation de chaque élément climatique sur les fibres de chanvre, nous avons réalisé le vieillissement et les analyses relatives. Trois matériaux PP/chanvre élaborés différemment sont analysés dans cette étude. Nous avons ainsi fait varier deux paramètres, la fraction volumique de fibre et la pression de compression. Ces paramètres sont résumés dans le Tableau 6-1.

### 6.3.1.1 Résultats des essais de traction

Les matériaux ont été soumis pendant 8 semaines à l'humidité relative. Chaque semaine, une série d'éprouvettes ont été testées mécaniquement afin de voir l'influence du vieillissement sur les propriétés du matériau. Les résultats de ces essais sont synthétisés sur la Fig. 6-8.

Tout d'abord, nous pouvons constater que les résistances à la traction des composites vieillis ont diminué avec le temps. Ils ont considérablement diminué après 2 semaines. Ils ont diminué de 14.3%, 20.5% and 22.8% pour les composites HR1, HR2 et HR3 respectivement. Ensuite, à partir de 8 semaines, le module d'Young a diminué de 29% (HR1), 40% (HR2) et 32% (HR3).

Les cycles subits par ces matériaux ont permis à l'eau de pénétrer dans les différents constituants et de faire subir aux fibres des cycles de gonflement et dégonflement. Ces cycles affaiblissent non seulement la résistance des fibres naturelles en dégradant les lignines mais dégradent aussi l'interface entre les fibres et la matrice.

Nous constatons aussi que le taux de fibres joue un rôle sur la résistance et surtout sur la manière avec laquelle les matériaux vont supporter l'humidité. La perte des propriétés mécaniques est assez constante suivant les configurations.

Enfin la pression imposée pendant l'élaboration a aussi un rôle important. La configuration HR3 permet d'obtenir de meilleures propriétés.

Nous venons de voir que l'absorption d'eau au sein du composite pouvait dégrader les propriétés du matériau. Cependant cette absorption a des limites, une fois que le composite est saturé en eau. Dans la partie suivante, nous allons voir en combien de jours le composite est saturé en eau.

**Tableau 6-1 Les configurations différentes du vieillissement de HR**

Composites	Température/ °C	Fraction volumique de fibre/ %	La pression/ MPa
HR1	190	11	0.4
HR2	190	19.5	0.4
HR3	190	19.5	0.6

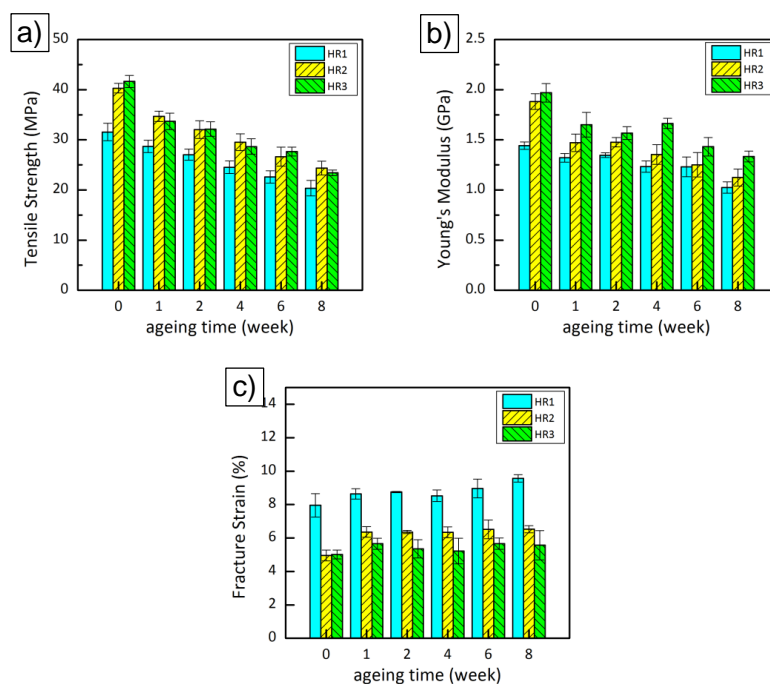


**Fig. 6-8 Les propriétés mécaniques des composites sous HR vieillissement, a) la contrainte maximale, b) le module d'Young, c) la déformation à la rupture.**

### 6.3.1.2 Absorption de l'eau

Dans cette partie, nous nous sommes intéressés à voir en combien de temps les différentes configurations présentées précédemment arrivaient à saturation en eau. Nous avons aussi regardé l'évolution de l'absorption dans le PP pur. Pour cela, nous avons pesé les structures avant et pendant les 8 semaines de vieillissement. La Fig. 6-9 ci-dessous montre l'évolution de la prise d'eau dans les structures en fonction du temps.

Nous constatons, en premier lieu que le polypropylène est quasiment insensible à la prise d'humidité. Cela est dû à son caractère hydrophobe et au fait

que c'est un polymère non polaire.

Ensuite nous pouvons constater une prise d'eau quasi linéaire sur un certain temps puis une saturation pour l'ensemble des trois configurations.

C'est la configuration HR2 (19.5% de fibre avec 0.4 MPa de pression) qui sature en premier. Cette saturation apparaît à 20 jours et atteint 11%.

Concernant les deux autres configurations HR1 (11% de fibre avec 0.4 MPa de pression) et HR3 (19.5% de fibre avec 0.6 MPa de pression) la prise d'humidité est quasiment identique. Elle apparaît au trentième jour pour atteindre 10%.

Ici aussi nous voyons clairement que le taux de fibres influence la prise d'eau. Ce résultat est assez logique étant donné le caractère hydrophile des fibres de chanvre [131, 134].

Par contre nous pouvons remarquer que la pression de fabrication joue un rôle important sur l'absorption d'eau. L'augmentation de la pression de 0.4 à 0.6 MPa permet de mieux protéger le matériau face à l'humidité.

C'est non seulement la nature des composants mais aussi la manière avec laquelle on les met en forme qui permet de les protéger face à l'humidité.

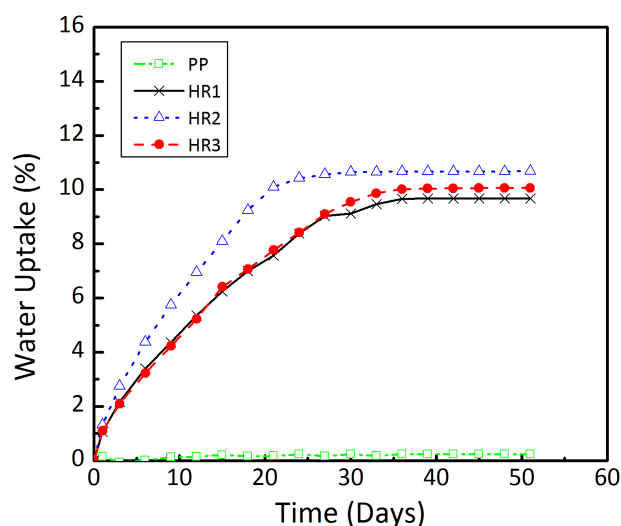


Fig. 6-9 Évolution de l'absorption de l'eau: pure PP, HR1, HR2 et HR3.

A la suite de cette étude face à l'humidité, nous avons regardé l'effet d'un vieillissement aux UV sur nos agro-composites.

### 6.3.2 Vieillissement au UV

Dans cette partie, nous avons voulu voir l'influence des UVs sur la tenue mécanique des agro-composites PP/chanvre dont la description est donnée dans le Tableau 6-1.

Les paramètres de vieillissement aux UVs ont été imposés selon la norme ISO 4892-2: 2006, comme indiqué dans le Tableau 6-2.

**Tableau 6-2 Les paramètres d'exposition du vieillissement au UV des composites**

Cycle d'exposition	rayonnement (W/m <sup>2</sup> )	Température du Black-standard (°C)	Température de la chambre (°C)	Humidité relative (%)
Sec en continu	50 ±2	65 ±3	38 ±3	50 ±10

#### 6.3.2.1 Résultats des essais de traction

La Fig. 6-10 présente les propriétés mécaniques des composites vieillis aux UVs jusqu'aux 8 semaines.

Nous pouvons constater que la perte de propriétés pour l'ensemble des configurations n'est pas immédiate comme dans le cas du vieillissement à l'humidité. Cette diminution apparaît à partir de la quatrième semaine.

Aussi nous voyons que l'ensemble des trois configurations subissent à peu près la même perte de propriétés même si la configuration HR3 (19.5% de fibre avec 0.6 MPa de pression) est la configuration la plus dégradée par ce vieillissement.

Nous pouvons remarquer que le vieillissement à 8 semaines aux UVs a fait chuter de 50% les propriétés initiales de nos matériaux.

### 6.3.2.2 Observation d'apparence

La Fig. 6-11 montre les photos des composites vieillies aux UVs. La couleur des échantillons a changé en passant du brun au blanc. Pendant les deux premières semaines, la couleur de la surface des composites n'a pas changé du tout. Mais après 4 semaines, la surface des échantillons a blanchi rapidement. Au bout de 8 semaines, nous avons constaté l'apparition de fissures macroscopiques à la surface de certains échantillons et une dégradation assez importante des matériaux.

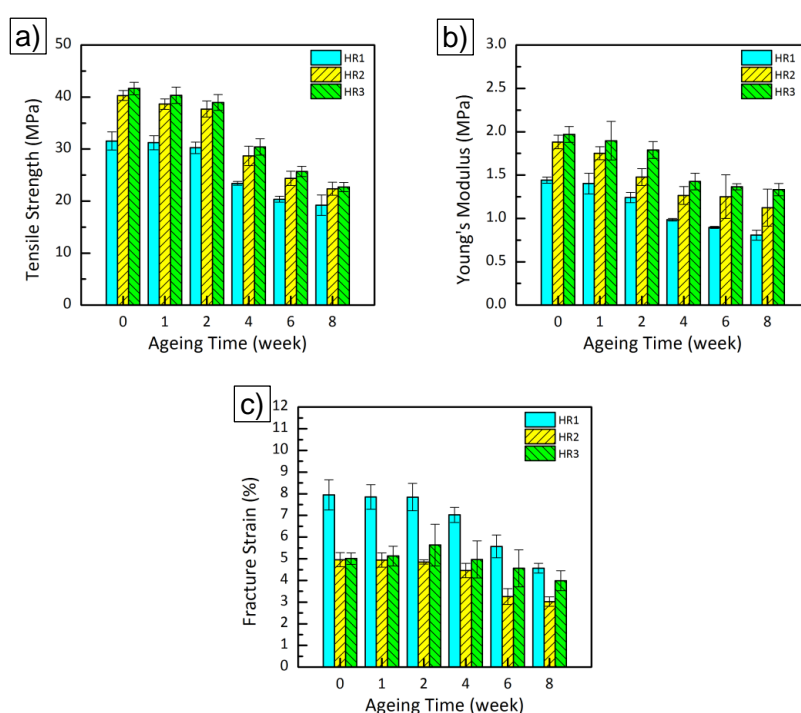


**Fig. 6-10** Les propriétés mécaniques des composites vieillies au UV, a) la contrainte maximale, b) le module d'Young, c) la déformation à la rupture.

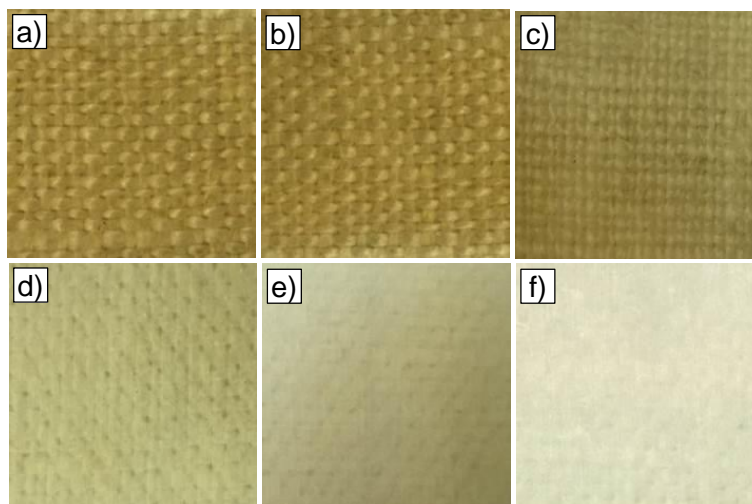


Fig. 6-11 Photos des composites HR3 vieillis, a) 0, b) 1, c) 2, d) 4, e) 6, f) 8 semaines.

## 6.4 Contraintes résiduelles dans les composites

Les contraintes résiduelles jouent un rôle important sur la tenue et la durée de vie des matériaux composites et des agro-matériaux en particulier. Cette partie du mémoire s'intéresse à la détermination des contraintes résiduelles dans chacun des plis de nos composites PP/chanvre et pour chacune des températures d'élaboration. Dans les agro-matériaux, les contraintes résiduelles sont essentiellement d'origine thermique et apparaissent pendant le processus de fabrication et surtout pendant le refroidissement. Elles sont générées par la différence de coefficient de dilatation thermique des matériaux assemblés.

Plusieurs méthodes existent pour déterminer ces contraintes mais la méthode la mieux adaptée à notre étude est la méthode du trou incrémental. Cette méthode est basée sur le principe de relaxation des contraintes après avoir percé un trou au centre d'une rosette de trois jauges de déformation.

Après avoir décrit succinctement la méthode, nous expliquerons comment nous avons déterminé les coefficients de calibration, puis montrerons les résultats obtenus sur nos matériaux.

### 6.4.1 La méthode du trou incrémentale

La méthode du trou incrémental est basée sur le principe de relaxation des contraintes. Pour cela une rosette de trois jauges de déformation est collée à l'endroit où l'on souhaite déterminer ces contraintes. Le perçage d'un trou de 2mm de diamètre relaxe les contraintes piégées dans le volume de matière qui vont créer en surface des déformations. En procédant ainsi de manière incrémentale, nous avons accès aux contraintes dans une fine épaisseur du composite, 1 mm pour notre étude.

Cette méthode peut se décomposer en trois étapes

- Percer un trou dans la zone d'intérêt.
- Mesurer les déformations autour du trou percé entre chaque incrément.
- Calculer les contraintes résiduelles.

Le problème est maintenant de relier les déformations mesurées en surface aux contraintes initialement présentes dans le matériau.

Nous faisons l'hypothèse que les contraintes résiduelles sont dans un état de plan de contrainte  $\sigma(x, y)$  avec  $\sigma_1$  et  $\sigma_2$  les contraintes principales. En changeant de système de coordonnées (Fig. 6-12 Diagramme schématisant le système coordonné), nous pouvons en déduire le tenseur cylindrique des contraintes  $\sigma(r, \theta)$ .

Aussi en posant  $X = \sigma_1 + \sigma_2$ ;  $Y = \sigma_1 - \sigma_2$ , pour obtenir :

$$\begin{cases} \sigma_r = \frac{1}{2}X + \frac{1}{2}Y \cos 2\beta \cos 2\theta + \frac{1}{2}Y \sin 2\beta \sin 2\theta \\ \sigma_\theta = \frac{1}{2}X - \frac{1}{2}Y \cos 2\beta \cos 2\theta - \frac{1}{2}Y \sin 2\beta \sin 2\theta \\ \tau_{r\theta} = -\frac{1}{2}Y \cos 2\beta \sin 2\theta + \frac{1}{2}Y \sin 2\beta \cos 2\theta \end{cases} \quad (6-2)$$

où,  $\beta$  est l'angle entre l'axe de contrainte principale  $\sigma_1$  et l'axe 'x',  $\theta$  est l'angle entre le jauge dans un repère cylindrique et l'axe de référence 'x'. En appliquant la loi de Hooke, nous obtenons:

$$\begin{Bmatrix} \varepsilon_r \\ \varepsilon_\theta \\ \varepsilon_{r\theta} \end{Bmatrix} = C \begin{Bmatrix} \sigma_r \\ \sigma_\theta \\ \sigma_{r\theta} \end{Bmatrix} = \begin{Bmatrix} C_{xx}f_1 & C_{xy}f_2 & C_{xs}f_3 \\ Z & Z & Z \\ Z & Z & Z \end{Bmatrix} \begin{Bmatrix} \sigma_r \\ \sigma_\theta \\ \sigma_{r\theta} \end{Bmatrix} \quad (6-3)$$

où, C est la matrice de souplesse,  $f_1, f_2, f_3$  sont des inconnues qui prennent en compte la géométrie du trou et les configurations des composites.

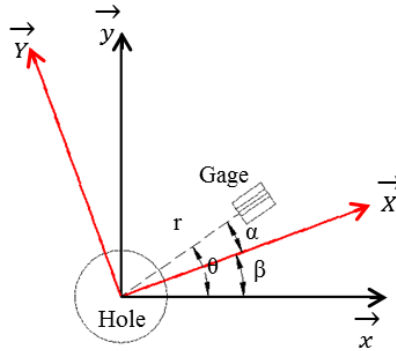


Fig. 6-12 Diagramme schématique du système coordonné

La déformation radiale autour du trou devient:

$$\varepsilon_r = AX + BY\cos 2(\theta - \beta) + CY\sin 2(\beta - \theta) \quad (6-4)$$

où,  $A = (C_{xx}f_1 + C_{xy}f_2)/2$ ,  $B = (C_{xx}f_1 - C_{xy}f_2)/2$ ,  $C = C_{xs}f_3$ .

En utilisant une rosette de jauges dans trois directions à  $\theta = 0, -\frac{3}{4}\pi, \frac{1}{2}\pi$ , les déformations sur chacune des trois jauges peuvent s'écrire:

$$\begin{cases} \varepsilon_1 = \varepsilon_0 = AX + BY\cos 2(0 - \beta) + CY\sin 2(\beta - 0) \\ \varepsilon_2 = \varepsilon_{-\frac{3}{4}\pi} = AX + BY\cos 2\left(-\frac{3}{4}\pi - \beta\right) + CY\sin 2\left(\beta + \frac{3}{4}\pi\right) \\ \varepsilon_3 = \varepsilon_{\frac{1}{2}\pi} = AX + BY\cos 2\left(\frac{1}{2}\pi - \beta\right) + CY\sin 2\left(\beta - \frac{1}{2}\pi\right) \end{cases} \quad (6-5)$$

En faisant l'hypothèse que les contraintes résiduelles sont homogènes sur toute l'épaisseur  $h_i$  du pli, entre chaque incrément, les déformations sont générées par le changement de géométrie du trou et la redistribution des contraintes.

La redistribution des contraintes entre chaque incrément est prise en compte

par l'équation 6-6. Il est facile d'obtenir les contraintes résiduelles pour le premier incrément, la difficulté est de déterminer les contraintes au n<sup>ième</sup> incrément. Les contraintes résiduelles dans la i<sup>ième</sup> couche (i<n) sont déjà connues avec  $\sigma_{1i}$ ,  $\sigma_{2i}$ ,  $\beta_i$ . La déformation provoquée par la libération des contraintes résiduelles dans la n<sup>ième</sup> couche est donné par:

$$\begin{aligned} \varepsilon_{in} = & A_{in}(\sigma_{1i} + \sigma_{2i}) + B_{in}(\sigma_{1i} - \sigma_{2i})\cos 2(\theta - \beta_i) \\ & + C_{in}(\sigma_{1i} - \sigma_{2i})\sin 2(\beta_i - \theta) \end{aligned} \quad (6-6)$$

où

$\sigma_{1i}$ ,  $\sigma_{2i}$ : les contraintes résiduelles dans la i<sup>ième</sup> couche.

$\varepsilon_{in}$ : la contribution de la i<sup>ième</sup> couche à la déformation totale après le n<sup>ième</sup> incrément.

$A_{in}$ ,  $B_{in}$ ,  $C_{in}$ : les coefficients de calibrations dans la i<sup>ième</sup> couche correspondant au n<sup>ième</sup> incrément.

$\beta_i$ : l'angle entre la direction principale des contraintes résiduelles dans la i<sup>ième</sup> couche et la direction  $\vec{x}$ .

$\theta$ : l'angle entre la jauge et la direction  $\vec{x}$ .

L'équation (6-6) permet de prendre en compte la redistribution du champ de contrainte. Par contre pour l'incrément n, la déformation s'écrit:

$$\begin{aligned} \varepsilon_{nn} = & A_{nn}(\sigma_{1n} + \sigma_{2n}) + B_{nn}(\sigma_{1n} - \sigma_{2n})\cos 2(\theta - \beta_n) + \\ & C_{nn}(\sigma_{1n} - \sigma_{2n})\sin 2(\beta_n - \theta) \end{aligned} \quad (6-7)$$

En écrivant cette relation sur chacune des trois jauges et en inversant le système, nous pouvons écrire les contraintes en fonction des déformations [152]:

$$\sigma_{1in} = \frac{\varepsilon_n^1(A_{nn} - B_{nn}\sin 2\theta_n + C_{nn}\cos 2\theta_n) - \varepsilon_n^2(A_{nn} - B_{nn}\cos 2\theta_n - C_{nn}\sin 2\theta_n)}{2A_{nn}B_{nn}(-\sin 2\theta_n + \cos 2\theta_n) + 2A_{nn}C_{nn}(\sin 2\theta_n + \cos 2\theta_n)}$$

$$\sigma_{2in} = \frac{-\varepsilon_n^1(A_{nn} + B_{nn}\sin 2\theta_n - \cos 2\theta_n) + \varepsilon_n^2(A_{nn} + B_{nn}\cos 2\theta_n + C_{nn}\sin 2\theta_n)}{2A_{nn}B_{nn}(-\sin 2\theta_n + \cos 2\theta_n) + 2A_{nn}C_{nn}(\sin 2\theta_n + \cos 2\theta_n)}$$

$$\theta_n = \frac{1}{2} \tan^{-1} \left[ \frac{C_{nn}(\varepsilon_n^3 - \varepsilon_n^1) - B_{nn}(2\varepsilon_n^2 - \varepsilon_n^1 - \varepsilon_n^3)}{C_{nn}(2\varepsilon_n^2 - \varepsilon_n^1 - \varepsilon_n^3) + B_{nn}(\varepsilon_n^3 - \varepsilon_n^1)} \right]$$

(6-8)

Le problème est maintenant de déterminer les coefficients  $A_{nn}$ ,  $B_{nn}$  et  $C_{nn}$ . Pour cela nous allons utiliser la méthode des éléments finis en simulant la relaxation des contraintes pour notre géométrie, nos conditions expérimentales et nos matériaux.

## 6.4.2 Détermination des coefficients de calibration

En appliquant la méthode du trou incrémental, le problème principal est de déterminer les coefficients de calibration. Pour cela, nous avons développé un outil informatique basé sur la méthode des éléments finis. Cet outil permet de simuler la relaxation des contraintes en fonction de nos données expérimentales. Nous avons utilisé le logiciel commercial ABAQUS/Standard pour l'ensemble des modélisations. La Fig. 6-13 montre le modèle utilisé.

Afin de déterminer les coefficients de calibration, nous avons supposé un état plan de contraintes, en effet, la contrainte normale à la surface est négligeable devant les autres contraintes.

Pour déterminer  $A_{in}$ , on suppose l'existence d'un état équi-biaxiale de contraintes résiduelles ( $\sigma_{1i} = \sigma_{2i} = \sigma$  et  $\beta=0$ ) au sein de la  $i$ ème couche dans le modèle, alors  $\sigma_{ri} = -\sigma$  et  $\sigma_{\theta i} = 0$ , dans le repère cylindrique. On obtient:  $A_{in} = \varepsilon_{in}/2\sigma$ .

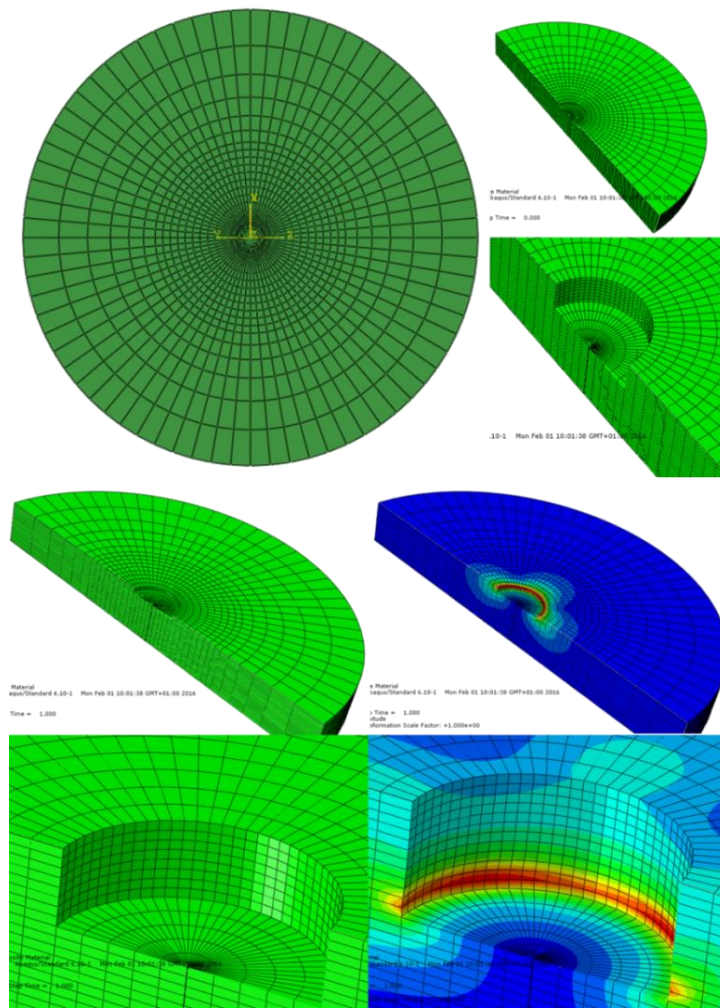


**Fig. 6-13** Mod èle d'éléments finis utilisé pour le calcul des coefficients de calibration

Concernant  $B_{in}$  et  $C_{in}$ , nous appliquons ici un état de contraintes dans la  $i$ ème couche dans le modèle avec  $\sigma_{1i} = -\sigma_{2i} = \sigma$  et  $\beta=0$ , alors  $\sigma_{ri} = -\sigma \cos 2\theta$  et  $\sigma_{r\theta i} = \sigma \sin 2\theta$ , dans le repère cylindrique. On obtient:  $B_{in} = \epsilon_{in}(\theta=0)/2\sigma$ , et  $C_{in} = -\epsilon_{in}(\theta=\pi/4)/2\sigma$ .

Dans ce travail, notre apport a été la détermination des coefficients de calibration adaptée à nos matériaux et à nos mesures. Cette méthode sera maintenant utilisée sur nos agro-matériaux avec les cinq températures d'élaboration. Ceci nous permettra de voir l'influence de la température sur le gradient de contraintes résiduelles.

## 6.4.3 Contraintes résiduelles

### 6.4.3.1 Influence de température

Les contraintes résiduelles ont été déterminées sur les agro-composites contenant 19,7% de fibres de chanvre, élaborés à une pression de 0.4 MPa et avec cinq températures différentes.

Nous avons percé un trou à fond plat de 2mm de diamètre au centre d'une rosette de trois jauges. Nous avons choisi de faire des incréments constants de 150 $\mu$ m d'épaisseur pour atteindre une profondeur totale de 1mm.

Les Fig. 6-14 et Fig. 6-15 montrent les contraintes résiduelles suivant les directions x et y, obtenues dans nos agro-matériaux en fonction de la profondeur. De plus ces contraintes sont données pour les cinq températures de fabrication.

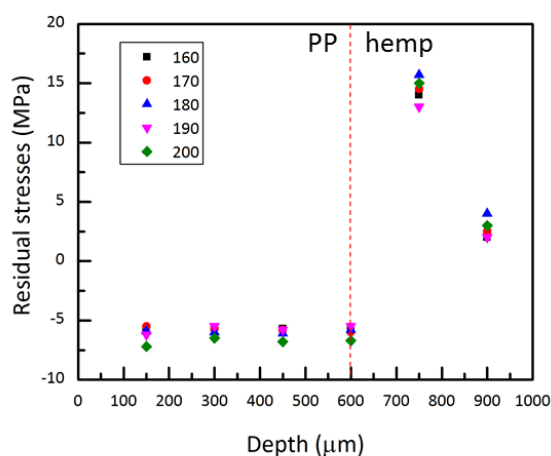
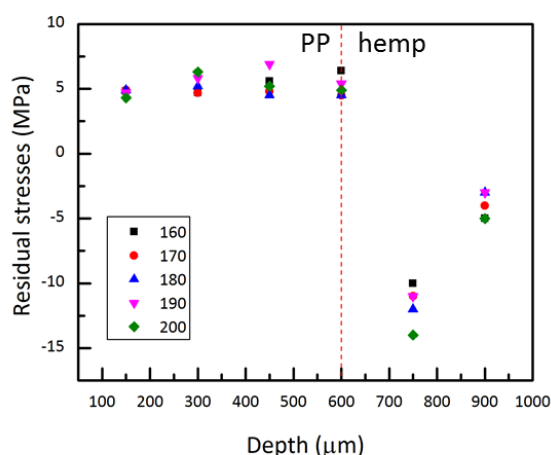


Fig. 6-14 Contraintes résiduelles  $\sigma_x$  en fonction de profondeur



**Fig. 6-15 C Contraintes résiduelles  $\sigma_y$  en fonction de profondeur**

Nous remarquons tout d'abord que les contraintes  $\sigma_x$  et  $\sigma_y$  sont équilibrées et sont de signe opposé.

Ensuite, nous constatons que les contraintes sont homogènes et constantes dans le PP, -5 MPa environ et qu'elles évoluent fortement dans les fibres de chanvres +15 et +5 MPa. Il est intéressant de constater le changement de signe des contraintes entre les différents plis.

Concernant la température, les contraintes résiduelles dans le PP n'évoluent pas beaucoup. Par contre dans les tissus de chanvre, la température affecte un peu plus les contraintes. Ici aussi nous pouvons constater qu'à 190°C, les contraintes résiduelles sont les plus faibles comparées aux autres températures.

## 6.5 Conclusions

Dans ce travail nous avons tout d'abord proposé un processus de fabrication d'agro-matériaux composites PP/tissus de chanvre. Nous avons constaté que la température imposée pendant la thermocompression jouait un rôle important sur le comportement mécanique des matériaux. Cinq températures ont été testées 160, 170, 180, 190 et 200 °C. Mécaniquement, nous avons pu constater qu'à 190°C, le comportement était le meilleur même si certaines différences sont assez faibles.

Nous avons ensuite soumis nos matériaux à des cycles de vieillissement à l'humidité et aux UVs. Nous avons aussi choisi de faire varier la pression de thermocompression et la fraction volumique de fibres tout en fabricant les composites à 190°C. Cette étude nous a permis de constater que ces deux types de vieillissement jouaient un rôle important sur le comportement mécanique des agro-matériaux. Aussi nous avons pu remarquer qu'avec un taux de fibres plus important, les composites certes sont plus résistants mais sont aussi plus sensibles au vieillissement.

Enfin, nous avons voulu voir l'influence de la température de thermocompression sur les contraintes résiduelles. La méthode du trou incrémental nous a permis d'inspecter les contraintes avec des pas de 150µm jusqu'à 1mm de profondeur. Cette méthode s'est montrée assez robuste et assez répétitive. Même si les intensités des contraintes sont assez faibles, elles peuvent nuire à la tenue des composants en service. Nous avons pu constater qu'à 190°C, les contraintes résiduelles étaient les plus faibles et donc les moins nocives pour nos agro-matériaux.

# List of Figures

Fig. 1-1 Schematic representation of plant fiber structure [3].....	7
Fig. 1-2 Chemical structure of cellulose.....	9
Fig. 1-3 Example of hemicellulose structure: L-arabino-D-xylane [15] .....	9
Fig. 1-4 The three alcoholic monomers of lignin .....	10
Fig. 1-5 Free water and bound water in polymer matrix [12] .....	24
Fig. 1-6 Effect of water on fibre–matrix interface [12].....	24
Fig. 1-7 Moisture absorption of the studied natural fibers at 23 °C/ 75% RH [92].....	25
Fig. 1-8 a) fickian diffusion at room temperature, b) non-fickian diffusion at elevated temperature [12] .....	26
Fig. 1-9 Typical thermogravimetric decomposition process of natural fibres [95, 96] .....	27
Fig. 1-10 Model of the structure of softwood lignin showing two chromophoric groups (A and B) [98] .....	29
Fig. 1-11 Oxidation reactions initiated by ultraviolet radiation [94].....	29
Fig. 1-12 Schematic representation of PP molecules after extensive photodegradation [94] .	30
Fig. 1-13 Schematic view of the effect of cooling on the matrix around a fibre. The bonded (constrained) case represents the situation after processing [99] .....	32
Fig. 1-14 Schematic view of residual stress formation in unbalanced cross-ply laminate [99] .....	32
Fig. 1-15 Laminate skin-core residual stress distribution (grey area) [99].....	33
Fig. 2-1 The received state of received (a) (b) hemp fabric and (c) polypropylene .....	40
Fig. 2-2 Dimensions and shape of the test samples .....	42
Fig. 2-3 The typical curve of the hemp fabric samples .....	43
Fig. 2-4 Gaps between hemp yarns .....	44
Fig. 2-5 Measurement of the width of the force-bearing hemp.....	44
Fig. 2-6 Widths measured by numerical microscope and Vernier Caliper.....	45
Fig. 2-7 Verification of the relationship coefficient between numerical microscope and Vernier Caliper .....	46
Fig. 2-8 Mechanical properties of hemp fabric, a) Tensile Strength; b) Young’s Modulus; c) Fracture Strain. ....	47
Fig. 2-9 SEM micrographs of the hemp fibers. a) and b) hemp fiber untested; c), d), e) and f) hemp fibers tested.....	48
Fig. 2-10 The spiral angle presents in the hemp yarns .....	49

## List of Figures

---

Fig. 2-11 Measurement of the spiral angle, a) Longitudinal direction; b) Transversal direction. .....	50
Fig. 2-12 Spiral angle alteration .....	50
Fig. 2-13 Basic diagram of the structure of a plant fiber [50] .....	51
Fig. 2-14 Simple representation of the reorientation of the microfibrils [122] .....	52
Fig. 2-15 Basic diagram of the reorientation of the hemp yarns .....	53
Fig. 2-16 Composites manufactured with different PP forms. a) PP granules, b) PP strips, c) PP sheets. ....	53
Fig. 2-17 Weight change of hemp when heated at a temperature .....	55
Fig. 2-18 The diagram of the moulds .....	56
Fig. 2-19 Mechanical properties of PP/hemp composites: a) Tensile Strength; b) Young's Modulus; c) Fracture Strain.....	58
Fig. 2-20 DSC thermograms of hemp fibers .....	59
Fig. 2-21 Color comparison of hemp fibers after treated under different temperatures .....	61
Fig. 2-22 mechanical properties of hemp fibers treated under different temperatures. a) Tensile Strength, b) Young's Modulus, c) Fracture Strain. ....	62
Fig. 2-23 SEM micrographs fo hemp fibers non-treated and treated under different temperatures: a) untreated fibers; b) treated at 160 °C; c) at 180 °C; d) at 200 °C; e) at 220 °C; f) at 240 °C. ....	63
Fig. 2-24 Tensile properties of PP/hemp composites under different pressures. a) Tensile Strength; b) Young's Modulus; c) Fracture Strain. ....	65
Fig. 2-25 SEM images of hemp/PP composites under different manufacturing pressure: a) b) 0.3 MPa; c) d) 0.5 MPa; e) f) 0.7 MPa. ....	66
Fig. 3-1 Mechanism of free radical formation from lignin degradation [98, 133] .....	72
Fig. 3-2 Ageing oven ATLAS SUNTEST XXL/XXL+.....	73
Fig. 3-3 Mechanical properties of relative humidity-aged PP/hemp composites under different conditions: 190 °C/0.4MPa/11%hemp; 190 °C/0.4MPa/19%hemp; 190 °C/0.6MPa/19%hemp, a) Tensile Strength; b) Young's Modulus; c) Fracture Strain .....	75
Fig. 3-4 Evolution of water uptake of composites: pure PP, HR1, HR2, HR3. ....	77
Fig. 3-5 Schematic curves representing four categories of recorded non-Fickian weight-gain sorption data in polymers and polymeric composites [135]. ....	79
Fig. 3-6 Diffusion case fitting plots for PP/hemp composites.....	81
Fig. 3-7 Swelling ration of humidity-aged PP/hemp composites. ....	84
Fig. 3-8 Mechanical properties of UV-aged PP/hemp composites under different conditions: 190 °C/0.4MPa/11%hemp; 190 °C/0.4MPa/19%hemp; 190 °C/0.6MPa/19%hemp, a) Tensile Strength; b) Young's Modulus; c) Fracture Strain.....	87

List of Figures

---

Fig. 3-9 Photos of PP/hemp composite HR1 after UV ageing of a) 0; b) 1; c) 2; d) 4; e) 6; and f) 8 weeks ..... 88

Fig. 3-10 Photos of PP/hemp composite HR2 after UV ageing of a) 0; b) 1; c) 2; d) 4; e) 6; and f) 8 weeks ..... 88

Fig. 3-11 Photos of PP/hemp composite HR3 after UV ageing of a) 0; b) 1; c) 2; d) 4; e) 6; and f) 8 weeks ..... 89

Fig. 3-12 SEM images of fracture morphology of aged composites after UV ageing. .... 89

Fig. 3-13 Development of cracks on PP surfaces during UV ageing: a) non-aged; b) 1 week; c) 2 weeks; d) 4 weeks; e) 6 weeks; f) 8 weeks..... 91

Fig. 3-14 Tensile test results of PP subjected up to 8 weeks of UV ageing: a) Young’s Modulus; b) Fracture Stress; c) Fracture Strain [140]. ..... 92

Fig. 3-15 XRD patterns of PP after UV ageing of 0 and 8 weeks [14]. ..... 93

Fig. 3-16 Reflection spectra of a) wood; b) lignin and c) cellulose [98]. ..... 94

Fig. 3-17 Guaiacoxy radical from irradiated softwood lignin [143]. ..... 94

Fig. 4-1 Hole-gage assembly in a stressed plate [108] ..... 100

Fig. 4-2 Strain as the radial distance between gage circle and ellipse is shown for uniaxial stress along a) axis x, b) axis y. c) the strain (in rectangular coordinates, proportional to  $K(\alpha)$ ) [108]. ..... 101

Fig. 4-3 Coordinate system diagram, the stress component and the location of strain-gage. 104

Fig. 4-4 The configuration of the strain-gage rosette ..... 106

Fig. 4-5 An example of the incremental analysis ..... 108

Fig. 4-6 The finite element model ..... 111

Fig. 4-7 Two types of applied loadings during the determination of the coefficients of calibration ..... 112

Fig. 4-8 Position of the strain-gage attached on the composites ..... 112

Fig. 4-9 Comparison of the hole quality ..... 115

Fig. 4-10 Configurations of the drilling devices ..... 116

Fig. 4-11 Measured strains of PP/hemp composites by the strain gages ..... 117

Fig. 4-12 Residual stress  $\sigma_x$  under different temperatures ..... 118

Fig. 4-13 Residual stress  $\sigma_y$  under different temperatures ..... 119

Fig. 4-14 Residual stress  $\sigma_x$  under different cooling rates ..... 120

Fig. 4-15 Residual stress  $\sigma_y$  under different cooling rates ..... 120

Fig. 4-16 Residual stress  $\sigma_x$  under different ageing time ..... 121

Fig. 4-17 Residual stress  $\sigma_y$  under different ageing time ..... 122

Fig. 6-1 Tissu de chanvre ..... 134

## List of Figures

---

Fig. 6-2 Propriétés mécaniques des chanvres, a) la contrainte maximale; b) Module d'Young; c) déformation à la rupture. ....	135
Fig. 6-3 La mesure de l'angle spirale, a) la direction longitudinale; b) la direction transversale .....	136
Fig. 6-4 Propriétés mécaniques des composites, a) la contrainte maximale; b) le module d'Young; c) la déformation à la rupture. ....	137
Fig. 6-5 Comparaison des couleurs des chanvres traités sous les températures différentes..	138
Fig. 6-6 Propriétés mécaniques des chanvres traités sous les températures différentes, a) la contrainte maximale, b) le module d'Young, c) la déformation à la rupture. ....	138
Fig. 6-7 Photographies MEB des chanvres, a) 160 °C, b) à 180 °C, c) 200 °C, d) 240 °C. ....	139
Fig. 6-8 Les propriétés mécaniques des composites sous HR vieillissement, a) la contrainte maximale, b) le module d'Young, c) la déformation à la rupture. ....	142
Fig. 6-9 Évolution de l'absorption de l'eau: pure PP, HR1, HR2 et HR3.....	143
Fig. 6-10 Les propriétés mécaniques des composites vieillis au UV, a) la contrainte maximale, b) le module d'Young, c) la déformation à la rupture. ....	145
Fig. 6-11 Photos des composites HR3 vieillis, a) 0, b) 1, c) 2, d) 4, e) 6, f) 8 semaines.....	146
Fig. 6-12 Diagramme schématique du système coordonné .....	148
Fig. 6-13 Le modèle des éléments finis.....	151
Fig. 6-14 Contraintes résiduelles $\sigma_x$ en fonction de profondeur.....	152
Fig. 6-15 C Contraintes résiduelles $\sigma_y$ en fonction de profondeur .....	153

# List of Tables

Table 1-1 Chemical composition of some natural fibers.....	8
Table 1-2 Factors effecting fiber quality at various stages of natural fiber production.....	11
Table 1-3 Factors affecting the physical and mechanical properties.....	11
Table 1-4 Physio-mechanical properties of some natural fibers with comparative values for E-glass.....	12
Table 1-5 Principal advantages and disadvantages of natural fibers as reinforcements in composites materials .....	14
Table 1-6 Three main stages of weight loss of natural fibers.....	28
Table 1-7 Overview of experimental techniques for residual stresses determination, percent accuracy estimates are for measurements of large stresses (~50% of yield stress), percentage numbers will be greater when measuring small stresses [107] .....	34
Table 2-1 Information on hemp fiber fabric.....	40
Table 2-2 Basic properties of polypropylene .....	40
Table 3-1 Different configurations of the aged composites .....	75
Table 3-2 Diffusion kinetic parameters.....	81
Table 3-3 Exposure parameters of UV ageing of PP/hemp composites.....	85
Table 4-1 The parameters of the strain gages.....	114
Tableau 6-1 Les configurations différentes du vieillissement de HR.....	142
Tableau 6-2 Les paramètres d'exposition du vieillissement au UV des composites.....	144



# References

- [1] Rowell, R.M., 1 - Natural fibres: types and properties, in *Properties and Performance of Natural-Fibre Composites*, K.L. Pickering, Editor. 2008, Woodhead Publishing. p. 3-66.
- [2] Kvavadze, E., et al., 30,000-Year-Old Wild Flax Fibers. *Science*, 2009. 325(5946): p. 1359-1359.
- [3] Pereira, P.H.F., et al., Vegetal fibers in polymeric composites: A review. *Polimeros*, 2015. 25(1): p. 9-22.
- [4] Abdul Khalil, H.P.S., A.H. Bhat, and A.F. Ireana Yusra, Green composites from sustainable cellulose nanofibrils: A review. *Carbohydrate Polymers*, 2012. 87(2): p. 963-979.
- [5] Pietak, A., et al., Atomic force microscopy characterization of the surface wettability of natural fibres. *Applied Surface Science*, 2007. 253(7): p. 3627-3635.
- [6] Thomas, S., et al., Natural Fibres: Structure, Properties and Applications, in *Cellulose Fibers: Bio- and Nano-Polymer Composites*, S. Kalia, B.S. Kaith, and I. Kaur, Editors. 2011, Springer Berlin Heidelberg. p. 3-42.
- [7] Faruk, O., et al., Biocomposites reinforced with natural fibers: 2000–2010. *Progress in Polymer Science*, 2012. 37(11): p. 1552-1596.
- [8] Hoareau, W., et al., Sugar cane bagasse and curaua lignins oxidized by chlorine dioxide and reacted with furfuryl alcohol: characterization and stability. *Polymer Degradation and Stability*, 2004. 86(3): p. 567-576.
- [9] Thakur, V.K. and M.K. Thakur, Processing and characterization of natural cellulose fibers/thermoset polymer composites. *Carbohydrate Polymers*, 2014. 109: p. 102-117.
- [10] Akil, H.M., et al., Kenaf fiber reinforced composites: A review. *Materials & Design*, 2011. 32(8–9): p. 4107-4121.
- [11] Cellulose. Available from: <http://www.fibersource.com/f-tutor/cellulose.htm>.
- [12] Azwa, Z., et al., A review on the degradability of polymeric composites based on natural fibres. *Materials & Design*, 2013. 47: p. 424-442.
- [13] Bogoeva-Gaceva, G., et al., Natural fiber eco-composites. *Polymer Composites*, 2007. 28(1): p. 98-107.
- [14] Eichhorn, S.J., et al., Review: current international research into cellulose nanofibres and nanocomposites. *Journal of Materials Science*, 2010. 45(1): p. 1-33.
- [15] Ebringerova, A., Z. Hromadkova, and T. Heinze, Hemicellulose. *Polysaccharides 1*:

## References

---

- Structure, Characterization and Use, 2005. 186: p. 1-67.
- [16] Xie, Y., et al., Silane coupling agents used for natural fiber/polymer composites: A review. *Composites Part A: Applied Science and Manufacturing*, 2010. 41(7): p. 806-819.
- [17] Meshitsuka, G. and A. Isogai, Chemical structures of cellulose, hemicellulose and lignin, in *Chemical Modification of Lignocellulosic Materials*, D.N.-S. Hon, Editor. 1996, Marcel Dekker, Inc. p. 11-33.
- [18] Bungay, H. Hemicellulose. July 1996; Available from: <http://www.rpi.edu/dept/chem-eng/Biotech-Environ/FUNDAMNT/hemicel.htm>.
- [19] Coma, V., Polysaccharide-based Biomaterials with Antimicrobial and Antioxidant Properties. *POLIMEROS-CIENCIA E TECNOLOGIA*, 2013. 23(3): p. 287-297.
- [20] Mukhopadhyay, S. and R. Fanguero, Physical Modification of Natural Fibers and Thermoplastic Films for Composites - A Review. *Journal of Thermoplastic Composite Materials*, 2009. 22(2): p. 135-162.
- [21] Summerscales, J., et al., A review of bast fibres and their composites. Part 1 – Fibres as reinforcements. *Composites Part A: Applied Science and Manufacturing*, 2010. 41(10): p. 1329-1335.
- [22] Thakur, V.K., M.K. Thakur, and R.K. Gupta, Review : Raw Natural Fiber-Based Polymer Composites. *INTERNATIONAL JOURNAL OF POLYMER ANALYSIS AND CHARACTERIZATION*, 2014. 19(3): p. 256-271.
- [23] Rodriguez, M.M. What is lignin? 2013; Available from: <http://www.howaboutlignin.blogspot.fr/2013/06/what-is-lignin.html>.
- [24] John, M.J. and R.D. Anandjiwala, Recent developments in chemical modification and characterization of natural fiber-reinforced composites. *POLYMER COMPOSITES*, 2008. 29(2): p. 187-207.
- [25] Dittenber, D.B. and H.V.S. GangaRao, Critical review of recent publications on use of natural composites in infrastructure. *Composites Part A: Applied Science and Manufacturing*, 2012. 43(8): p. 1419-1429.
- [26] Nishino, T., Natural fibre sources, in *Green composites: Polymer composites and the environment*, C. Baillie, Editor. 2004, Woodhead Publishing Ltd & CRC Press LLC: Cambridge England.
- [27] Mwaikambo, L.Y., TENSILE PROPERTIES OF ALKALISED JUTE FIBRES. *BioResources*; Vol 4, No 2 (2009), 2009.
- [28] Genet, M., et al., The influence of cellulose content on tensile strength in tree roots. *Plant and Soil*, 2005. 278(1-2): p. 1-9.
- [29] Sefain, M.Z., et al., Thermal behaviour of cyanoethylated cellulose. *Thermochimica*

- Acta, 1994. 231: p. 257-265.
- [30] Sawpan, M.A., K.L. Pickering, and A. Fernyhough, Effect of various chemical treatments on the fibre structure and tensile properties of industrial hemp fibres. *Composites Part A: Applied Science and Manufacturing*, 2011. 42(8): p. 888-895.
- [31] Mwaikambo, L. and M. Ansell, Mechanical properties of alkali treated plant fibres and their potential as reinforcement materials. I. Hemp fibres. *Journal of materials science*, 2006. 41(8): p. 2483-2496.
- [32] Mwaikambo, L. and M. Ansell, Mechanical properties of alkali treated plant fibres and their potential as reinforcement materials II. Sisal fibres. *Journal of materials science*, 2006. 41(8): p. 2497-2508.
- [33] Shahzad, A., A Study in Physical and Mechanical Properties of Hemp Fibres. *Advances in Materials Science and Engineering*, 2013. 2013: p. 9.
- [34] Hargitai, H., I. Rácz, and R.D. Anandjiwala, Development of HEMP fiber reinforced polypropylene composites. *Journal of Thermoplastic Composite Materials*, 2008. 21(2): p. 165-174.
- [35] Wambua, P., J. Ivens, and I. Verpoest, Natural fibres: can they replace glass in fibre reinforced plastics? *Composites Science and Technology*, 2003. 63(9): p. 1259-1264.
- [36] Ahmad, I., A. Baharum, and I. Abdullah, Effect of extrusion rate and fiber loading on mechanical properties of Twaron fiber-thermoplastic natural rubber (TPNR) composites. *Journal of reinforced plastics and composites*, 2006. 25(9): p. 957-965.
- [37] Bledzki, A.K. and J. Gassan, Composites reinforced with cellulose based fibres. *Progress in Polymer Science*, 1999. 24(2): p. 221-274.
- [38] Baley, C., Analysis of the flax fibres tensile behaviour and analysis of the tensile stiffness increase. *Composites Part A: Applied Science and Manufacturing*, 2002. 33(7): p. 939-948.
- [39] Bodros, E. and C. Baley, Study of the tensile properties of stinging nettle fibres (*Urtica dioica*). *Materials Letters*, 2008. 62(14): p. 2143-2145.
- [40] Saheb, D.N. and J. Jog, Natural fiber polymer composites: a review. *Advances in polymer technology*, 1999. 18(4): p. 351-363.
- [41] Karmaker, A.C. and J.P. Shneider, Mechanical performance of short jute fibre reinforced polypropylene. *Journal of Materials Science Letters*, 1996. 15(3): p. 201-202.
- [42] Shah, A.N. and S.C. Lakkad, Mechanical properties of jute-reinforced plastics. *Fibre Science and Technology*, 1981. 15(1): p. 41-46.
- [43] Roe, P.J. and M.P. Ansell, Jute-reinforced polyester composites. *Journal of Materials Science*, 1985. 20(11): p. 4015-4020.

- [44] Holbery, J. and D. Houston, Natural-fiber-reinforced polymer composites in automotive applications. *Jom*, 2006. 58(11): p. 80-86.
- [45] Beckermann, G.W. and K.L. Pickering, Engineering and evaluation of hemp fibre reinforced polypropylene composites: Micro-mechanics and strength prediction modelling. *Composites Part A: Applied Science and Manufacturing*, 2009. 40(2): p. 210-217.
- [46] Kumar, S., et al., Behavior of Kevlar/epoxy composite plates under ballistic impact. *Journal of Reinforced Plastics and Composites*, 2009.
- [47] Natural fibres: Ancient fabrics, high-tech geotextiles. 2009; Available from: <http://www.naturalfibres2009.org/en/fibres/index.html>.
- [48] Thakur, V.K., et al., Green composites: An introduction, in *Green composites from natural resources*, V.K. Thakur, Editor. 2013, CRC Press.
- [49] Shahzad, A., Hemp fiber and its composites—a review. *Journal of Composite Materials*, 2012. 46(8): p. 973-986.
- [50] BALEY, C., *Fibres naturelles de renfort pour matériaux composites*. 2004: Ed. Techniques Ingénieur.
- [51] Lei, Y., et al., Preparation and properties of recycled HDPE/natural fiber composites. *Composites Part A: Applied Science and Manufacturing*, 2007. 38(7): p. 1664-1674.
- [52] Facca, A.G., M.T. Kortschot, and N. Yan, Predicting the elastic modulus of natural fibre reinforced thermoplastics. *Composites Part A: Applied Science and Manufacturing*, 2006. 37(10): p. 1660-1671.
- [53] Li, Y., C. Hu, and Y. Yu, Interfacial studies of sisal fiber reinforced high density polyethylene (HDPE) composites. *Composites Part A: Applied Science and Manufacturing*, 2008. 39(4): p. 570-578.
- [54] Torres, F.G. and M.L. Cubillas, Study of the interfacial properties of natural fibre reinforced polyethylene. *Polymer Testing*, 2005. 24(6): p. 694-698.
- [55] Araújo, J.R., W.R. Waldman, and M.A. De Paoli, Thermal properties of high density polyethylene composites with natural fibres: Coupling agent effect. *Polymer Degradation and Stability*, 2008. 93(10): p. 1770-1775.
- [56] Brahmakumar, M., C. Pavithran, and R.M. Pillai, Coconut fibre reinforced polyethylene composites: effect of natural waxy surface layer of the fibre on fibre/matrix interfacial bonding and strength of composites. *Composites Science and Technology*, 2005. 65(3–4): p. 563-569.
- [57] Abdelmouleh, M., et al., Short natural-fibre reinforced polyethylene and natural rubber composites: Effect of silane coupling agents and fibres loading. *Composites Science and Technology*, 2007. 67(7–8): p. 1627-1639.

## References

---

- [58] Paul, A., K. Joseph, and S. Thomas, Effect of surface treatments on the electrical properties of low-density polyethylene composites reinforced with short sisal fibers. *Composites Science and Technology*, 1997. 57(1): p. 67-79.
- [59] Paul, A. and S. Thomas, Electrical properties of natural - fiber - reinforced low density polyethylene composites: A comparison with carbon black and glass - fiber - filled low density polyethylene composites. *Journal of applied polymer science*, 1997. 63(2): p. 247-266.
- [60] Zampaloni, M., et al., Kenaf natural fiber reinforced polypropylene composites: A discussion on manufacturing problems and solutions. *Composites Part A: Applied Science and Manufacturing*, 2007. 38(6): p. 1569-1580.
- [61] Mohanty, A.K., L.T. Drzal, and M. Misra, Engineered natural fiber reinforced polypropylene composites: influence of surface modifications and novel powder impregnation processing. *Journal of Adhesion Science and Technology*, 2002. 16(8): p. 999-1015.
- [62] Tajvidi, M., R.H. Falk, and J.C. Hermanson, Effect of natural fibers on thermal and mechanical properties of natural fiber polypropylene composites studied by dynamic mechanical analysis. *Journal of Applied Polymer Science*, 2006. 101(6): p. 4341-4349.
- [63] Li, H. and M.M. Sain, High Stiffness Natural Fiber - Reinforced Hybrid Polypropylene Composites. *Polymer-Plastics Technology and Engineering*, 2003. 42(5): p. 853-862.
- [64] Espert, A., F. Vilaplana, and S. Karlsson, Comparison of water absorption in natural cellulosic fibres from wood and one-year crops in polypropylene composites and its influence on their mechanical properties. *Composites Part A: Applied Science and Manufacturing*, 2004. 35(11): p. 1267-1276.
- [65] Sain, M., et al., Flame retardant and mechanical properties of natural fibre-PP composites containing magnesium hydroxide. *Polymer Degradation and Stability*, 2004. 83(2): p. 363-367.
- [66] Zafeiropoulos, N.E., et al., Engineering and characterisation of the interface in flax fibre/polypropylene composite materials. Part I. Development and investigation of surface treatments. *Composites Part A: Applied Science and Manufacturing*, 2002. 33(8): p. 1083-1093.
- [67] Gassan, J. and A.K. Bledzki, Possibilities to Improve the Properties of Natural Fiber Reinforced Plastics by Fiber Modification – Jute Polypropylene Composites –. *Applied Composite Materials*, 2000. 7(5-6): p. 373-385.
- [68] Kim, S.-J., et al., Mechanical properties of polypropylene/natural fiber composites: Comparison of wood fiber and cotton fiber. *Polymer Testing*, 2008. 27(7): p. 801-806.

## References

---

- [69] Al - Khanbashi, A., K. Al - Kaabi, and A. Hammami, Date palm fibers as polymeric matrix reinforcement: fiber characterization. *Polymer composites*, 2005. 26(4): p. 486-497.
- [70] Ganan, P., et al., Surface modification of sisal fibers: effects on the mechanical and thermal properties of their epoxy composites. *Polymer composites*, 2005. 26(2): p. 121-127.
- [71] Sreekala, M.S., et al., Stress-relaxation behaviour in composites based on short oil-palm fibres and phenol formaldehyde resin. *Composites Science and Technology*, 2001. 61(9): p. 1175-1188.
- [72] Siró, I. and D. Plackett, Microfibrillated cellulose and new nanocomposite materials: a review. *Cellulose*, 2010. 17(3): p. 459-494.
- [73] Huber, T., et al., A critical review of all-cellulose composites. *Journal of Materials Science*, 2012. 47(3): p. 1171-1186.
- [74] Gindl, W. and J. Keckes, All-cellulose nanocomposite. *Polymer*, 2005. 46(23): p. 10221-10225.
- [75] Nishino, T. and N. Arimoto, All-cellulose composite prepared by selective dissolving of fiber surface. *Biomacromolecules*, 2007. 8(9): p. 2712-2716.
- [76] Nishino, T., I. Matsuda, and K. Hirao, All-cellulose composite. *Macromolecules*, 2004. 37(20): p. 7683-7687.
- [77] Soykeabkaew, N., et al., All-cellulose composites by surface selective dissolution of aligned ligno-cellulosic fibres. *Composites Science and Technology*, 2008. 68(10-11): p. 2201-2207.
- [78] Halpin, J.C. and J. Kardos, The Halpin-Tsai equations: a review. *Polymer engineering and science*, 1976. 16(5): p. 344-352.
- [79] Mackenzie, J.K., The Elastic Constants of a Solid containing Spherical Holes. *Proceedings of the Physical Society. Section B*, 1950. 63(1): p. 2.
- [80] Madsen, B., A. Thygesen, and H. Lilholt, Plant fibre composites – porosity and volumetric interaction. *Composites Science and Technology*, 2007. 67(7-8): p. 1584-1600.
- [81] Khondker, O.A., et al., A novel processing technique for thermoplastic manufacturing of unidirectional composites reinforced with jute yarns. *Composites Part A: Applied Science and Manufacturing*, 2006. 37(12): p. 2274-2284.
- [82] Lee, S.-H., et al., Evaluation of interphase properties in a cellulose fiber-reinforced polypropylene composite by nanoindentation and finite element analysis. *Composites Part A: Applied Science and Manufacturing*, 2007. 38(6): p. 1517-1524.

- [83] Ganster, J., H.P. Fink, and M. Pinnow, High-tenacity man-made cellulose fibre reinforced thermoplastics – Injection moulding compounds with polypropylene and alternative matrices. *Composites Part A: Applied Science and Manufacturing*, 2006. 37(10): p. 1796-1804.
- [84] Amash, A. and P. Zugenmaier, Morphology and properties of isotropic and oriented samples of cellulose fibre–polypropylene composites. *Polymer*, 2000. 41(4): p. 1589-1596.
- [85] Ljungberg, N., J.Y. Cavaille, and L. Heux, Nanocomposites of isotactic polypropylene reinforced with rod-like cellulose whiskers. *Polymer*, 2006. 47(18): p. 6285-6292.
- [86] Qiu, W., T. Endo, and T. Hirotsu, Structure and properties of composites of highly crystalline cellulose with polypropylene: Effects of polypropylene molecular weight. *European Polymer Journal*, 2006. 42(5): p. 1059-1068.
- [87] Madsen, B. and H. Lilholt, Physical and mechanical properties of unidirectional plant fibre composites—an evaluation of the influence of porosity. *Composites Science and Technology*, 2003. 63(9): p. 1265-1272.
- [88] Panthapulakkal, S. and M. Sain, Agro-residue reinforced high-density polyethylene composites: Fiber characterization and analysis of composite properties. *Composites Part A: Applied Science and Manufacturing*, 2007. 38(6): p. 1445-1454.
- [89] Beg, M.D.H. and K.L. Pickering, Accelerated weathering of unbleached and bleached Kraft wood fibre reinforced polypropylene composites. *Polymer Degradation and Stability*, 2008. 93(10): p. 1939-1946.
- [90] Assarar, M., et al., Influence of water ageing on mechanical properties and damage events of two reinforced composite materials: Flax–fibres and glass–fibres. *Materials & Design*, 2011. 32(2): p. 788-795.
- [91] Athijayamani, A., et al., Effect of moisture absorption on the mechanical properties of randomly oriented natural fibers/polyester hybrid composite. *Materials Science and Engineering: A*, 2009. 517(1–2): p. 344-353.
- [92] Methacanon, P., et al., Properties and potential application of the selected natural fibers as limited life geotextiles. *Carbohydrate Polymers*, 2010. 82(4): p. 1090-1096.
- [93] Dhakal, H.N., Z.Y. Zhang, and M.O.W. Richardson, Effect of water absorption on the mechanical properties of hemp fibre reinforced unsaturated polyester composites. *Composites Science and Technology*, 2007. 67(7–8): p. 1674-1683.
- [94] Joseph, P.V., et al., Environmental effects on the degradation behaviour of sisal fibre reinforced polypropylene composites. *Composites Science and Technology*, 2002. 62(10–11): p. 1357-1372.
- [95] Suardana, N.P.G., M.S. Ku, and J.K. Lim, Effects of diammonium phosphate on the

- flammability and mechanical properties of bio-composites. *Materials & Design*, 2011. 32(4): p. 1990-1999.
- [96] Lee, S.-H. and S. Wang, Biodegradable polymers/bamboo fiber biocomposite with bio-based coupling agent. *Composites Part A: Applied Science and Manufacturing*, 2006. 37(1): p. 80-91.
- [97] Hollaway, L.C., A review of the present and future utilisation of FRP composites in the civil infrastructure with reference to their important in-service properties. *Construction and Building Materials*, 2010. 24(12): p. 2419-2445.
- [98] George, B., et al., Photodegradation and photostabilisation of wood – the state of the art. *Polymer Degradation and Stability*, 2005. 88(2): p. 268-274.
- [99] Parlevliet, P.P., H.E.N. Bersee, and A. Beukers, Residual stresses in thermoplastic composites—A study of the literature—Part I: Formation of residual stresses. *Composites Part A: Applied Science and Manufacturing*, 2006. 37(11): p. 1847-1857.
- [100] Parlevliet, P.P., H.E.N. Bersee, and A. Beukers, Residual stresses in thermoplastic composites—A study of the literature—Part II: Experimental techniques. *Composites Part A: Applied Science and Manufacturing*, 2007. 38(3): p. 651-665.
- [101] Parlevliet, P.P., H.E.N. Bersee, and A. Beukers, Residual stresses in thermoplastic composites – a study of the literature. Part III: Effects of thermal residual stresses. *Composites Part A: Applied Science and Manufacturing*, 2007. 38(6): p. 1581-1596.
- [102] Barnes, J.A. and G.E. Byerly, The formation of residual stresses in laminated thermoplastic composites. *Composites Science and Technology*, 1994. 51(4): p. 479-494.
- [103] Manson, J.-A.E. and J.C. Seferis, Process simulated laminate (PSL): a methodology to internal stress characterization in advanced composite materials. *Journal of composite materials*, 1992. 26(3): p. 405-431.
- [104] Withers, P.J. and H.K.D.H. Bhadeshia, Residual stress. Part 1 – Measurement techniques. *Materials Science and Technology*, 2001. 17(4): p. 355-365.
- [105] Niku-Lari, A., J. Lu, and J. Flavenot, Measurement of residual stress distribution by the incremental hole-drilling method. Pergamon Press, *Advances in Surface Treatments. Technology--Applications--Effects.*, 1987. 4: p. 199-219.
- [106] Nairn, J.A. and P. Zoller, Matrix solidification and the resulting residual thermal stresses in composites. *Journal of Materials Science*, 1985. 20(1): p. 355-367.
- [107] Schajer, G.S. and C.O. Ruud, Overview of residual stresses and their measurement. *Practical residual stress measurement methods*. John Wiley & Sons, 2013: p. 1-27.
- [108] Rendler, N. and I. Vigness, Hole-drilling strain-gage method of measuring residual stresses. *Experimental Mechanics*, 1966. 6(12): p. 577-586.

## References

---

- [109] Sasaki, K., M. Kishida, and T. Itoh, The accuracy of residual stress measurement by the hole-drilling method. *Experimental mechanics*, 1997. 37(3): p. 250-257.
- [110] Choi, S. and L. Broutman, Residual stresses in plastic pipes and fittings. 1. Methods for experimental analysis. *POLYMER-KOREA*, 1997. 21(1): p. 71-82.
- [111] Micro-Measurements, V., Measurement of residual stresses by the hole drilling strain gage method. 2005, Tech Note TN-503-6.
- [112] Ruud, C.O., A review of selected non-destructive methods for residual stress measurement. *NDT International*, 1982. 15(1): p. 15-23.
- [113] Kandil, F., et al., A review of residual stress measurement methods. *A Guide to Technique Selection*, NPL, Report MATC (A), 2001. 4.
- [114] Withers, P.J. and H.K.D.H. Bhadeshia, Residual stress. Part 2 – Nature and origins. *Materials Science and Technology*, 2001. 17(4): p. 366-375.
- [115] Rong, M.Z., et al., The effect of fiber treatment on the mechanical properties of unidirectional sisal-reinforced epoxy composites. *Composites Science and Technology*, 2001. 61(10): p. 1437-1447.
- [116] Oksman, K., L. Wallström, and L. Berglund, Morphology and mechanical properties of unidirectional sisal–epoxy composites. *Journal of Applied Polymer Science*, 2002. 84(13): p. 2358-2365.
- [117] Bledzki, A., H.P. Fink, and K. Specht, Unidirectional hemp and flax EP - and PP - composites: Influence of defined fiber treatments. *Journal of Applied Polymer Science*, 2004. 93(5): p. 2150-2156.
- [118] Brahim, S.B. and R.B. Cheikh, Influence of fibre orientation and volume fraction on the tensile properties of unidirectional Alfa-polyester composite. *Composites Science and Technology*, 2007. 67(1): p. 140-147.
- [119] Charlet, K., et al., Characteristics of Hermès flax fibres as a function of their location in the stem and properties of the derived unidirectional composites. *Composites Part A: Applied Science and Manufacturing*, 2007. 38(8): p. 1912-1921.
- [120] Madsen, B., P. Hoffmeyer, and H. Lilholt, Hemp yarn reinforced composites – II. Tensile properties. *Composites Part A: Applied Science and Manufacturing*, 2007. 38(10): p. 2204-2215.
- [121] Madsen, B., et al., Hemp yarn reinforced composites – I. Yarn characteristics. *Composites Part A: Applied Science and Manufacturing*, 2007. 38(10): p. 2194-2203.
- [122] Charlet, K., et al. Relation entre la microstructure et le comportement mécanique d'une fibre de lin. in *JNC 15/AMAC*. 2007.
- [123] Pérez - Rigueiro, J., et al., Tensile properties of Attacus atlas silk submerged in liquid

- media. *Journal of applied polymer science*, 2001. 82(1): p. 53-62.
- [124] DURABLE, C.G.A.D., Les filières industrielles stratégiques de l'économie verte. 2010, Ministère de l'Écologie, de l'Énergie, du Développement durable et de la Mer en charge des Technologies vertes et des Négociations sur le Climat, Rapport.
- [125] Aziz, S.H. and M.P. Ansell, The effect of alkalization and fibre alignment on the mechanical and thermal properties of kenaf and hemp bast fibre composites: Part 1 – polyester resin matrix. *Composites Science and Technology*, 2004. 64(9): p. 1219-1230.
- [126] Aziz, S.H. and M.P. Ansell, The effect of alkalization and fibre alignment on the mechanical and thermal properties of kenaf and hemp bast fibre composites: part 2 – cashew nut shell liquid matrix. *Composites Science and Technology*, 2004. 64(9): p. 1231-1238.
- [127] Akita, K. and M. Kase, Determination of kinetic parameters for pyrolysis of cellulose and cellulose treated with ammonium phosphate by differential thermal analysis and thermal gravimetric analysis. *Journal of Polymer Science Part A - 1: Polymer Chemistry*, 1967. 5(4): p. 833-848.
- [128] Yang, H., et al., Characteristics of hemicellulose, cellulose and lignin pyrolysis. *Fuel*, 2007. 86(12–13): p. 1781-1788.
- [129] Derbyshire, H. and E. Miller, The photodegradation of wood during solar irradiation. *Holz als Roh-und Werkstoff*, 1981. 39(8): p. 341-350.
- [130] Ku, H., et al., A review on the tensile properties of natural fiber reinforced polymer composites. *Composites Part B: Engineering*, 2011. 42(4): p. 856-873.
- [131] Law, T. and Z. Ishak, Water absorption and dimensional stability of short kenaf fiber - filled polypropylene composites treated with maleated polypropylene. *Journal of Applied Polymer Science*, 2011. 120(1): p. 563-572.
- [132] Pothan, L.A., S. Thomas, and N. Neelakantan, Short banana fiber reinforced polyester composites: mechanical, failure and aging characteristics. *Journal of reinforced plastics and composites*, 1997. 16(8): p. 744-765.
- [133] Kamoun, C., et al., Etude par spectroscopie de résonance paramagnétique électronique de la photodégradation des lignines extraites du bois de pin radiata (*Pinus radiata* D. Don). *Ann. For. Sci.*, 1999. 56(7): p. 563-578.
- [134] Mohanty, A., M. Misra, and G. Hinrichsen, Biofibres, biodegradable polymers and biocomposites: an overview. *Macromolecular materials and Engineering*, 2000. 276(1): p. 1-24.
- [135] Weitsman, Y.J., Anomalous fluid sorption in polymeric composites and its relation to fluid-induced damage. *Composites Part A: Applied Science and Manufacturing*, 2006.

- 37(4): p. 617-623.
- [136] Scida, D., et al., Influence of hygrothermal ageing on the damage mechanisms of flax-fibre reinforced epoxy composite. *Composites Part B: Engineering*, 2013. 48: p. 51-58.
- [137] Retegi, A., et al., Effects of hygrothermal ageing on mechanical properties of flax pulps and their polypropylene matrix composites. *Journal of applied polymer science*, 2006. 102(4): p. 3438-3445.
- [138] Cherif, Z.E., et al., Influence of textile treatment on mechanical and sorption properties of flax/epoxy composites. *Polymer Composites*, 2013. 34(10): p. 1761-1773.
- [139] Shen, C.-H. and G.S. Springer, Moisture absorption and desorption of composite materials. *Journal of Composite Materials*, 1976. 10(1): p. 2-20.
- [140] Han, H., Study of agro-composite hemp/polypropylene: treatment of fibers, morphological and mechanical characterization. 2015, Troyes.
- [141] Jin, S. and X. Gong, Study of mechanical properties and performance of aging hemp fibers. *World Journal of Engineering*, 2011. 8(4): p. 325-330.
- [142] Rabello, M.S. and J.R. White, The role of physical structure and morphology in the photodegradation behaviour of polypropylene. *Polymer Degradation and Stability*, 1997. 56(1): p. 55-73.
- [143] Sundell, P. and M. De Meier. Influence of acetylation on discoloration and weathering of (coated) wood. in *Workshop on photodegradation COST E. 2001*.
- [144] Mathar, J., Determination of initial stresses by measuring the deformation around drilled holes. *Trans. ASME*, 1934. 56(4): p. 249-254.
- [145] Bert, C.W. and G.L. Thompson, A method for measuring planar residual stresses in rectangularly orthotropic materials. *Journal of Composite Materials*, 1968. 2(2): p. 244-253.
- [146] Naik, N. and R. Sahani. Measurement of Residual Stresses in Composites by Hole Drilling Method.(Retroactive Coverage). in *V International Congress on Experimental Mechanics*. 1984.
- [147] Wang, J.-y., Measurement of residual stress by the hole-drilling method: General stress-strain relationship and its solution. *Experimental mechanics*, 1988. 28(4): p. 355-358.
- [148] Prasad, C.B., R. Prabhakaran, and S. Tompkins, Determination of calibration constants for the hole-drilling residual stress measurement technique applied to orthotropic composites—Part I: Theoretical considerations. *Composite Structures*, 1987. 8(2): p. 105-118.
- [149] Prasad, C.B., R. Prabhakaran, and S. Tompkins, Determination of calibration constants for the hole-drilling residual stress measurement technique applied to orthotropic composites—Part II: Experimental evaluations. *Composite Structures*, 1987. 8(3): p.

- 165-172.
- [150] Schajer, G. and L. Yang, Residual-stress measurement in orthotropic materials using the hole-drilling method. *Experimental Mechanics*, 1994. 34(4): p. 324-333.
- [151] Shokrieh, M.M., Simulation of central hole drilling process for measurement of residual stresses in isotropic, orthotropic, and laminated composite plates. *Journal of Composite materials*, 2007. 41(4): p. 435-452.
- [152] Sicot, O., et al., Determination of residual stress in composite laminates using the incremental hole-drilling method. *Journal of composite materials*, 2003. 37(9): p. 831-844.
- [153] Sicot, O., et al., Influence of experimental parameters on determination of residual stress using the incremental hole-drilling method. *Composites science and technology*, 2004. 64(2): p. 171-180.
- [154] Wen, Z., Contribution à l'étude des contraintes résiduelles sur le comportement mécanique des composites stratifiés±θ. 2015, Troyes.
- [155] Gigliotti, M., F. Jacquemin, and A. Vautrin, Assessment of approximate models to evaluate transient and cyclical hygrothermoelastic stress in composite plates. *International Journal of Solids and Structures*, 2007. 44(3-4): p. 733-759.
- [156] Gigliotti, M., et al., Transient and cyclical hygrothermoelastic stress in laminated composite plates: Modelling and experimental assessment. *Mechanics of Materials*, 2007. 39(8): p. 729-745.

# XiaoHui ZHANG

Doctorat : Matériaux, Mécanique, Optique et Nanotechnologie

Année 2016

## Elaboration des chanvre/PP composites et étude des contraintes résiduelles et du comportement de vieillissements

Depuis quelques années les matériaux composites à base de fibres naturelles sont de plus en plus utilisés pour les nouvelles performances qu'ils proposent. C'est surtout au niveau des fibres naturelles que de nouvelles propriétés sont proposées

Dans ce travail, nous nous sommes essentiellement intéressés aux fibres naturelles de chanvre. Ces fibres sont déjà fortement utilisées dans l'automobile et la construction. En Europe, ces fibres sont produites principalement en France et plus particulièrement dans l'Aube.

Pour développer des agro-composites hautes performances, c'est sous la forme de fibres longues et de tissus que nous avons choisi d'orienter ce travail de thèse.

Nous avons choisi la thermocompression pour élaborer des plaques avec des tissus de chanvre et une matrice en polypropylène (PP).

Ce travail permet de voir l'influence des conditions d'élaboration sur le comportement mécaniques de ces agro-composites. Cette thèse permet aussi de voir l'effet du vieillissement aux UV et à l'Humidité sur les performances de ces matériaux. Enfin une analyse des contraintes résiduelles par la méthode du trou incrémental permet de voir leurs effets sur ces agro-matériaux.

**Mots clés :** fibres végétales - matières plastiques renforcées avec des fibres - contraintes résiduelles - matériaux, détérioration - matériaux, propriétés mécaniques.

## Manufacturing of Hemp/PP Composites and Study of its Residual Stress and Aging Behavior

In recent years composite materials based on natural fibers are more and more used for their new performances. Natural fibers propose attractive environmental, mechanical and thermal properties.

In this work, we are firstly interested in hemp fibers.

These fibers are already used in the automotive and construction industry. In Europe, these fibers are produced mainly in France and especially in Aube.

To develop agro-composites with high performances, we have focused this thesis on hemp woven. We chose to elaborate the plates with hemp woven and a polypropylene matrix (PP) by compression molding.

This work allows us to see the influence of elaboration conditions on the mechanical behavior of these agro-composites. This thesis also allows us to see the effect of aging conditions UV and humidity on the performance of these materials. Finally an analysis of residual stresses determined by the hole drilling method is proposed to see their effects on the agro-materials.

**Keywords:** plant fibers - fiber reinforced plastics - residual stresses - materials, deterioration - materials, mechanical properties.

Thèse réalisée en partenariat entre :

